NASA Contractor Report 179477

Improved Silicon Carbide for Advanced Heat Engines

T.J. Whalen and W.L. Winterbottom
Ford Motor Company
Dearborn, Michigan

September 1986

Prepared for
Lewis Research Center
Under Contract NAS3-24384

Date for general release September 1988

National Aeronautics and
Space Admini

(NASA-CR-179477) IMPROVED SILICON CARBIDE FOR ADVANCED HEAT ENGINES Annual Report (Ford Motor Co.) 103 p CSCL 11C

N89-15251

Unclas
G3/27 0184820

FOREWORD

The experimental planning and the processes of mixing, forming, sintering, and testing of SiC samples were performed by the Research Staff of Ford Motor Company at the Scientific Laboratory, Dearborn, Michigan.

The principal investigator was Dr. Thomas J. Whalen and the program manager was Dr. Walter L. Winterbottom. Ms. Nancy Shaw of NASA Lewis Research Center is project manager. Significant contributions throughout the first year of the program have been made by W. Trela, Dr. R. M. Williams, Dr. S. Shinozaki, Dr. R. Govila, B. N. Juterbock, L. R. Reatherford, and V. Mindroiu. Contributions to the experimental work and the report preparation also have been made by J. A. Mangels, J. R. Baer, E. L. Cartwright, and R. C. Elder.

TABLE OF CONTENTS

EXECUTIVE SUMMARY

This report prepared by the Research Staff, Ford Motor Company is the first annual technical report for the program entitled "Improved Silicon Carbide for Advanced Heat Engines". The program is conducted for the National Aeronautics and Space Administration (NASA) under contract number NA53-24384. This report includes work performed during the period February 12, 1985 to February 15, 1986.

The objective of the program is the development of high strength, high reliability silicon carbide parts having complex shapes suitable for use in advanced heat engines. The fabrication methods used are to be adaptable for the mass production of such parts on an economically sound basis. Injection molding is the method selected for use in the program. These objectives are to be accomplished in a two phase program: Phase I - achieve a 20% improvement in strength and a 100% increase in Weibull modulus of the baseline material; Phase II - produce a complex shaped part, a gas turbine rotor for example, with the optimal mechanical properties attained in Phase I.

Eight tasks are included in Phase I covering the characterization of the properties of a baseline material, the improvement of those properties and the fabrication of complex shaped parts. Activities during the first contract year were directed to two of these task areas.

Initial problems in sintering to full density were experienced in the program which delayed the start of the baseline characterization. As a result, significant alterations were made in the dewaxing and sintering processes planned for use. Vacuum dewaxing and sintering processes were developed under Task VII and were used in baseline processing. The baseline characterization was completed in the first year of the program. Material and process improvements are ongoing throughout the program.

Task I

The objective of Task I was to characterize the Ford baseline starting materials (Ibiden beta SiC; carbon and boron sintering aids) and determine the mechanical properties of test bars produced by the baseline process. The properties measured were the chemical composition, polyphase distribution, particle size distribution, surface area, specific gravity, and packing density. The binder materials used in the molding mix were characterized by Thermal Gravimetric Analysis and Differential Scanning Calorimetry. MOR bars were individually formed by injection molding, dewaxed in vacuum, and sintered in vacuum. Machined test bars were measured for room temperature and elevated temperature strength. A determination of Weibull characteristic strength and modulus at room temperature was made on statistically significant sample sizes. Mean strength and stress rupture at elevated temperatures, fracture origins, microstructure, and density were measured on representative samples.

A group of 276 test bars were injection molded for the baseline study, and 122 were sintered and machined for testing.

A total of 48 MOR bars were tested for strength at room temperature, 1000^0 C, 1200^0 C and 1400^0 C . The results of these tests indicated the baseline materials have a room temperature characteristic strength of 316 MPa (45.8 Ksi) with a Weibull modulus of 8. The mean strengths at room temperature, 1000^0 C, 1200^0C and 1400^0 C were 299 (43.3 Ksi), 285 MPa (41.4 Ksi), 298 MPa (43.2 Ksi), and 325 MPa (47.2 Ksi) respectively. The mean stress rupture life at 1400^oC of five samples tested at 172 MPa (25 Ksi) stress was 62 hours and at 207 MPa (30 Ksi) stress was 14 hours.

Task VII

The objectives of Task VII are to improve the processing and properties of the SiC material. During the first year, a number of experimental studies were carried out to facilitate selection of the baseline composition, the dewaxing and sintering processes, and injection molding parameters which would give fully dense materials with MOR strengths of at least 310 MPa (45 Ksi). Vacuum dewaxing and sintering and high-shear dry mixing processes were developed and utilized in producing a baseline material which met the minimum strength requirement. Concerted efforts to further reduce the flaw size and improve mechanical properties using hot-roll and high-shear milling methods were ineffective.

A fluid mixing process was studied under Task VII, when it became obvious that materials prepared with the dry mixing process were strength limited by flaws introduced in the mixing process. Reductions in flaw size and improved properties have been achieved with the fluid mixing process. This process has been scaled up, process controls have been added, and statistical process control data are being collected.

Future Plans

Because of the strength improvements achieved by fluid mixing, Task VII, a revised set of goals for injection molded SiC has been established. The new Phase I goals are: i) Weibull characteristic strength of 710 MPa (80 Ksi); ii) Weibull modulus of 16.

In the coming year, the program focus will be on the development of process and material strength improvements under Task II. Turbocharger molding studies (Ford funded) will be initiated in order to test the complex-shape moldability of the improved materials developed in Task II.

INTRODUCTION

This is the first annual technical report prepared by the Ford Motor Company on "Improved Silicon Carbide for Advanced Heat Engines". The program is being conducted for the National Aeronautics and Space Administration (NASA) under contract number NAS3-24384. The period February 12, 1985 to February 15, 1986 is covered by this report.

The objective of this program is to develop high strength, high reliability silicon carbide parts, having complex shapes suitable for use in advanced heat engines. The fabrication method is to be adaptable to mass production of such parts on an economically sound basis.

The original program schedule is shown in Figure I-1. Two phases of development are shown which are to be completed in 60 months. Phase I contains the fabrication, evaluation and optimization of test bars, and is divided into four tasks:

Task I

Fabricate and characterize the baseline silicon carbide material.

Task II

Improve silicon carbide MOR bars with process and material improvements by iterative, statistically designed experiments and show a 20% increase in strength and a 100% increase in Weibull modulus.

Task III

Characterize the improved process and material.

Task VII

Conduct studies to develop advanced ceramic compositions and processing techniques.

TASK NO.	DESCRIPTION	% EFFORT
I	BASELINE CHARAC.	5
II	MOR MATRIX	25
III	OPTIMIZED MOR	5
IV	BASELINE LG.SHAPE	5
V	LG.SHAPE MATRIX	25
VI	OPTIM. LG. SHAPE	10
VII	MAT'L./PROC. IMP.	15
VIII	T'CHARGER FAB.	5
IX	RPTS./PROJ. MGMT.	5

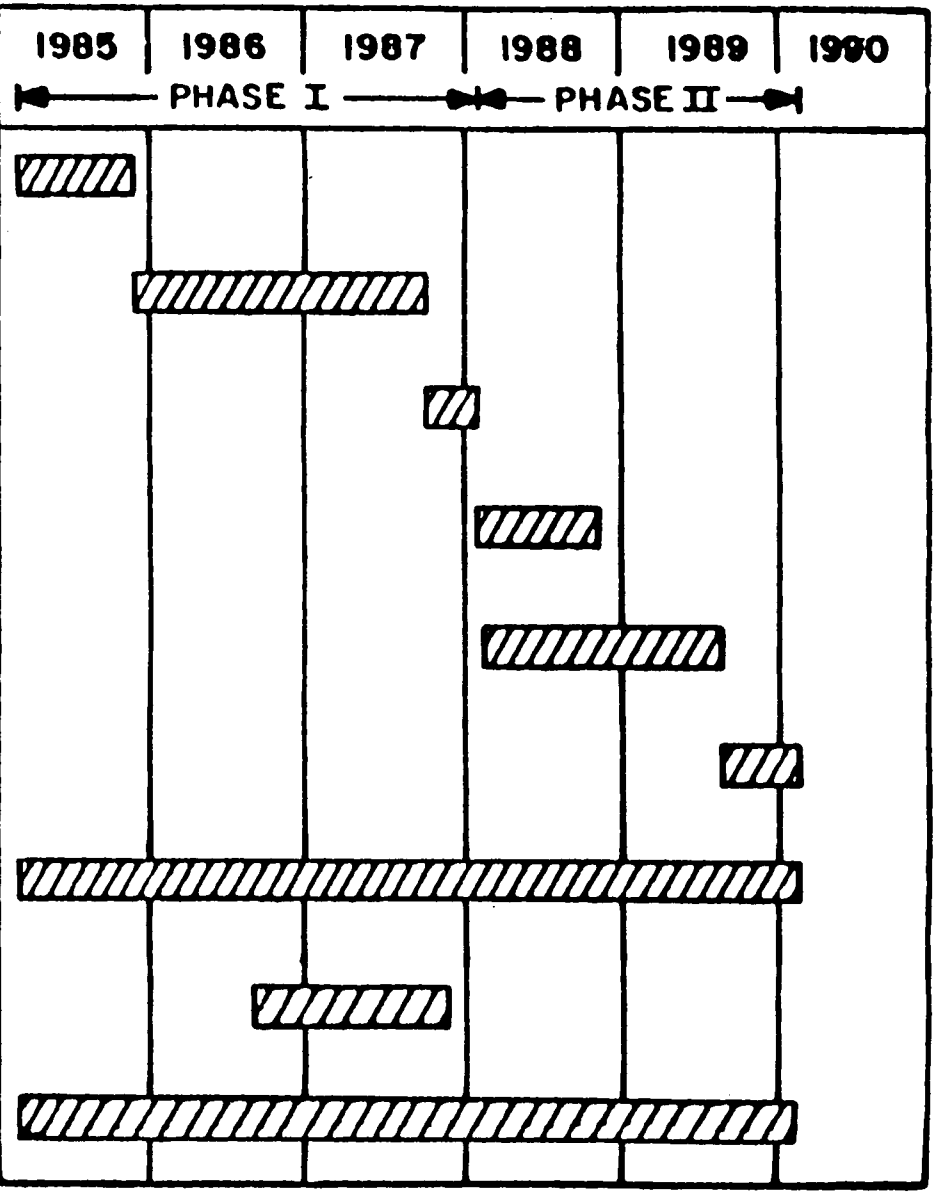

Fig. I-1 Timing Chart

Task VIII

Form a turbocharger rotor from the best material and process available in the last quarter of 1986 to supplement the findings of the other tasks with simpler shapes and to provide early data on the processing of a complex shape for Tasks IV, V, and VI. (Ford supports this task as a cost-sharing effort.)

Task I of Phase I has been completed and is reported along with results from Task VII studies in this annual report.

Phase II involves the fabrication, evaluation and optimization of a large shape that has potential application in a heat engine. This effort is divided into four tasks:

Task IV

Fabricate and characterize a large, complex part.

Task V

Use iterative, statistically designed studies to improve the properties of this large shape.

Task VI

Fabricate and evaluate the large complex shape developed in Task V.

Task VII

Conduct studies to develop advanced ceramic compositions and processing techniques.

Many process and material variables have been identified, and more than 20 of them have been studied during the first year of the program (results for 14 are included in this report). A similar number of variables will be evaluated in statistically designed experiments during the second year of the program. Variables related to powder processing in the mixing through dewaxing steps are being placed under statistical process control as well. Plans for Task II and Task VII in the coming year have been approved by NASA management.

EXPERIMENTAL WORK

Task I - BASELINE MATERIALS CHARACTERIZATION

The Ford baseline process was patterned after ceramic processing methods developed previously at Ford for injection molding other materials. The process involves the dry mixing of powders, adding a wax mixture to the powders, homogenizing with a high-shear mixer, injection molding to form test bars in a four-cavity mold, dewaxing in a vacuum furnace and sintering in a vacuum furnace. Six subtasks are considered for reporting and are listed as follows:

I.1. Characterization of Starting Materials

I.2. Preparation of Molding Mix, Injection Molding and Evaluation of Molded Test Bars

I.3. Dewaxing of Molded Bars

I.4. Sintering of Dewaxed Bars

I.5. MOR Characterization and Fractography

I.6. Process/Property Relationships

I.1. Characterization of Starting Materials

The chemical and physical characteristics of the various materials used in the baseline materials were evaluated. The materials tested included:

Beta Silicon Carbide Powder (Ibiden UF lot 0166)
Amorphous Boron (Starck lot S 3506)
Lampblack Carbon (Monsanto TL 246)

Chemical analyses were performed by Luvac Inc., Boylston Mass. Total carbon was determined by a combustion technique (Leco EC 12 system) in which the sample is heated with an induction coil in a stream of oxygen and the resultant CO_2 determined by an infra-red detector. The oxygen content was determined (Leco TZ 136) by heating the sample in a stream of He in a dc electric furnace to promote reaction with a graphite crucible; the resulting CO_2 is detected by I.R. Trace elements were detected by emission spectroscopy.

The data are given in Table I.1-I. The SiC has an oxygen content typical of ultra-fine particle size SiC material with a thin SiO_2 covering amounting to approximately 1.6 wt%. The carbon content is higher than stoichiometry, indicating the presence of about 0.7 % free carbon. The metallic constituents are present only in small amounts. The boron and carbon contain some oxygen, probably due to adsorbed moisture, and other impurities. However, since these sintering aids are used in small concentrations (1 to 2 wt%), they have only a minor affect on the composition of the sintered SiC.

The particle size distributions were determined by the Elzone electric sensing zone analytical technique (Particle Data Laboratories, Elmhurst Ill.). In this technique, particles are suspended in a conductive fluid which flows serially through an orifice under a differential pressure. Electrodes are immersed on each side of the orifice, and as each particle passes through the aperture, it replaces a volume of the liquid, momentarily changing the value of the resistance between the electrodes. This change produces a voltage pulse of short duration with a magnitude

proportional to particle volume. In an analysis, the series of pulses is electronically amplified, scaled and counted. The measurement of particle volume is the basis for these data, and a computer calculates the diameter of a sphere of equivalent volume.

The results are given in Table I.1-II. The particle diameter from the volume distribution is always larger than the diameter from the frequency distribution since the volume increases as a function of the diameter cubed. An interpretation of the data is complex since the size measure is influenced by the irregular surfaces and shapes of the particles. The median value is generally used as the estimate of particle diameter.

The particle size distributions are shown in Figure I.1-1.

Surface area determinations were made at Ford using the single point BET nitrogen absorption technique with a Quantachrome "Monosorb" analyzer (Quantachrome Inc., Norcross, Ga.). The data were:

Ibiden UF	SiC	Lot 0166	21.5 M^2/g
Starck	B	Lot S-3506	12.1 M^2/g
Monsanto	C	Lot TL-246	53.1 M^2/g

The high surface area and coarse mean particle diameter that characterize the carbon black indicate that the particles contain a large amount of internal porosity. This is characterisitc of an agglomerated powder.

Polytype analysis of silicon carbide was performed at Ford by X-ray diffraction analysis. Absolute intensities for the four principal SiC polytypes - 3C, 4H, 6H and 15R - were calculated using a single crystal analysis method developed by Ruska et al([1]). These intensities were then transformed into relative numbers proportional to the peak areas expected in a powder diffraction spectrum of the pure polytypes. Each diffraction

---

[1]. J. Ruska, L. Gauckler, J. Lorenz and H. V. Rexer, "the Quantitative Calculation of SiC Polytypes from Measurements of X-Ray Diffraction Peak Intensities," J. Mat. Sci. 14(8) 2013-2017 (1979).

TABLE I.1-I

POWDER COMPOSITIONS
(Weight %)

ELEMENT	UF-SiC	BORON	CARBON
C	30.41	0.36	98.6
O	0.85	1.71	1.12
Al	0.046	0.040	
Fe	0.043	0.17	<0.005
Ca	0.019	0.046	
Mg	0.015	0.55	
Ti	0.005	0.047	
Zr	0.005		
S			0.25

TABLE I.1-II

PARTICLE DIAMETER OF STARTING POWDERS

Statistical Property	Volume Dist. (micrometers)	Frequency Dist. (micrometers)
SiC		
Median	1.05	0.61
Mode	1.16	0.64
Geometric Mean	1.04	0.59
Arithmetic Mean	1.18	0.65
Boron		
Median	2.19	1.26
Mode	1.91	1.35
Geometric Mean	2.33	1.27
Arithmetic Mean	2.70	1.37
Carbon Black		
Median	7.04	0.29
Mode	11.17	0.17
Geometric Mean	5.62	0.34

Particle Size Distribution of Powders

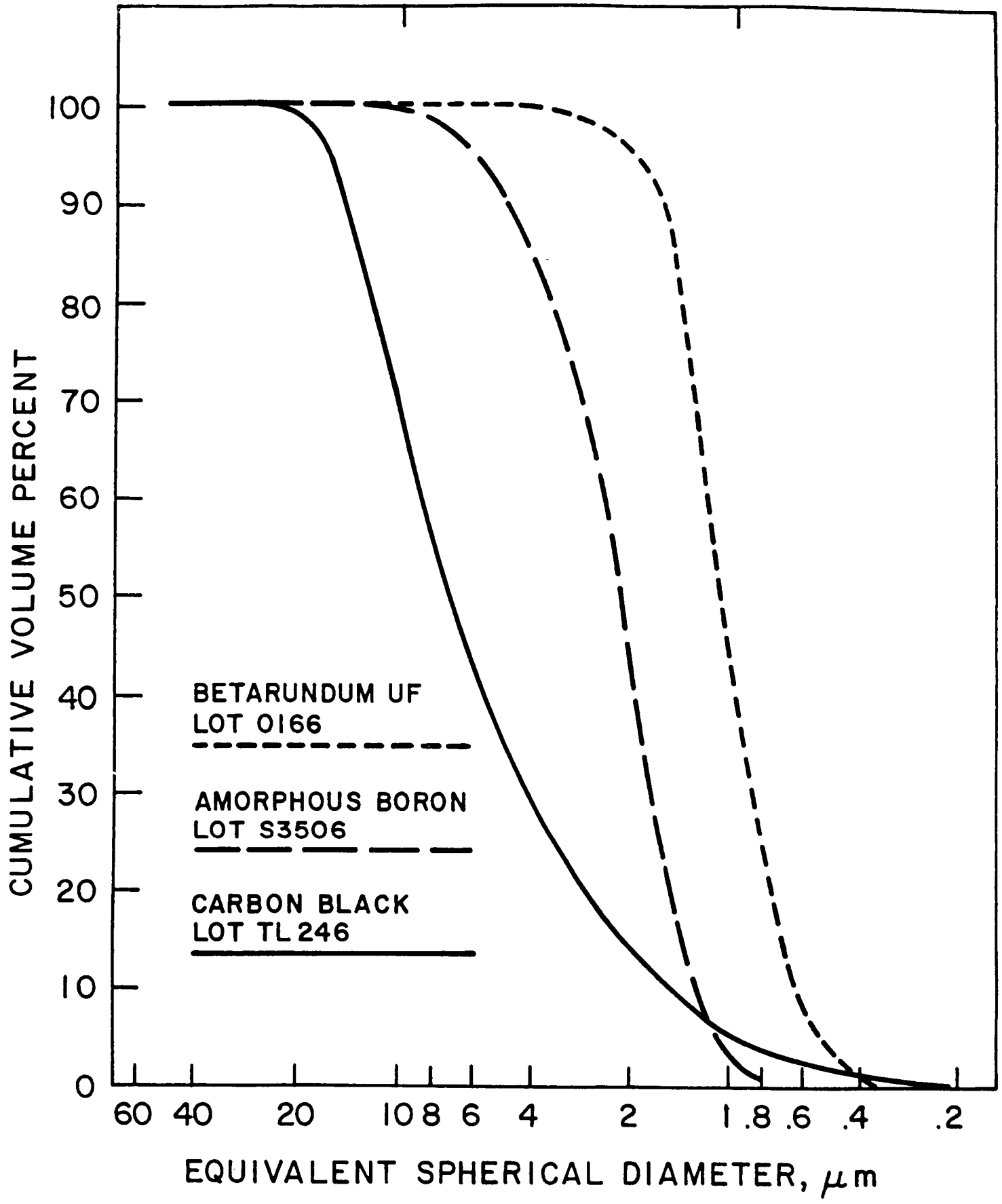

Fig. I.1-1

spectrum was automatically step-scanned using Cu Ka x-rays and a Philips vertical diffractometer equipped with a diffracted beam graphite monochrometer. The scanning parameters used were 2 Theta = 0.05^0, t = 15 sec. A total of eight peak areas, or observations ranging from 2.66 to 2.17 Angstroms, was used to calculate the relative volume fractions of the four polytypes and any poorly crystallized, disordered material. Next, the spectrum, stored on magnetic disk, was evaluated with a least squares peak fitting program to obtain the peak areas assuming a linear background and Lorentzian peak shapes. The volume fractions of the SiC polytypes were calculated from these peak areas.

The polyphase data show that the SiC powder is primarily 3C (cubic) phase (85%) with the remaining amount determined to be a disordered phase with no clearcut X-ray pattern.

The morphology of the beta-SiC powder is shown in the SEM micrographs of Figure I.1-2. In general, the particles are equiaxed and rounded, with a few grains showing well defined cleavage faces. As shown, a significant fraction of the particles is under one micrometer in diameter, and the grain size distribution is narrow.

The properties of the thermoplastic binders used to provide moldability during the injection molding process were evaluated by thermal gravimetric analysis (TGA) and differential scanning calorimetry (DSC). The progressive weight changes as measured by TGA occur when the material is heated at a controlled rate in specific environments. DSC measures heat absorption or evolution during the heating process and provides information on phase transformations.

The TGA curves, Figure I.1-3, are dominated by the weight losses of the major component which vaporize in argon in the 224-305°C range. The most rapid evolution occurs at 272°C. A minor inflection in the rate curve (dotted) at about 350°C is related to the loss of a secondary binder. The weight losses are significantly affected by the atmosphere. The use of vacuum heating lowers the temperatures of vaporization by 70-85°C.

Morphology of Betarundum UF

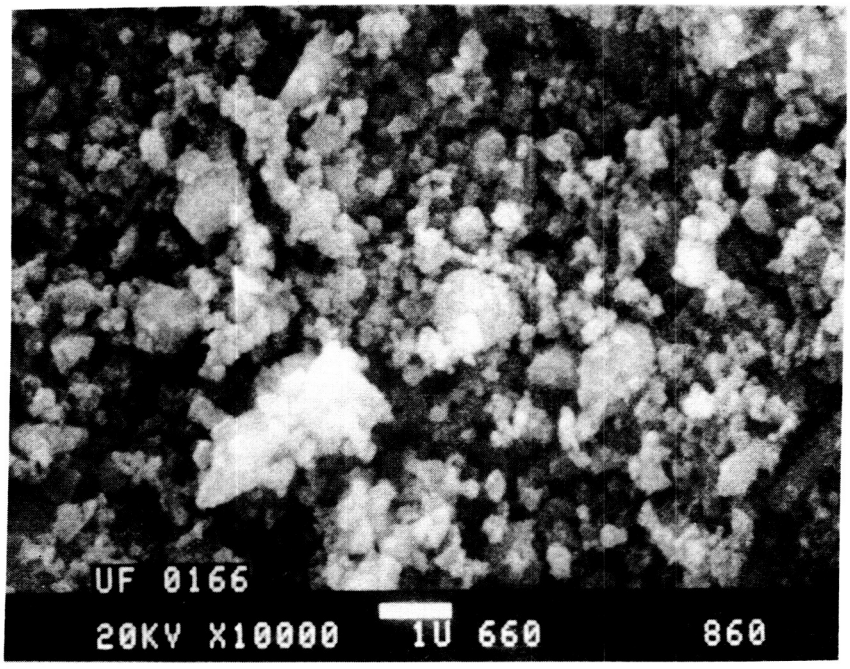

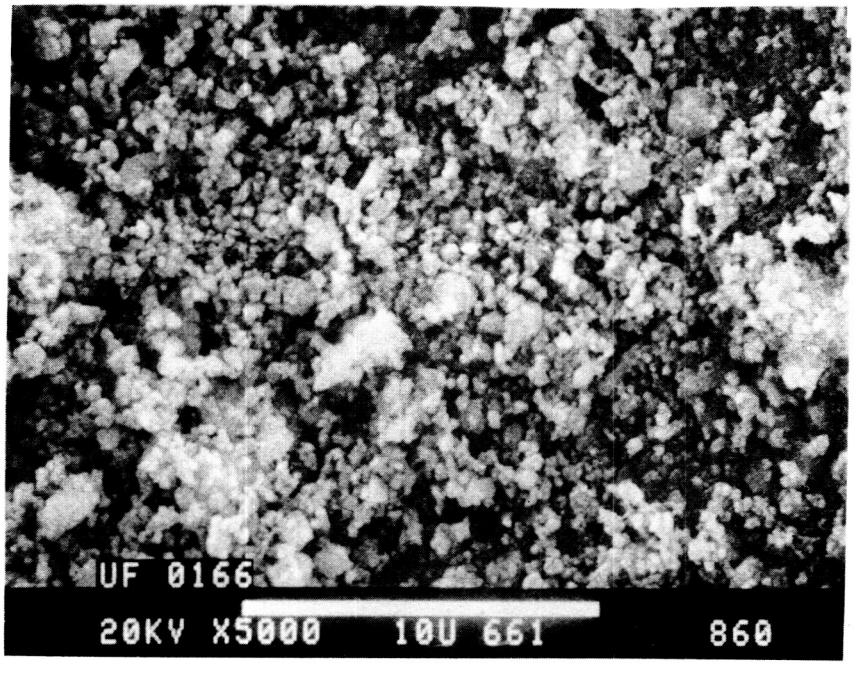

Fig. I.1-2

THERMOGRAVIMETRIC ANALYSIS
VACUUM 8 mm Hg
BASELINE WAX

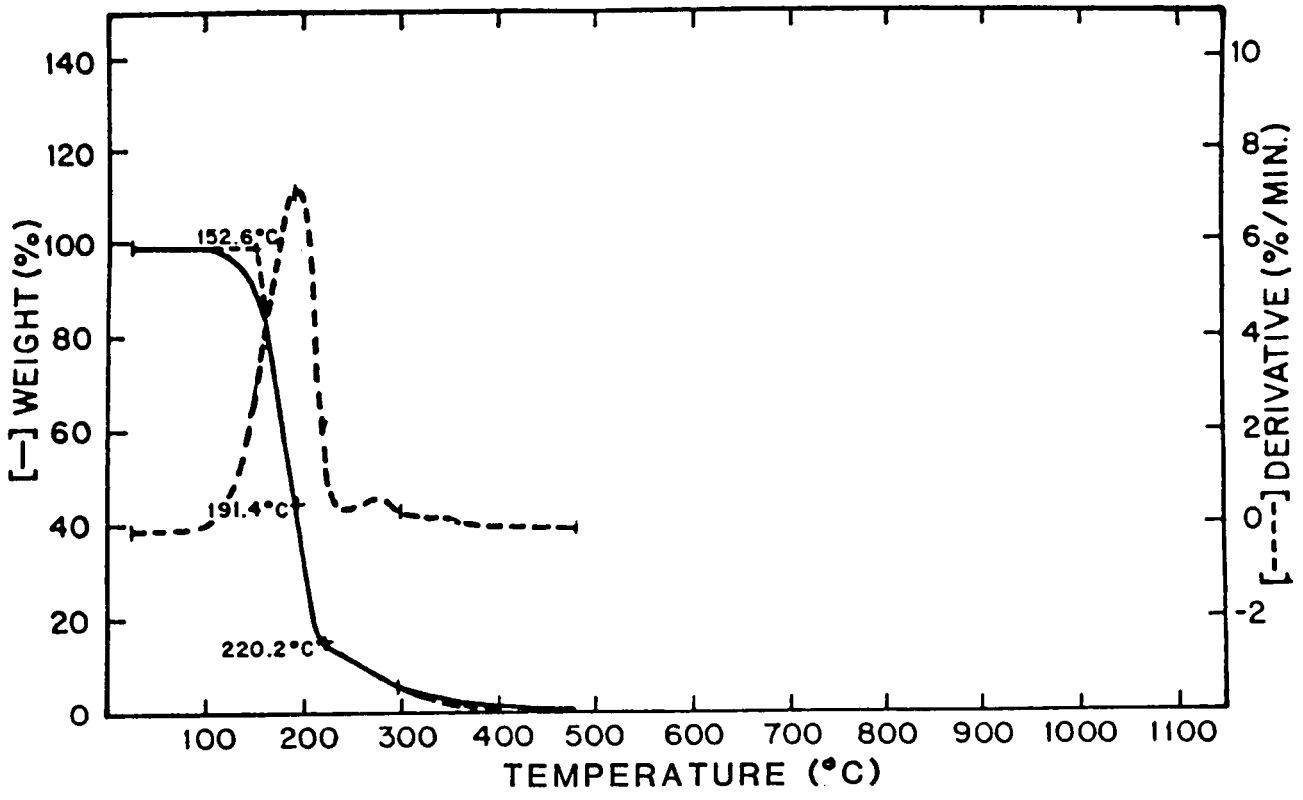

ARGON 100 ML/MIN.
BASELINE WAX

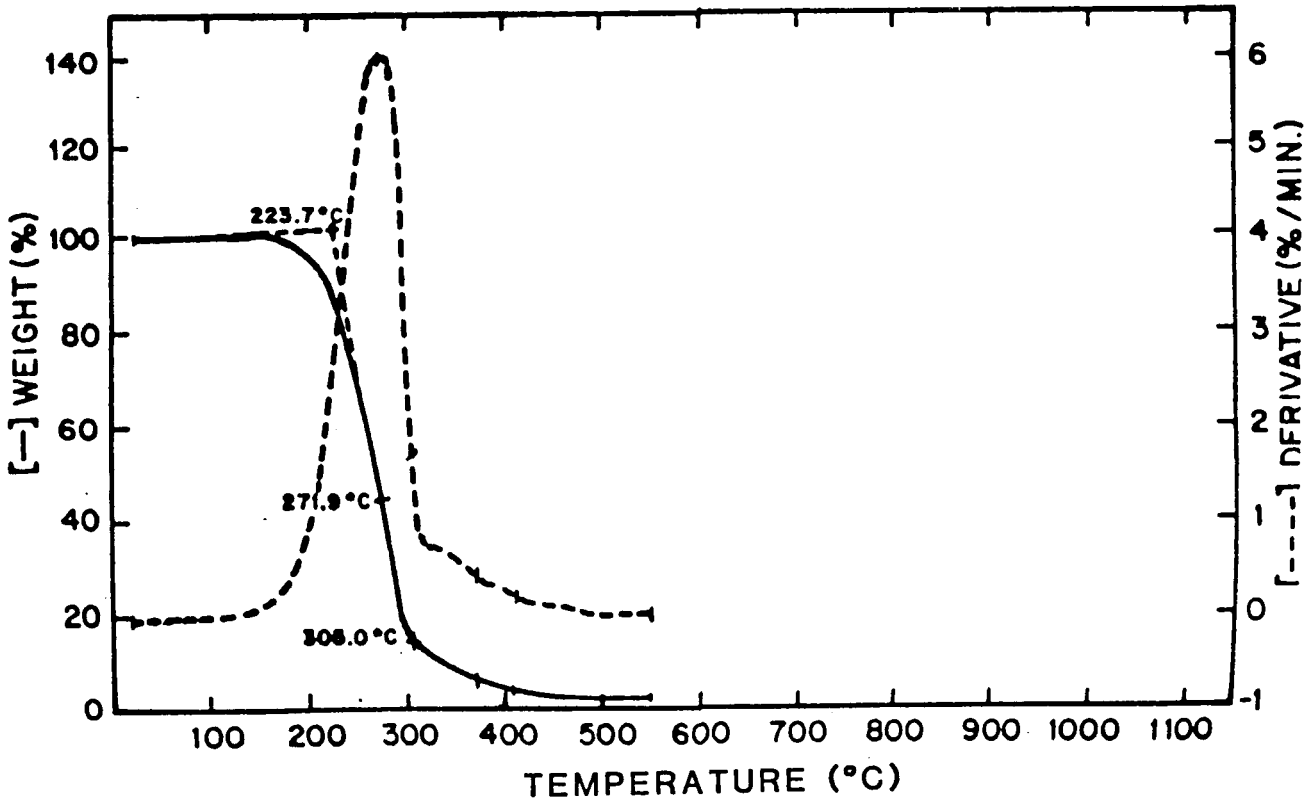

Fig. I.1-3

The DSC curve, Figure I.1-4, shows glass transition and the melting points of the major constituent at 35° and 56°C, respectively. The secondary binder is more refractory, melting at about 75°C, and the lubricant melts at about 108°C.

I.2. Preparation of Molding Mix, Injection Molding, and Evaluation of Molded Test Bars

The most promising composition evaluated in Task VII, Matrix 1, was selected for the baseline and designated as NASA 4G. It consisted of Betarundum UF SiC powder with additions of 2.0 % carbon black and 1.0 % amorphous boron as sintering aids. A solids loading of 55.5 % by volume and 44.5 % binder was employed. The processing steps were:

1. Dry mixing of SiC powder and sintering aids using a V-blender

2. Blending of powders with molten binders in a heated double planetary mixer to produce a thermoplastic moldable mix

3. Homogenization of the warm mix in a high-shear Haake mill[2].

4. Reheating mix under agitation and injection molding test bars

Examination of the blended mix (step 2) disclosed the presence of inhomogeneities of light gray color and rounded or oval shape. Step 3 was introduced in order to improve homogeneity.

To provide sufficient volume of baseline material for molding trials and test bar production, four thousand grams of the blended mix (step 2) were processed through the Haake mill in 32 batches. Samples were taken from each batch and inspected in the optical microscope at 100X magnification

[2]The Haake mill consists of two counter rotating, triangular rolls with rounded apexes and a 90° axial twist; the rolls can be adjusted to provide a narrow gap which produces a high intensity shearing action as the mix passes between the rolls.

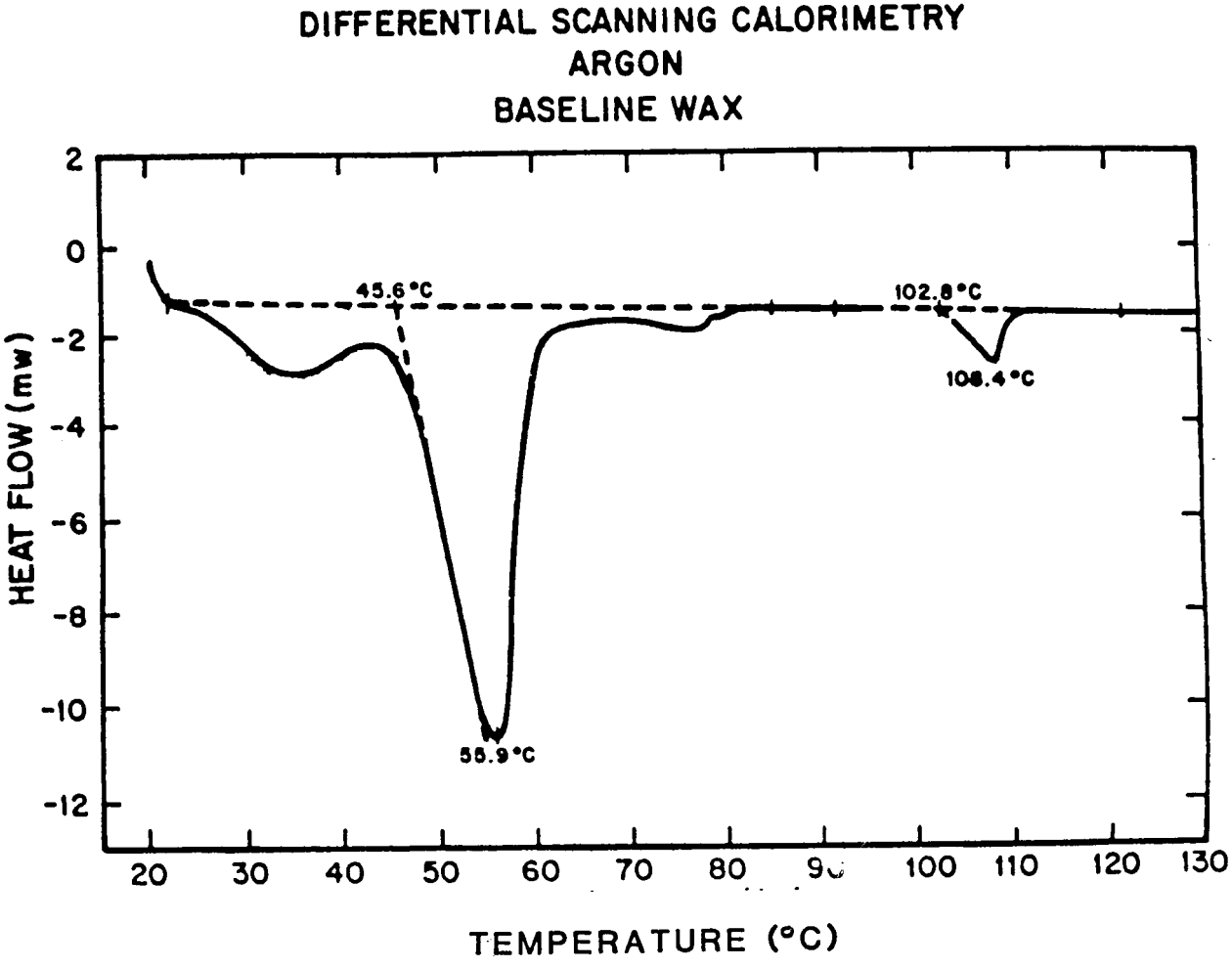
DIFFERENTIAL SCANNING CALORIMETRY
ARGON
BASELINE WAX
HEAT FLOW (mw)
2
0
-2
-4
-6
-8
-10
-12
45.6°C
55.9°C
102.8°C
108.4°C
20
30
40
50
60
70
80
100
110
120
130
TEMPERATURE (°C)

Fig. I.1-4

for inhomogeneities which were quantified by size and frequency. The most prevalent type of inhomogeneity observed was a rounded to oval shaped gray area, typically 25-75 micrometers in diameter and numbering about 12 per square millimeter. Occasional red spots were noted as well. Representative fracture surfaces of the mixes are shown in Figure I.2-1 under polarized light at 100X magnification. The effectiveness of the high-shear remixing is evaluated by comparing the initially blended mix, step 2, and the homogenized mix, step 3. The relationship between the defects (agglomerates) noted at this stage of processing with failure origins is considered in Section I.5.

The process of high shear mixing was evaluated by assessing agglomerate size using statistical process control charts as shown in Figure I.2-2. The parameter under control is the maximum agglomerate size. All the data fall within the upper and lower statistical control limits which indicates that the high-shear mixing process is under control. A summary of the process control parameters applied in the mixing and molding of the baseline bars is shown in Table I.2-I.

The statistical process control chart for the molding process is shown in Figure I.2-3. The plotted points are an average (or range) of four samples shot consecutively. In this case, the molded density is the control parameter; and as shown, two observations fall on the lower control limit. X-ray inspection of these bars indicated that large voids were present. The problem was corrected when a small air leak in the delivery tube on the molder was detected and repaired.

I.3. Dewaxing of Molded Bars

Dewaxing of the baseline bars was carried out in a vacuum dewaxing facility which was controlled and monitored for pressure, temperature and rate of temperature change. For dewaxing, the bars were packed in coarse particles of carbon contained in four saggers, each of which contained three layers of bars. Saggers 1 and 2 (top) were stacked at the rear of the furnace and saggers 3 and 4 (top) were stacked at the front of the

Optical Photomicrographs of Batch Materials

Polarized Light, 100 X

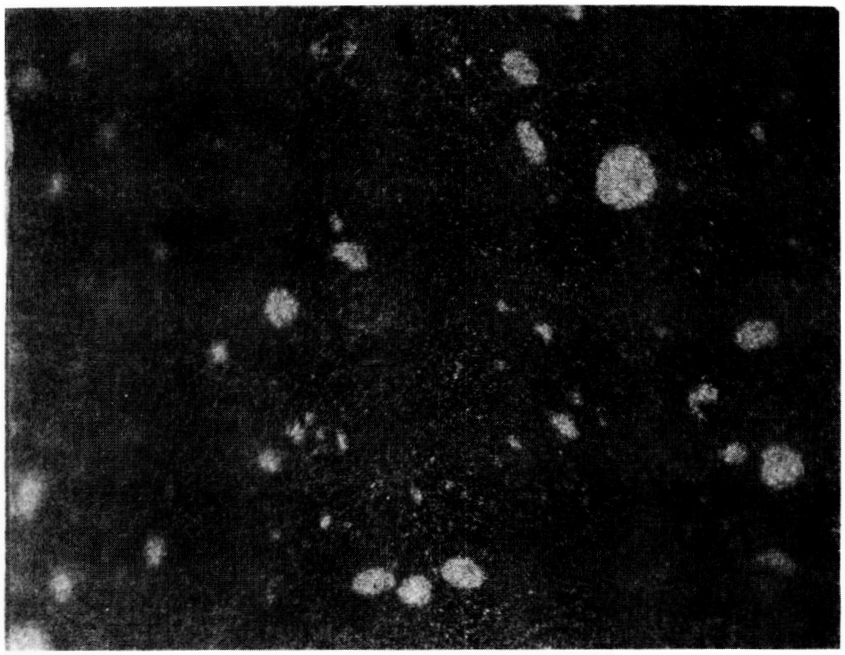

After Initial Blending (Step 2)

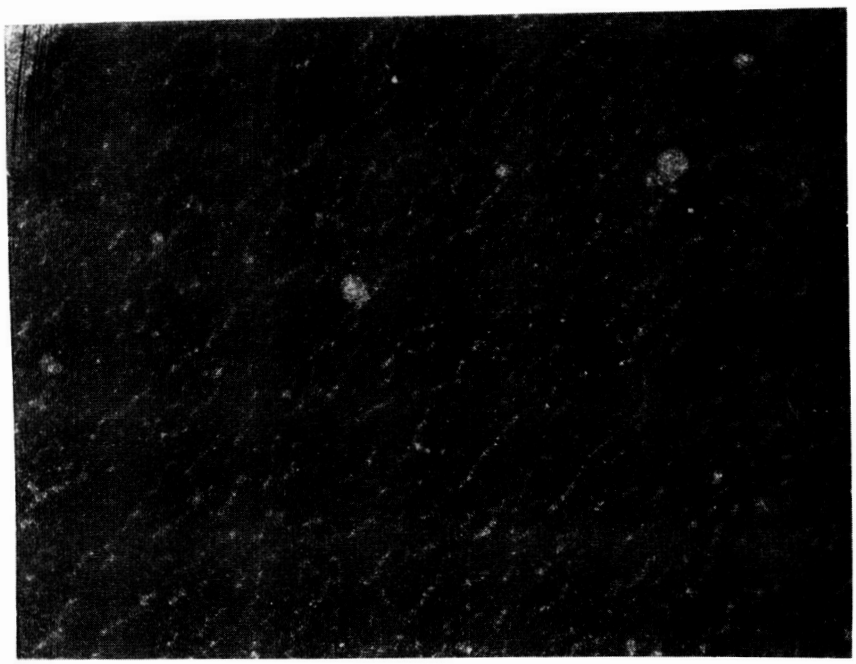

After Haake Mill Homogenization (Step 3)

Fig. I.2-1

STATISTICAL PROCESS CONTROL CHART
HIGH SHEAR MIXING PROCESS

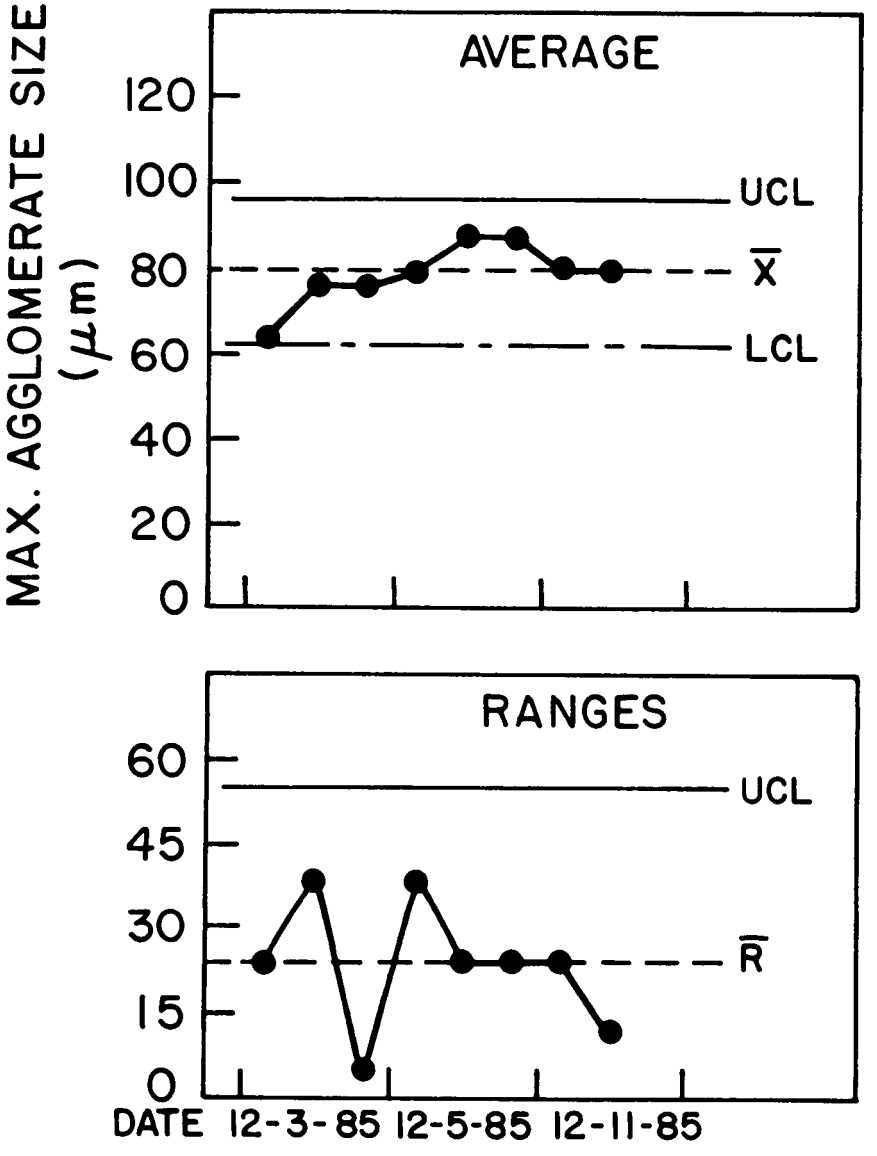

EACH POINT IS AVERAGE OR RANGE
OF FOUR SAMPLES

Fig. I.2-2

TABLE I.2-I

PROCESS CONTROL PARAMETERS

MOLDING MIX/TEST BARS

MOLDING MIX:

PROCESS	SAMPLES	QUALITY CHECK
FORMULATION	---	BATCH NO. DEFINES COMPOSITION RECORD LOT NOS. AND AMOUNTS OF ALL INGREDIENTS
BLENDING	3/BATCH	RETAINED FOR RECORDS
MIXING (LO SHEAR)	3(MELT)	X-RAY
	5(MELT)	VISUAL @ 100X[1]
	10(GRANULATED)	VISUAL @ 100X
MIXING (HI SHEAR)	1(BATCH)	VISUAL @ 100X

TEST BARS

MOLDED	100%	SERIALIZED[2]
	100%	WEIGHT : LENGTH
	100%	VISUAL
	100%	X-RAY
	25%	DENSITY
	RANDOM	VISUAL @ 100%

1 VISUAL @ 100X OF FRACTURE SURFACE EXAMINED FOR INHOMOGENEITIES

2 SERIALIZED SEQUENTIALLY...IDENTIFIES SHOT NUMBER, CAVITY NUMBER, DATE, EQUIPMENT, OPERATOR, MATERIAL, CONDITIONS...

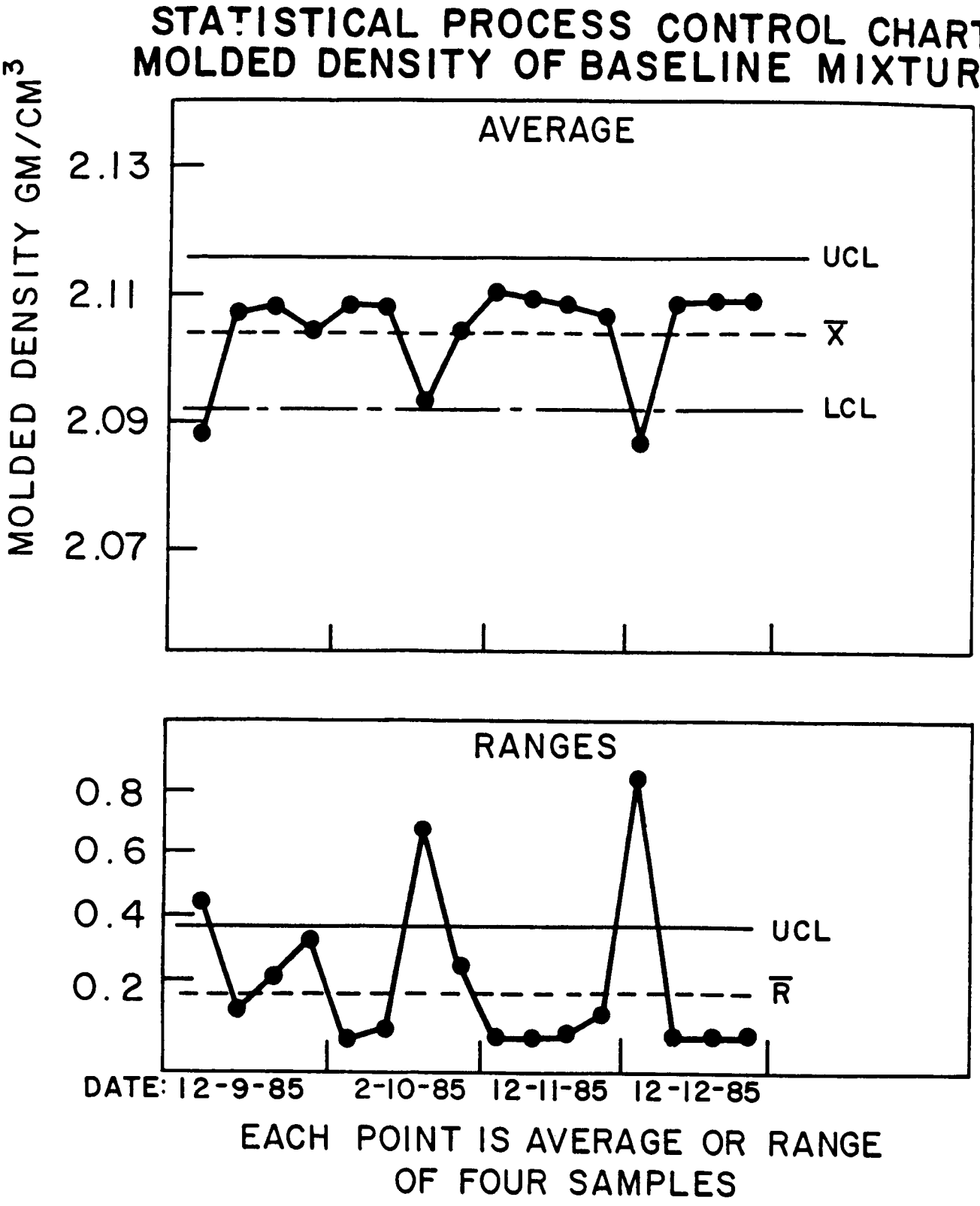
STATISTICAL PROCESS CONTROL CHART
MOLDED DENSITY OF BASELINE MIXTURE
MOLDED DENSITY GM/CM3
AVERAGE
2.13
2.11
2.09
2.07
UCL
X̄
LCL
RANGES
0.8
0.6
0.4
0.2
UCL
R̄
DATE: 12-9-85
2-10-85
12-11-85
12-12-85
EACH POINT IS AVERAGE OR RANGE
OF FOUR SAMPLES

Fig. I.2-3.

furnace. A single run was used to dewax 127 bars.

Following dewaxing, the M.O.R. bars were measured for warpage (100 % inspection), density (100 %), percent binder removal (100 %), and shrinkage (25 %).

Some warpage was observed in the dewaxed bars, and the position of the bars within the dewaxing furnace and the influence of mold cavity were examined as possible factors. The mean values of the amount of warpage (measured as the maximum deviation of a test bar face from a flat surface) due to dewaxing are listed in Table I.3-I. It can be seen that very low warpage was measured for the first layer in saggers 1, 2, and 3, and much larger warpage was observed in the second and third layers. In sagger 4, layers 1 and 2 showed more warpage than layer 3. A statistical analysis of these data was performed and results are given in Table I.3-II. In comparing the four saggers, no statistically significant differences were detected. When the layers were compared for all the saggers, it was found that layer 1 is statistically different from layers 2 and 3.

Another correlation was found between warpage and the location of the cavity in the four-cavity mold (cooling circuit in only one side) that was used in forming the bar. This correlation was independent of the sagger effect described above. It was found that at the .05 probability level, cavity 1 produced bars with significantly greater tendency for warpage than cavity 2 or 4. This effect is probably due to a small, steady increase in mold temperature that occurs as the mold cavities are filled. The mold cavity filling sequence is 1 - 3 - 2 - 4. A $3^{0}C$ increase in mold temperature during the filling of cavities 2 and 4 above the mold temperature during the filling of cavity 1, is believed to account for higher strain in bars from cavity 1 and the greater warpage in the bars molded in that cavity. Adjustments have been made in the cooling circuit of the mold to alleviate the problem.

The amount of binder removed from the bars during dewaxing was found to

TABLE I.3-I

MEAN VALUES OF WARPAGE

DURING DEWAXING OF BASELINE MOR BARS
(Units of 0.001 inches)

SAGGER NUMBER	LAYER NUMBERS 1	2	3
1	0.1*	1.8	3.0
2	0.5	2.3	3.8
3	0.9	3.7	3.7
4	2.1	2.1	0.3

Overall Mean = 1.94

TABLE I.3-II

STATISTICAL ANALYSIS OF

SIGNIFICANT DIFFERENCES IN WARPAGE

DURING DEWAXING AS A FUNCTION

OF POSITION IN FURNACE

COMPARISON BETWEEN SAGGERS

1 vs 2	2 vs 3	3 vs 4	1 vs 3	2 vs 4	1 vs 4
No	No	No	No	No	No

COMPARISON BETWEEN LAYERS

1 vs 2	2 vs 3	1 vs 3
Yes .005*	No	Yes .001

* Probability of Significance from Student's t Test

vary significantly as a function of position within the furnace, the length of time the heated mix was in the molder where vaporization could occur, and the molded density. Future dewaxing runs will be loaded in a random order so that these effects can be studied independently.

The shrinkage of the baseline material (NASA 4G) during dewaxing is considerably larger than that normally observed in injection-molded bars. Table I.3-III contains data on the mean linear shrinkage of NASA 4 compositions processed under different conditions and at several solids loading levels. As indicated, solids loading has a minor effect on shrinkage while processing under high shear conditions (hot-roll milling or Haake milling) results in significantly higher shrinkages. The fluid-mixing process, discussed in Section VII.5, results in low shrinkage which is believed to be more desireable for large, complex-shaped parts.

I.4. The Sintering Process

Sintering of the baseline bars was carried out in vacuum at 2100^{0}C for 10 minutes in 3 sintering runs. The as-sintered test bars were inspected visually and by x-ray and the densities determined. The average densities of the bars before and after machining are given in Table I.4-I. The results illustrate the uniformity and reproducibility of the three sintering runs. An SPC chart, generated by plotting the average density of five groups of bars randomly selected (four bars per group) from each sintering run, is given in Figure I.4-1. The chart indicates the sintering process is under control.

TABLE I.3-III

SHRINKAGE DURING DEWAXING

NASA 4 COMPOSITIONS

DEWAX # 011886

NO.	PROCESS	SOLIDS LOADING %	MEAN LINEAR SHRINK %
NASA 4 A	Dry Mixed	55.5	0.20
		58.5	-0.08
		61.5	-0.10
NASA 4B	Hot Roll Milled	55.5	2.08
NASA 4G BASELINE	Haake Milled	55.5	3.89
NASA 4E	Fluid Mixed	57.5	0.18

(- = Expansion)

TABLE I.4-I

BULK DENSITY DATA FOR BASELINE RUNS

SINTER RUN	NO.	AS SINTERED			AFTER MACHINING		
		Density (g/cc)	ST. DEV.	%T.D.*	Density (g/cc)	ST. DEV.	%T.D.*
V26	47	2.991	0.019	94.4	3.033	0.023	95.7
V27	48	2.981	0.021	94.0	3.012	0.011	95.0
V29	27	2.989	0.014	94.3	3.031	0.014	95.6

* Based on density of 3.17 for fully dense material

STATISTICAL PROCESS CONTROL CHART
BASELINE SINTERING PROCESS

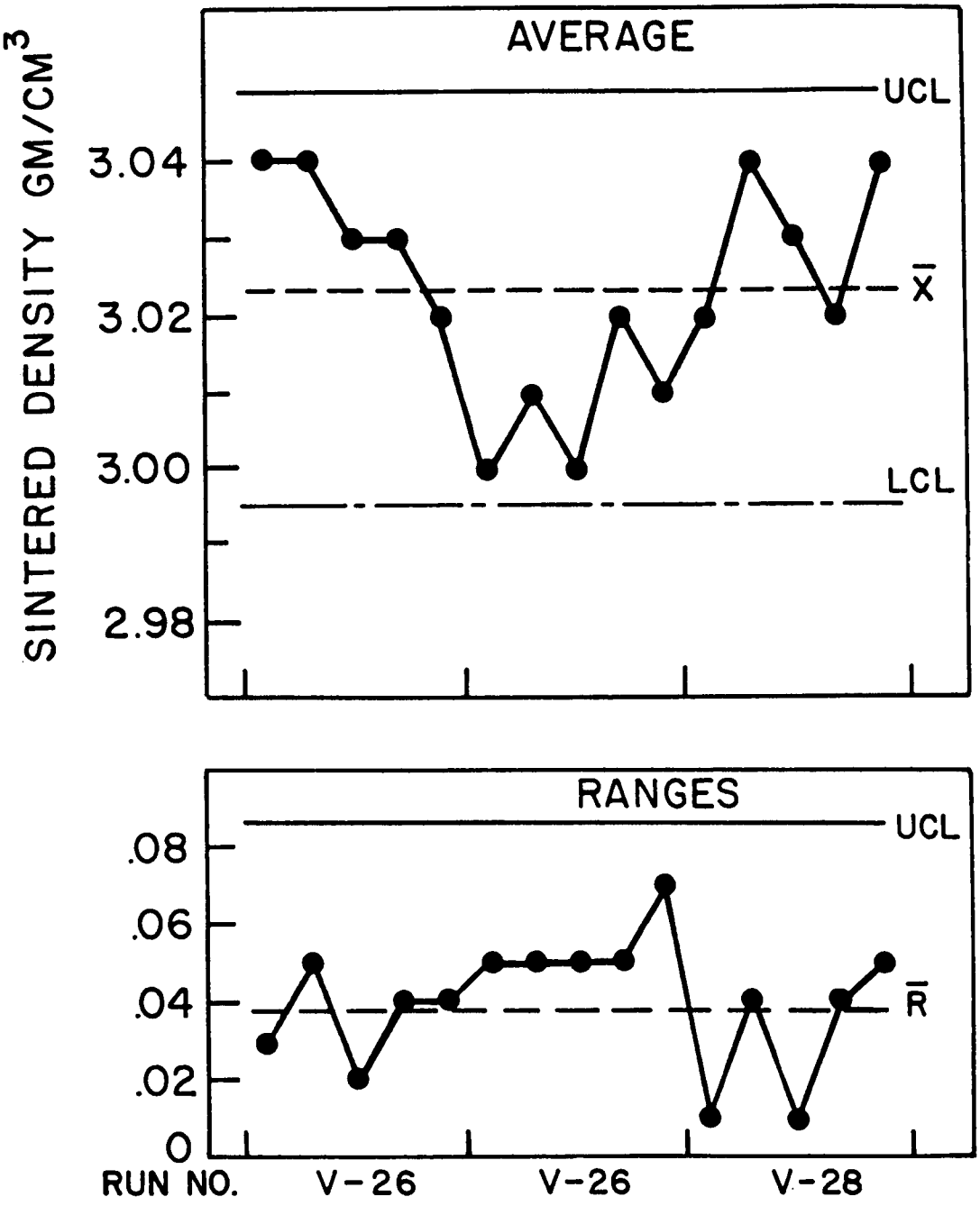

EACH POINT IS AVERAGE OR RANGE
OF FOUR SAMPLES

Fig. I.4-1

I.5. Characterization and Evaluation of Baseline Specimens

I.5.1. Composition and Microstructure

Chemical analysis of the sintered test bars indicates that vacuum sintering very effectively reduces the oxygen content to a low level, Table I.5.1-I. The higher carbon content is a reflection of the 2 wt% carbon black added as sintering aid. The increased concentration of the metallic elements, Cr, Ni, and Fe reflects the pick-up of metallic particles during processing. The origin of the metal pick-up has been traced to a granulation of the mix prior to molding during baseline processing. The structural effects of these metallic inclusions after the sintering process are considered in Section I.6.2.

A cross section of an unmachined, baseline MOR bar is shown in Figure I.5.1-1. The unetched microstructure of the bar is uniform except for a dark appearing surface layer approximately ten micrometers thick which is visible at the bottom of the photograph. There is a random distribution of generally rounded low density inclusions with sizes up to 80 micrometers which are believed to be related to the gray spots noted in the green bodies.

An electrolytic etch (KOH solution) of the polished surface was used to enhance the grain structure as shown in Figure I.5.1-2(a). A grain size of 6 micrometers is typical, and the pores are small and evenly distributed. No evidence was found of the needle or feather type structure that characterizes an over sintered material. The inclusions were visible as highly reflective regions, Figure I.5.1-2(b), with more porosity and grain growth than in the surrounding material.

The as-etched microstructure adjacent to the surface is shown in the optical micrograph in Figure I.5.1-3(a). There is some evidence of volatilization in this zone when the structure with small irregular crystals is compared with the more equiaxed crystals of the interior region. The surface zone is clearly resolved with the SEM as shown in the micrograph of the fracture surface, Figure I.5.1-3(b). The dark zone is

TABLE I.5.1-I

CHEMICAL COMPOSITION - SINTERED BASELINE MOR BARS

	Starting Powder (0166)	Sintered Bar (Sample 1140)
O	0.95	0.006
C	29.5	30.3
Ni		0.052
Cu		0.007
Fe	0.043	0.208
Co		0.025
Al	0.046	0.024
Ca	0.019	<0.002
Cr		0.009
Mg	0.015	<0.002

Microstructure of Sintered Unmachined Baseline Specimen

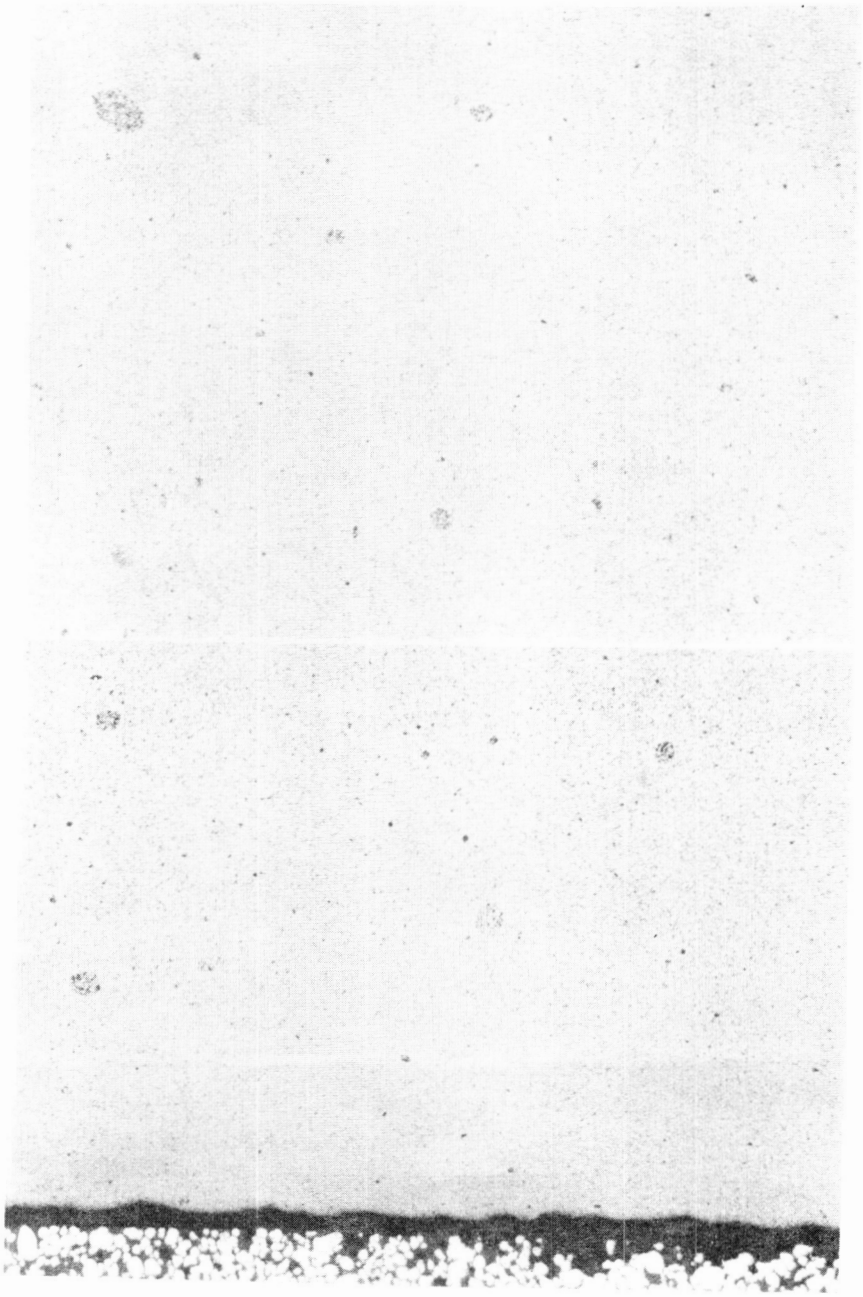

Fig. I.5.1-1

Microstructure of Sintered Unmachined Baseline Specimen

Electrolytic KOH etch

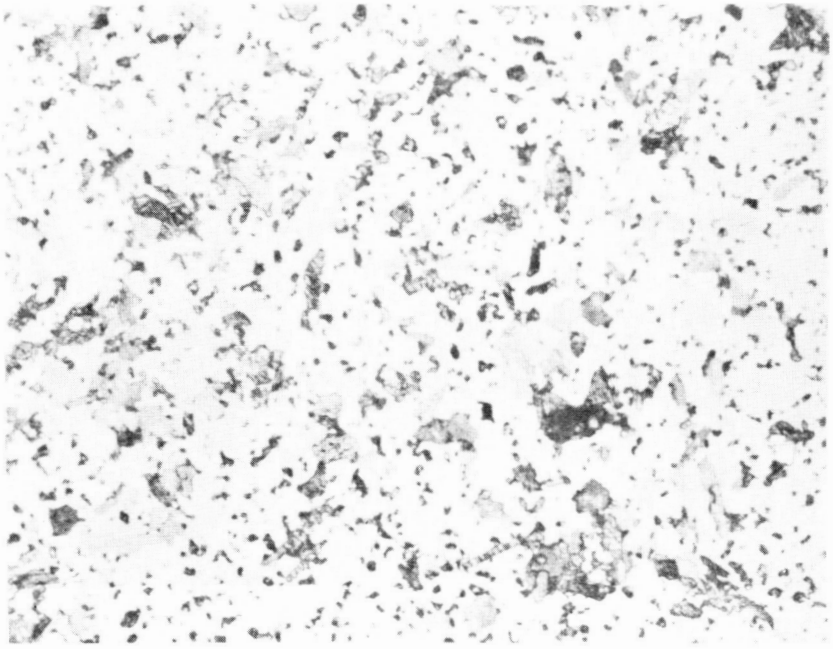

(a) Overall microstructure of interior of bar

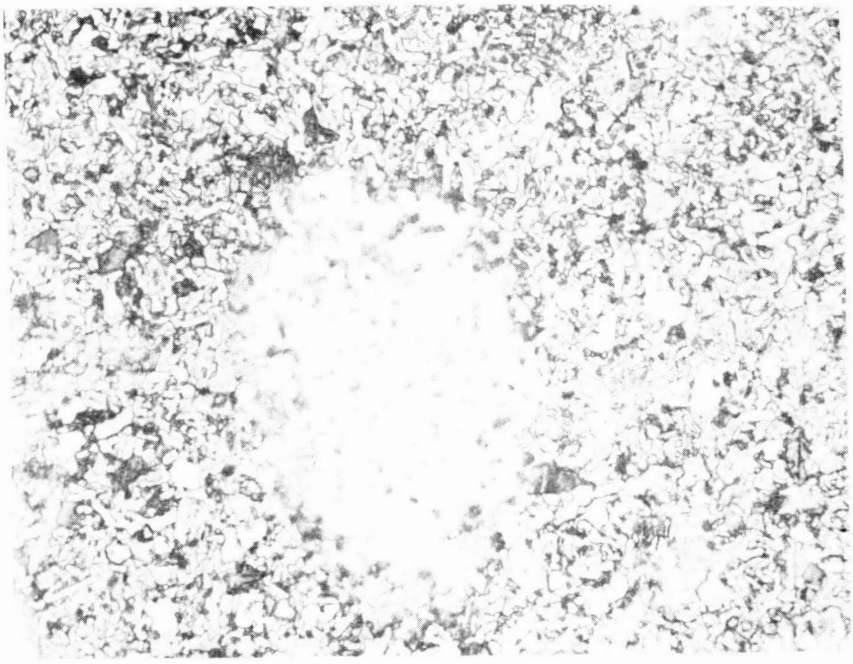

(b) Typical inclusion

Fig. I.5.1-2

Microstructure of Sintered Unmachined Baseline Specimen

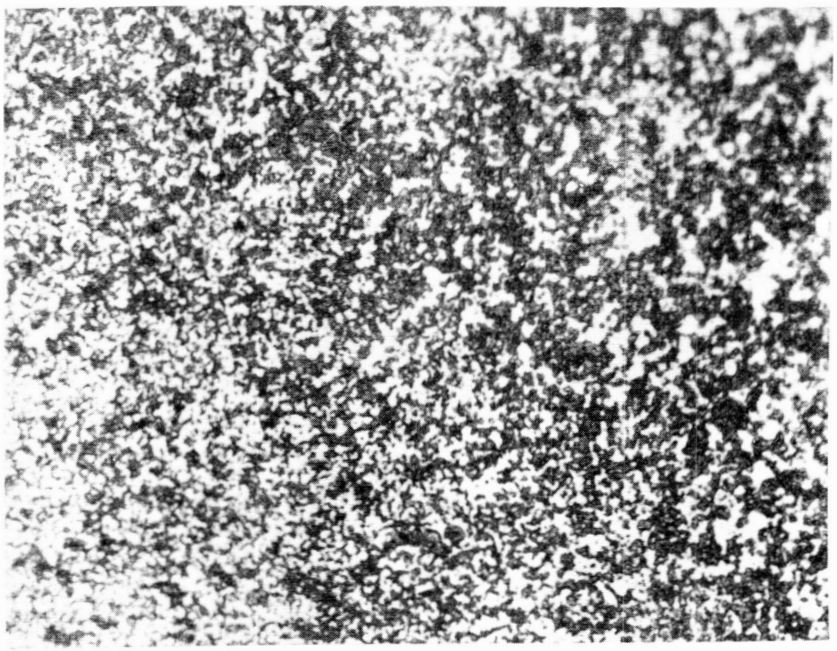

(a) Edge of bar showing surface deterioration

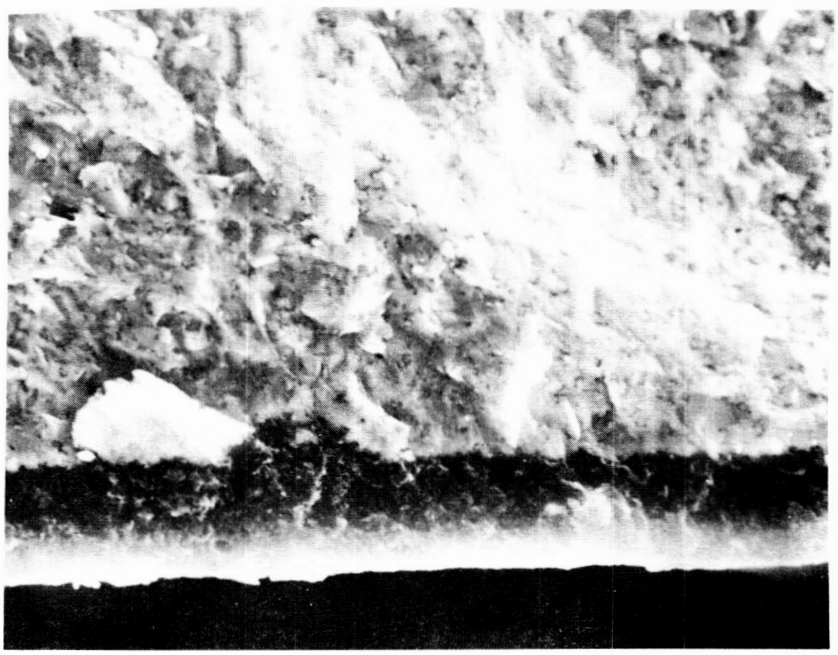

(b) S.E.M. micrograph showing surface modification

Fig. I.5.1-3

approximately 15 micrometers thick in this area and is assumed to be related to the volatization occurring during vacuum sintering.

I.5.2. Phase Composition

A quantitative x-ray diffraction analysis was made on a sintered, unmachined baseline bar. The phase distribution data obtained from a crushed sample (- 44 microns) are given in Figure I.5.2-1: 52.9 % crystallized beta SiC (3C) and structurally undefined components (47.1 %). The figure illustrates the working curves derived from the digital recordings of x-ray peak areas as a function of the diffraction angle. The unidentified structure is attributed to highly faulted, disordered crystallites which do not yield analyzable peaks; this structure is stable to 2100°C. There is close agreement with the analysis of dry pressed SiC based on this composition reported by Williams et al.[3]

I.5.3. Mechanical Testing

The sintered test bars which passed x-ray and visual inspection were machined to parallelepipeds approximately 9.8 x 4.9 x 51 mm by diamond grinding and were chamfered parallel to the long axis of the bar. All surfaces, except for the ends, had a 10 micro-inch finish or better. The room temperature testing was done on an Instron testing machine with a crosshead speed of 0.5 mm/min., using a four-point test fixture of 20 mm upper span and 40 mm lower span. All of the machined test bars were x-rayed and specimens with gross flaws within the center inch were discarded. Test bars were selected from the available specimens of each baseline run in proportion to the number sintered in the run. A total of 30 specimens were selected for room temperature testing, 18 for elevated temperature testing, and 10 for stress rupture evaluation at elevated temperature.

The baseline MOR data are summarized in Table I.5.3-I. The room

[3] R. Williams, B. Juterbock, S. Shinozaki, C. Peters and T. Whalen, Bull. Am. Cer. Soc. 64(10) (1985) p. 1385.

WORKING DIAGRAM FOR QUANTITATIVE POLYTYPE ANALYSIS
OF BASELINE UNMACHINED SiC COMPOSITION

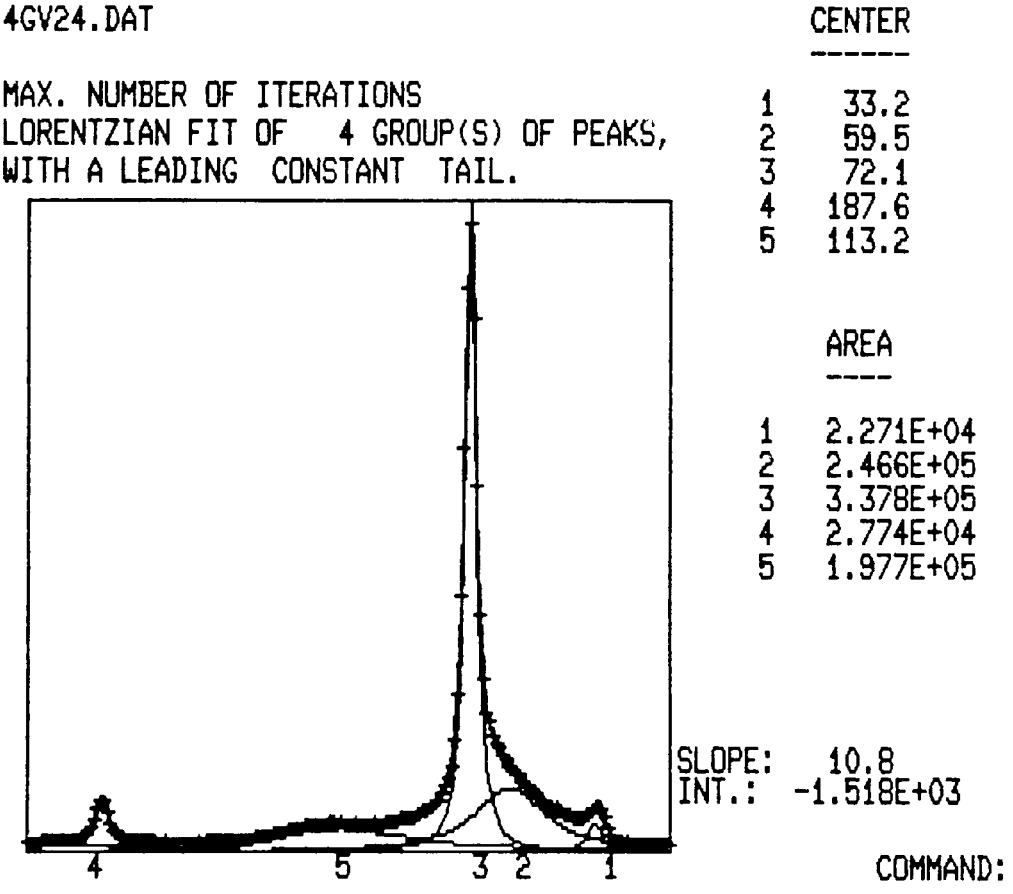

Well-characterized β-SiC (3C)	52.9%
Disordered, undifferentiated phases	47.1%

Fig. I.5.2-1

TABLE I.5.3-I

M.O.R. BASELINE RESULTS

		RT	1000°C	1200°C	1400°C
$\bar{\sigma}$	Ksi	45.8			
	mPa	(315)			
m		8.0			
X	Ksi	43.3	41.4	43.2	47.2
	mPa	(299)	(285)	(298)	(325)
n		30	6	6	6

temperature MOR results for the three baseline sintering runs are:

	Mean MOR Value (MPa)
V-26	298 (43.19 Ksi)
V-27	299 (43.38 Ksi)
V-29	300 (43.60 Ksi)

No significant difference in the MOR values for the three runs was found on the basis of the Student's t test which tests for significant differences in the means. A Weibull plot of the room temperature baseline data is given in Figure I.5.3-1. A detailed statistical analysis of some of the data is given Table I.5.3-II.

At room temperature, a mean MOR value of 299 MPa (43.3 ksi) and a Weibull characteristic value of 316 MPa (45.8 ksi) with a Weibull modulus of 8.0 were calculated.

The high temperature MOR data indicate a gradual increase in mean values of strength with increasing temperature. These mean MOR strengths are plotted in Figure I.5.3-2 as a function of test temperature, and a range of one standard deviation is shown above and below the plotted means as an indication of uncertainty. When the Student's t test was applied to the high temperature data, only the differences between the means at 1000^{o}_{C} and the means at 1400^{o}_{C} were significant, and then only at the 0.09 level of probability.

Flexural stress rupture measurements were made at $1400^{o}C$. Ten specimens were tested for durability under load at stresses of 172 and 207 MPa. Hot pressed SiC fixtures with an identical geometry to the fixtures used in room temperature tests were employed. The data reported in Figure I.5.3-III show the wide variation of life times found in the test. A significant decrease in durability occurs at the higher stress level. These characteristics are typical of a heterogeneous material and depend upon the location and size of the strength controlling flaws.

NUMBER OF SAMPLES = 30.00
WEIBULL CHARACTERISTIC VALUE = 316 MPa (45.8 Ksi)
WEIBULL SLOPE = 7.97
DISTRIBUTION MEAN = 297 MPa (43.1 Ksi)
STANDARD DEVIATION = 44 MPa (6.43 Ksi)

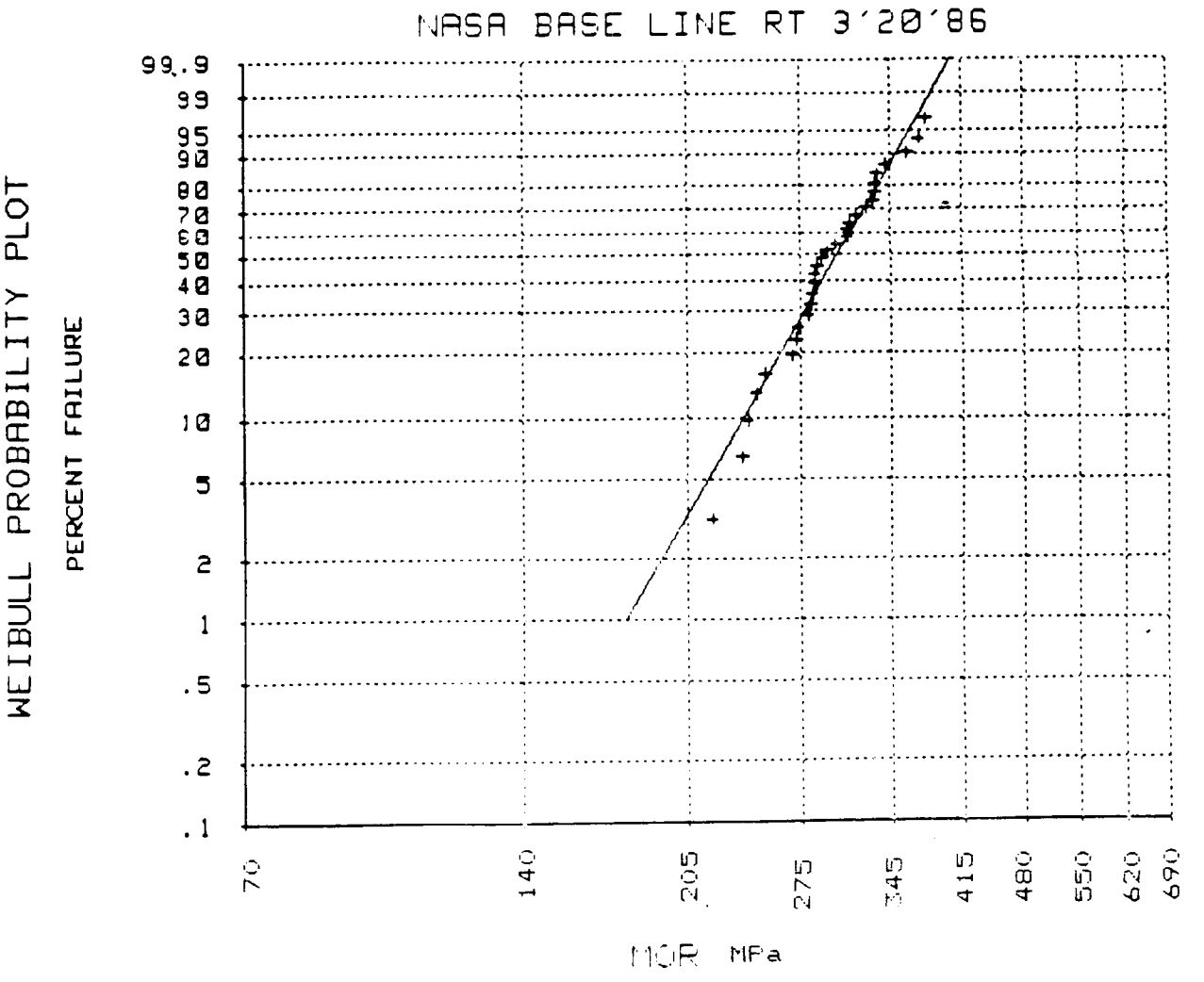

Fig. I.5-3-1

TABLE I.5.3-11

MOR BASELINE RESULTS

D E S C R I P T I V E S T A T I S T I C S

Mean	=	43.33
Median	=	42.48
MOR Has No Mode		
Variance	=	32.85
Std. Dev	=	5.732
Range	=	22.87
Minimum	=	31.95
Maximum	=	54.82
N	=	30

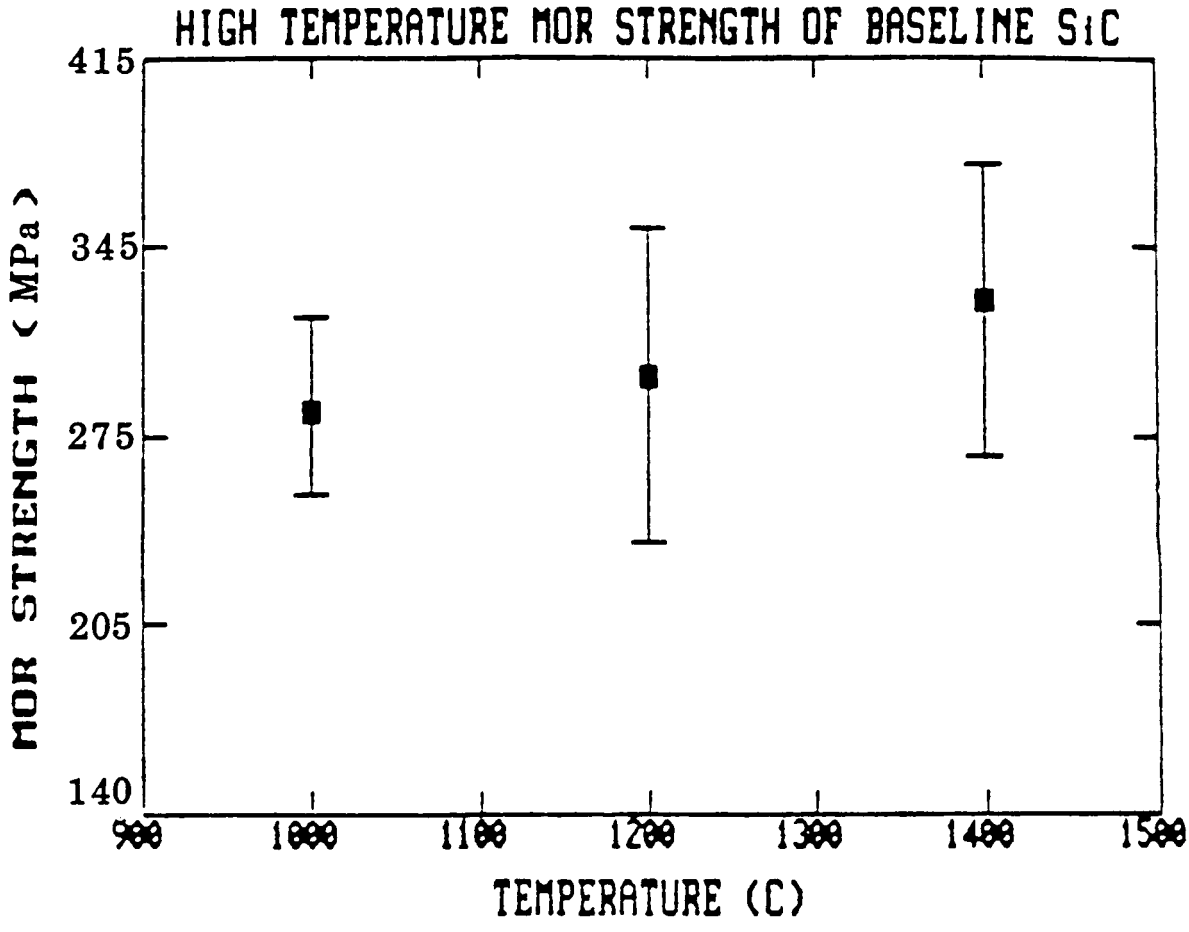
HIGH TEMPERATURE MOR STRENGTH OF BASELINE SiC
MOR STRENGTH (MPa)
415
345
275
205
140
900
1000
1100
1200
1300
1400
1500
TEMPERATURE (C)

Fig. I.5.3-2

TABLE I.5.3-III

FLEXURAL STRESS RUPTURE RESULTS FOR SINTERED SiC
(4G Database Specimens)

Test Temperature: 1400°C

Applied Stress (MPa)	Failure Time (h)
(25 Ksi)	
172	36
172	102
172	6
172	5
172	163
(30 Ksi	
207	6
207	6.6
207	38.6
207	*
207	7
207	12

* Instant Failure - Machining Flaw

I.5.4. Fractograpic Analysis of Baseline Bars

The origins of failure in the baseline room temperature test bars were located by visual examination using a binocular microscope under 30X magnification. The origins were delineated by placing the two broken halves together and surveying the tensile region of the fracture surface using oblique lighting. Fracture origins were identified in the 25 samples which fractured into two pieces. Five samples fractured into three or more fragments and certain identification of the initial fracture origin was impossible. In every case, the identified failure origins were clearly visible defects, surrounded by radiating hackle markings. No definitive correlations were found between the locations of the fracture origins and x-ray or visual indications of bulk or surface flaws. The data are summarized in Table I.5.4-I(A & B).

Representative samples were examined in the scanning electron microscope to determine the microstructural and chemical nature of the defects. Three types of flaws observed as fracture origins are shown in Figures I.5.4-1 through I.5.4-3. Figure I.5.4-1 shows an inclusion as the initiation site located at the edge of the bar, and the energy dispersive x-ray spectrum clearly identifies the flaw as an iron-containing particle. The failure origin shown in Figure I.5.4-2 is a porous, boron-rich area close to the bar surface. The x-ray map at the bottom of the figure indicates the boron-rich areas. The failure origin indicated by the arrow in Figure I.5.4-3 is a flaw in which the concentration of sulfur is above the level of the surrounding microstructure. Chemical analyses of the carbon black sintering aid used in the baseline composition have shown that sulfur is a residual element, and it is hypothesized that the fracture origin shown is a carbon-rich agglomerate. It is believed that all these strength-controlling flaws are traceable to the mixing techniques utilized in the preparation of the baseline material.

A more detailed discussion of the microstructural characterization of the injection molded and sintered material is given in Section I.6.2 of this report.

TABLE I.5.4-IA

FRACTOGRAPHY - ROOM TEMPERATURE BASELINE

MOR mPa	B.D. (g/cc)	LOCATION	FRACTURE ORIGIN TYPE (30X)	S.E.M.
237	3.052	Edge	Small pit-proj.	Morphology indicates possible Fe, but not detected - probably machining defect
252	2.995	Surface	Pits	C, shown by presence of S and Cl, Fig.I.5.4-6
295	2.997	Interior	Deep pits	Hole containing well-developed crystals, Fe
273	3.005	Interior, near edge	Shallow pit-proj.	
285	2.982	Surface	Small triangular crack	
285	3.012	Edge	Small pit-proj.	
331	3.025	Surface	Shallow pit-proj.	
310	3.048	Surface	Indistinct-discolored area	
270	3.052	Surface	Pit-proj.	
334	3.071	Surface	Small shallow pits	
310	3.072	Interior	Shallow pits break within inclusion	Clearly defined B
272	3.004	Surface	Indis. sm. pits	
284	3.022	Edge	Indis. shallow discolored area	
312	3.064	Surface, near edge	Small, shallow pit-proj.	
284	3.067	Surface, near edge	Small, shallow pit-proj.	

220	2.883	Edge	Pit-proj.	Clearly def. Fe, Fig.I.5.4-4
246	3.011	Surface	Pit-proj.	Clearly def. B, Fig.I.5.4-5
280	2.992	Surface	Pit-proj.	
241	2.984	Surface	Shallow pit-proj.	Clearly defined B
287	3.013	Interior, very close to surface	Shallow pit, broke thru flaw	
318	3.006	Surface	Pit-proj.	No conclusive evidence of source
302	3.004	Edge	Indis. shallow discolored area	
283	3.019	Interior	Small pit-proj.	
341	3.072	Surface	Lg. porous area	
333	3.054	Interior, near edge	Pore-proj.	

TABLE I.5.4-IB

SUMMARY OF FRACTOGRAPHY

LOCATION OF ORIGIN	NUMBER	%
EDGE	5	20
SURFACE	14	56
INTERIOR	6	24

LOCATION OF BREAK	NUMBER	%
AROUND PIT-PROJ DEFECT	13	52
THROUGH DEFECT	11	44
CRACK	1	4

PROJ - Surface Projection Matching Pit on a joining fracture surface

S.E.M. ANALYSIS	NUMBER	%
CLEARLY DEFINED BORON	3	36
CLEARLY DEFINED Fe	2	25
POSSIBLE Fe	1	13
CLEARLY DEFINED C	1	13
NOT ANALYZABLE	1	13

SEM Micrograph of Iron-Rich Surface Defect

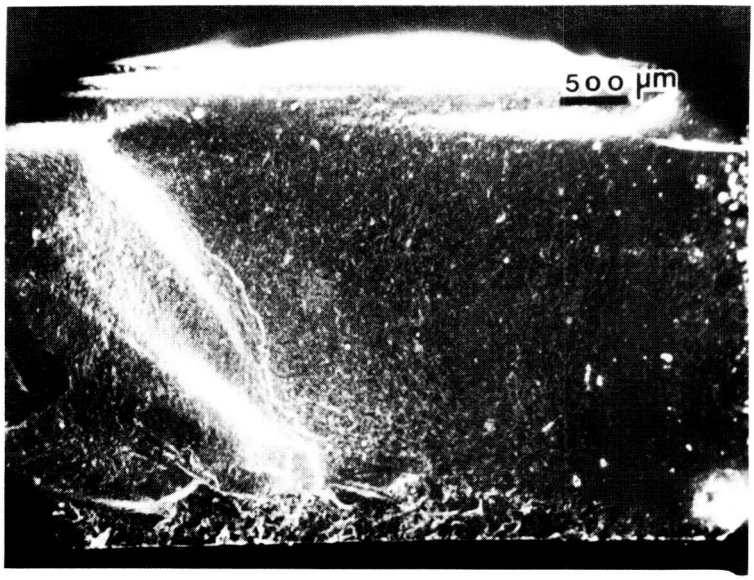

← Fracture Origin

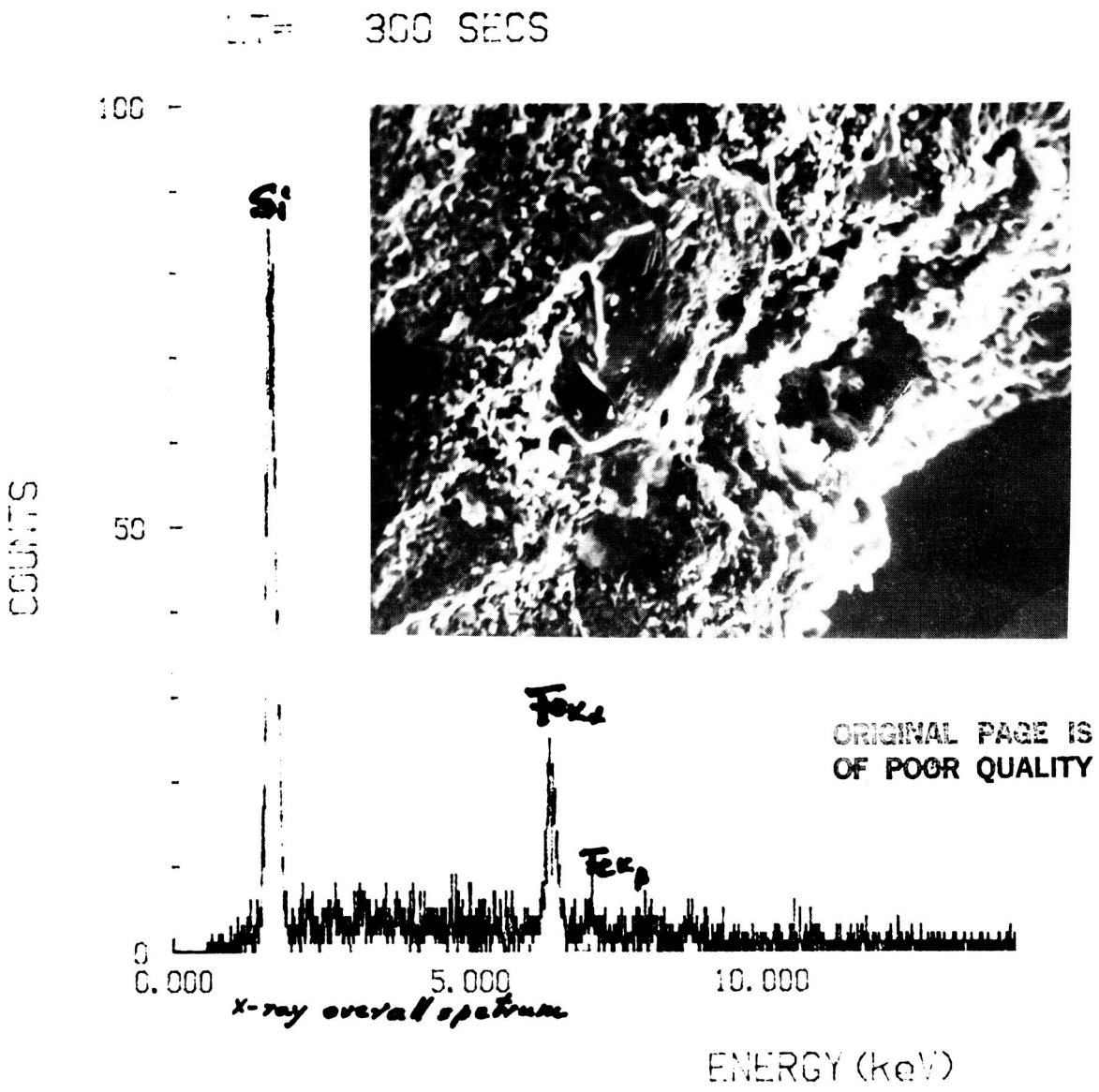

x-ray overall spectrum

Fig. I.5.4-1

SEM Micrographs of Fracture Surface Showing Boron-Rich Flaw Origin

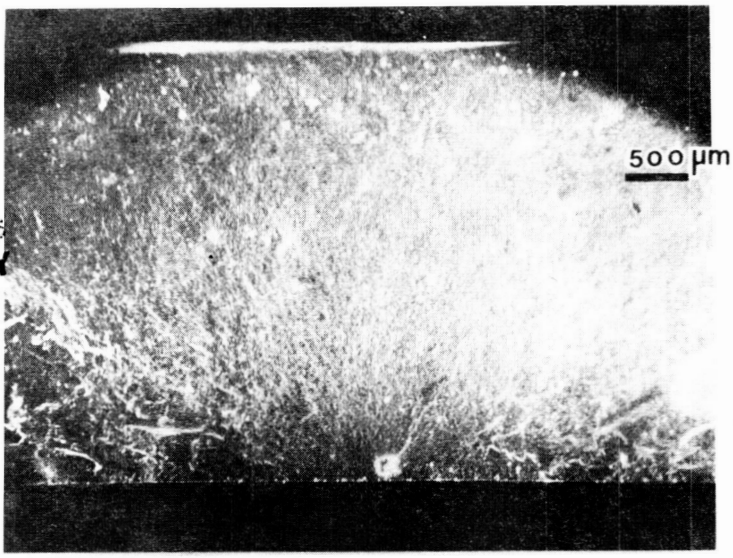

FRACTURE ORIGIN

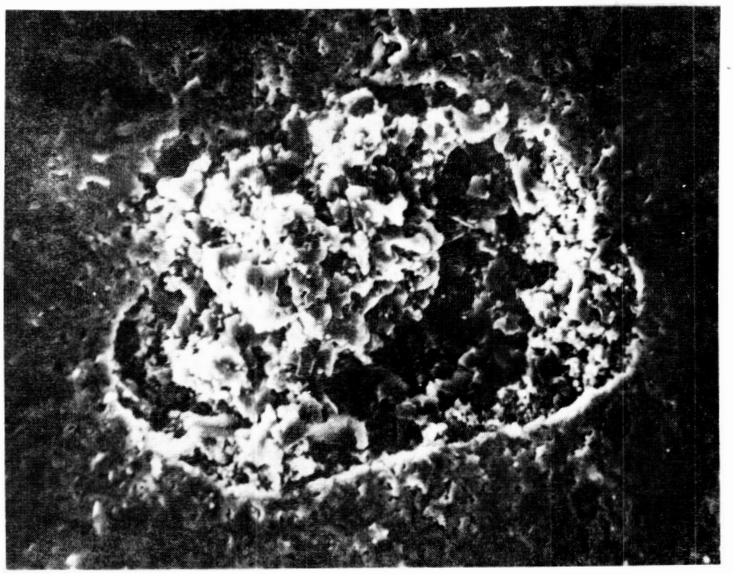

FLAW

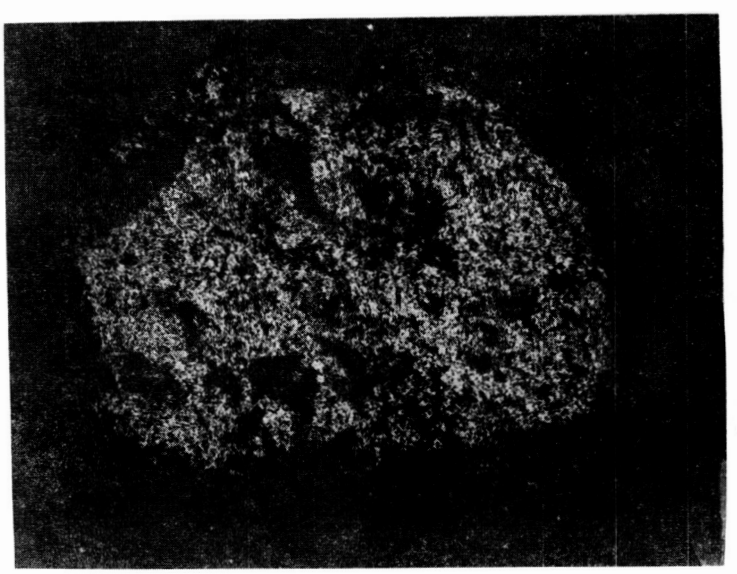

BORON MAP

Fig. I.5.4-2

SEM Micrographs of Fracture Surface Showing Sulfur-Rich flaw Origin

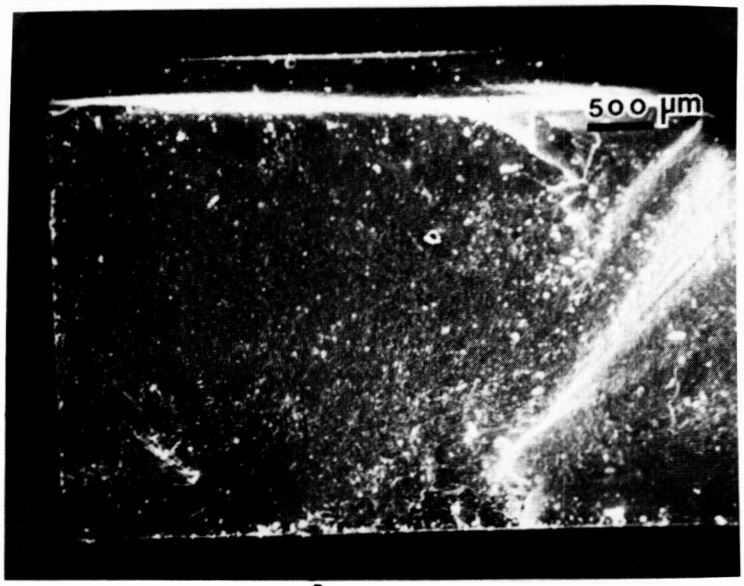

Fracture Origin

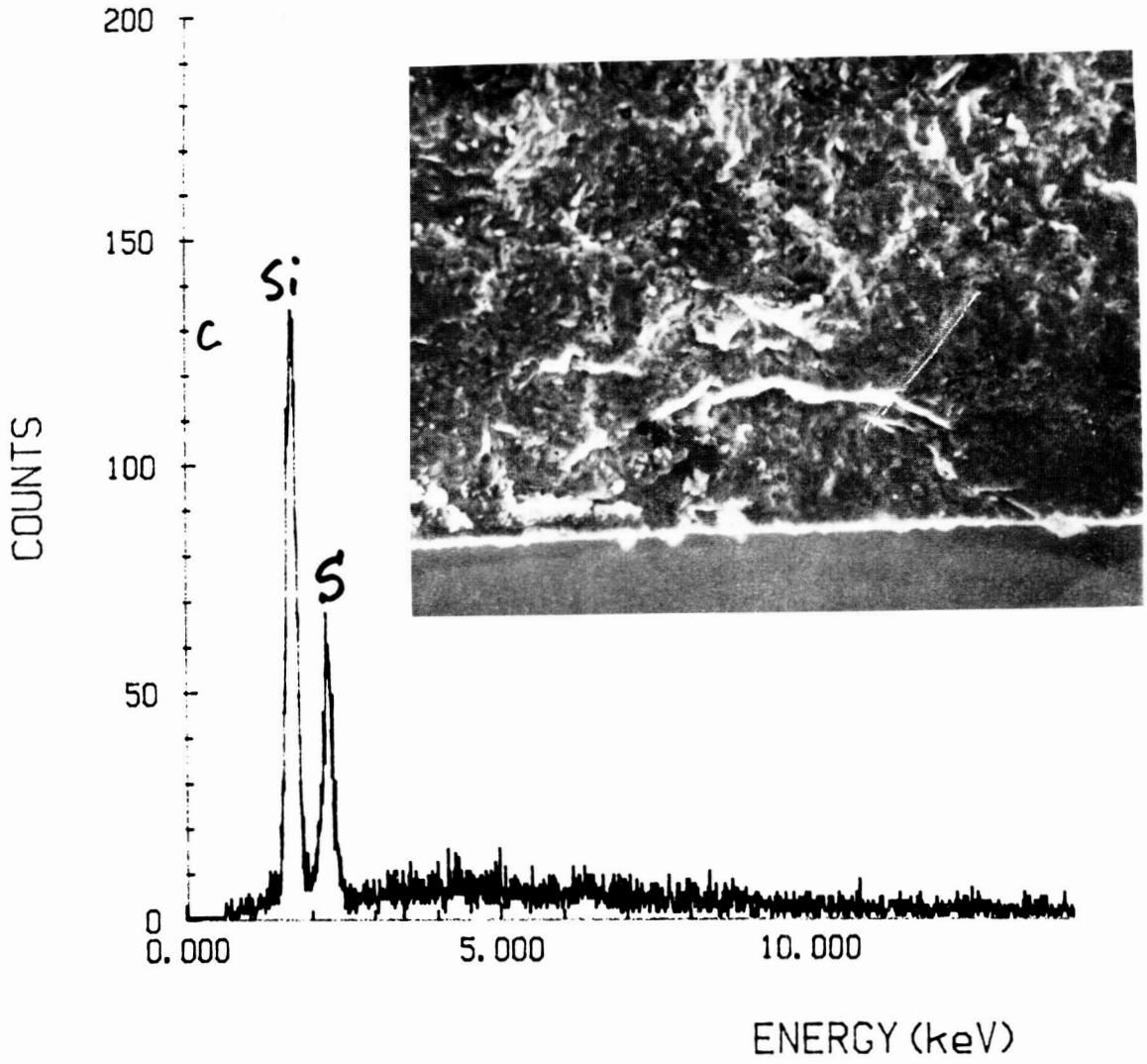

Fig. I.5.4-3

I.6. Processing/Property Relationships

I.6.1. Analysis of The Sintering Process

The baseline sintering process was carried out in vacuum at 2100°C for 10 minutes. With the short time at temperature required to limit the dissociation of SiC in vacuum, there was concern that temperature uniformity during sintering might be a problem. A statistical analysis of the properties of the MOR bars, identified according to their position in the sintering furnace, was carried out in order to assess this possibility.

In a sintering run, the bars are placed in a vertical position in a graphite holder as shown schematically in Figure I.6.1-1. Two groups of bars are indicated: one group (O) designated as the outermost from the center of the holder, and the second group (I) designated as the inside group. The properties of the inner and outer groupings are compared.

The sintering results for the baseline density data, runs V-26, V-27 and V-29, are summarized in Table I.6.1-I. It can be seen that the percent of theoretical density is reproducible for the inner and outer groups at the sintering temperature of 2100°C and that the average densities for the two groups differ by more than a standard diviation. The student "t" test for differences of means shows that the outside group is stronger than the inside group at the 0.026 level of significance.

An indication of the effect of temperature on density is given by the data for run V-25 sintered 25°C lower in temperature. At the lower sintering temperature, the density is reduced by about 2% in the outer grouping of bars. If it is assumed that a temperature gradient is responsible for the difference, then the variation in density found between bars sintered at 2100°C and 2075°C can be used to estimate the gradient. If a linear relationship between sinter temperature and density is assumed, it is estimated that the sinter temperature for the inner group is 15°C lower

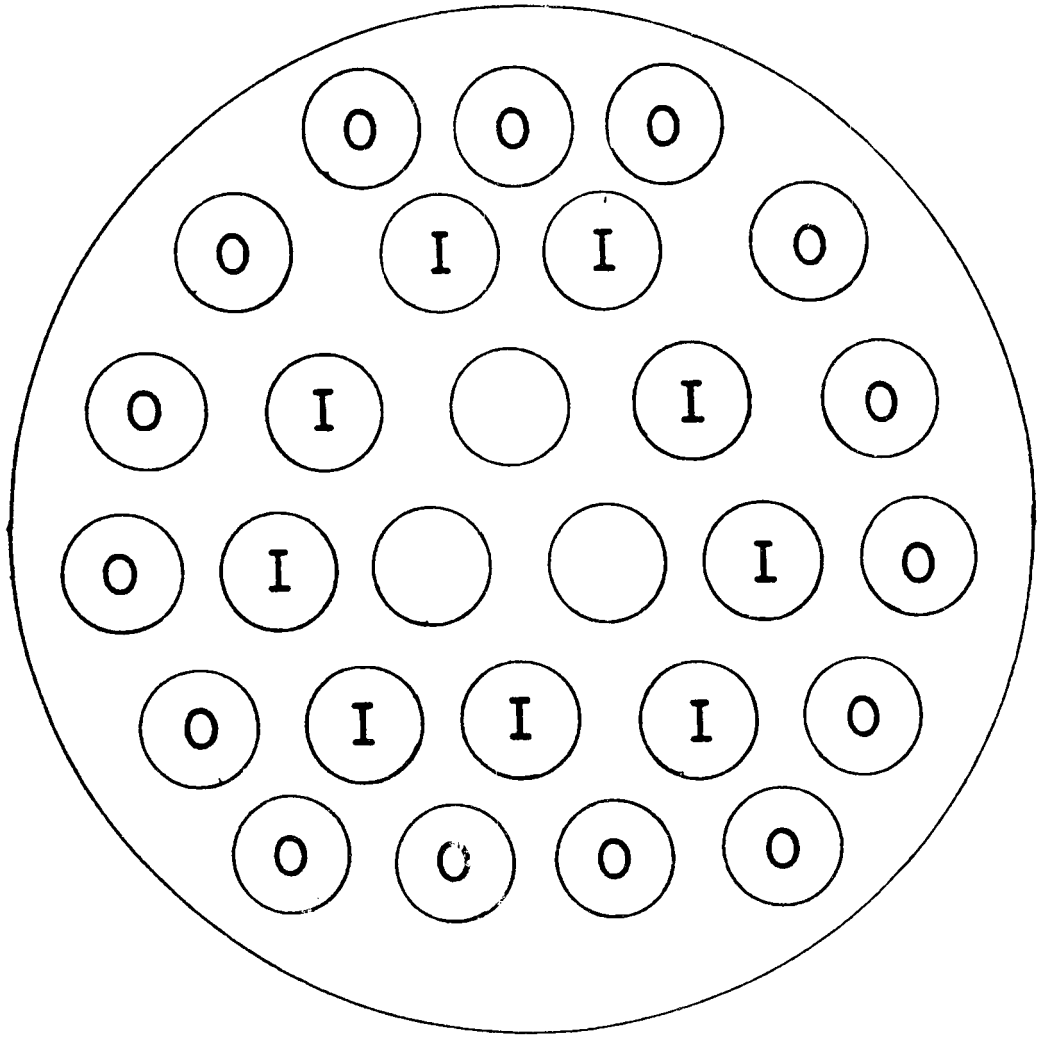

VACUUM FURNACE SAMPLE HOLDER

Fig. I.6.1-1

TABLE I.6.1-I

NASA 4G BASELINE BARS
(Unmachined Specimens)

SINTER NO.	INNER GROUP			OUTER GROUP		
	n	X	σ	n	X	σ
V-24 Warped Bars 2100°C - 10 Min.	20	93.1	0.4	30	94.2	0.5
V-25 Lucifer Dewax 2075°C - 10 Min.	-	-	-	20	92.6	0.5
V-26 Lucifer Dewax 2100°C - 10 Min.	20	93.8	0.3	30	94.8	0.4
V-27 Lucifer Dewax 2100°C - 10 Min.	13	93.4	0.2	30	94.5	0.4
V-29 Lucifer Dewax 2100°C - 10 Min.	-	-	-	27	94.3	0.5

than the outer group in runs V-26, V-27 and V-29.

The data indicate that sinter density and strength are very sensitive to small firing temperature/time differences under the particular conditions utilized in this study. The results emphasize the need for close control of the sintering furnace and temperature gradients in a vacuum sintering process.

I.6.2. Microstructural Analysis

Microstructural analyses were performed on the baseline material by means of scanning electron microscopy (SEM), electron microprobe analysis (EMPA), optical microscopy, and energy dispersive x-ray spectrometry (EDX). Analyses of the material were made at each of the distinguishable steps in processing from the green body stage through sintering. Defects were identified, and an attempt was made to determine the processing step in which they originated. The morphology and chemical characteristics of the defective regions provided the basis for a definitive relationship in most cases between the defect and the process origin.

As Molded Green Body

Four types of defects were observed on the fracture surfaces of the as-molded green body:

Gray Spots: Observed with optical microscopy in the green body as illustrated in Figure I.6.2-1. The characteristics observed in studies of this type of defect are: i) shapes are either spherical or elliptical; ii) analyses with the SEM show that the defect is more dense than the matrix and is often surrounded by a less dense or porous ring, Figure I.6.2-2; and iii) the chemistry is similar to that of the matrix.

Green, Grey spots

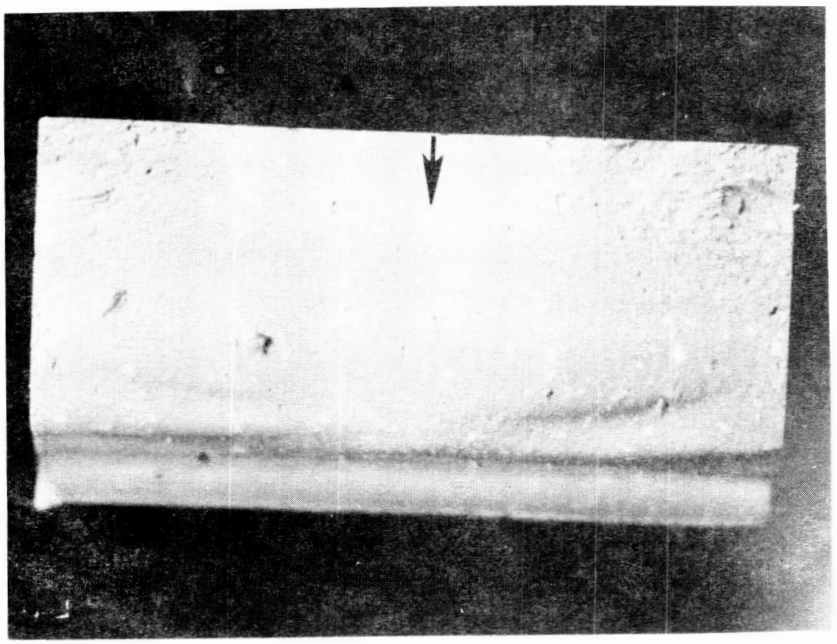

Fig. I.6.2-1

Sintered, Grey Spots

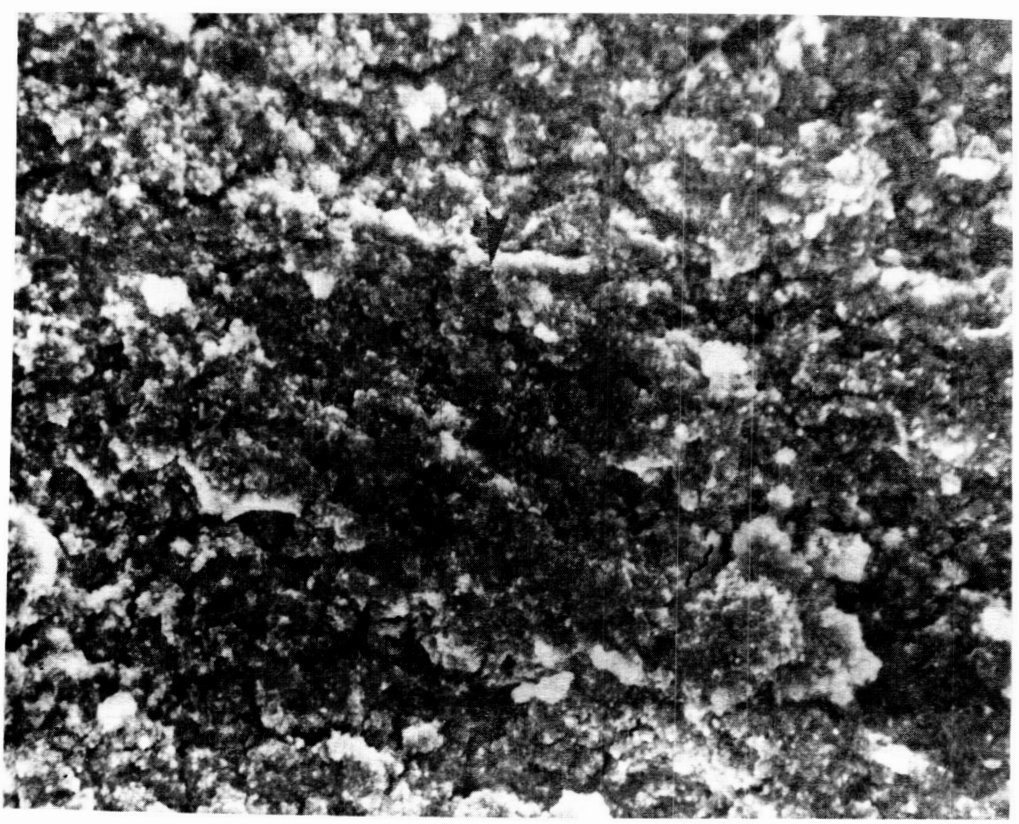

Fig. I.6.2-2

More detailed analyses of the microstructure of the defect and the matrix indicate that the inhomogeneous distribution of binder in the molding mix may be responsible for the flaw.

. Red Spots: Observed with optical microscopy in the green body. Figure I.6.2-3, location (a), illustrates the nature of the spot as observed in the SEM; the defect at location (b) is a SiC agglomerate (discussed below). The characteristics observed are: i) various shapes and sizes observed; ii) distribution is less dense than that of the gray spots; and iii) an x-ray map for boron (EMPA) shows the major constituent of the red spot, Figure I.6.2-4(a); minor concentrations of K, Cl, Fe, Cu, and Zn were detected in the flaw which are associated with the amorphous boron additive. The Si map in Figure I.6.2-4(b) shows the red spot does not contain Si.

The results indicate that the red spot defect is a result of the agglomeration of the boron particles used as a sintering aid.

. SiC & Carbon Agglomerates: The SEM micrograph shown in Figure I.6.2-3, location (b), illustrates this defect. The characteristics observed are: i) the agglomerates do not tend to separate along the plain of fracture but tend to pull out in one of the fracture pieces; ii) SiC and Carbon agglomerates can be distinguished only by chemical analysis; and iii) SiC agglomerates are more numerous than carbon agglomerates.

The characteristics indicate that the agglomerates result from inadequate dispersion of the powdered solids during the preparation of the molding mix.

The identification and subsequent characterization of these flaws has contributed significantly to an improved understanding of the materials and processes used in the program. The development of improved processing methods and process control criteria as described in the report is largely due to the emphasis placed on this part of the program.

Green: a; red spot b; SiC agglomerate

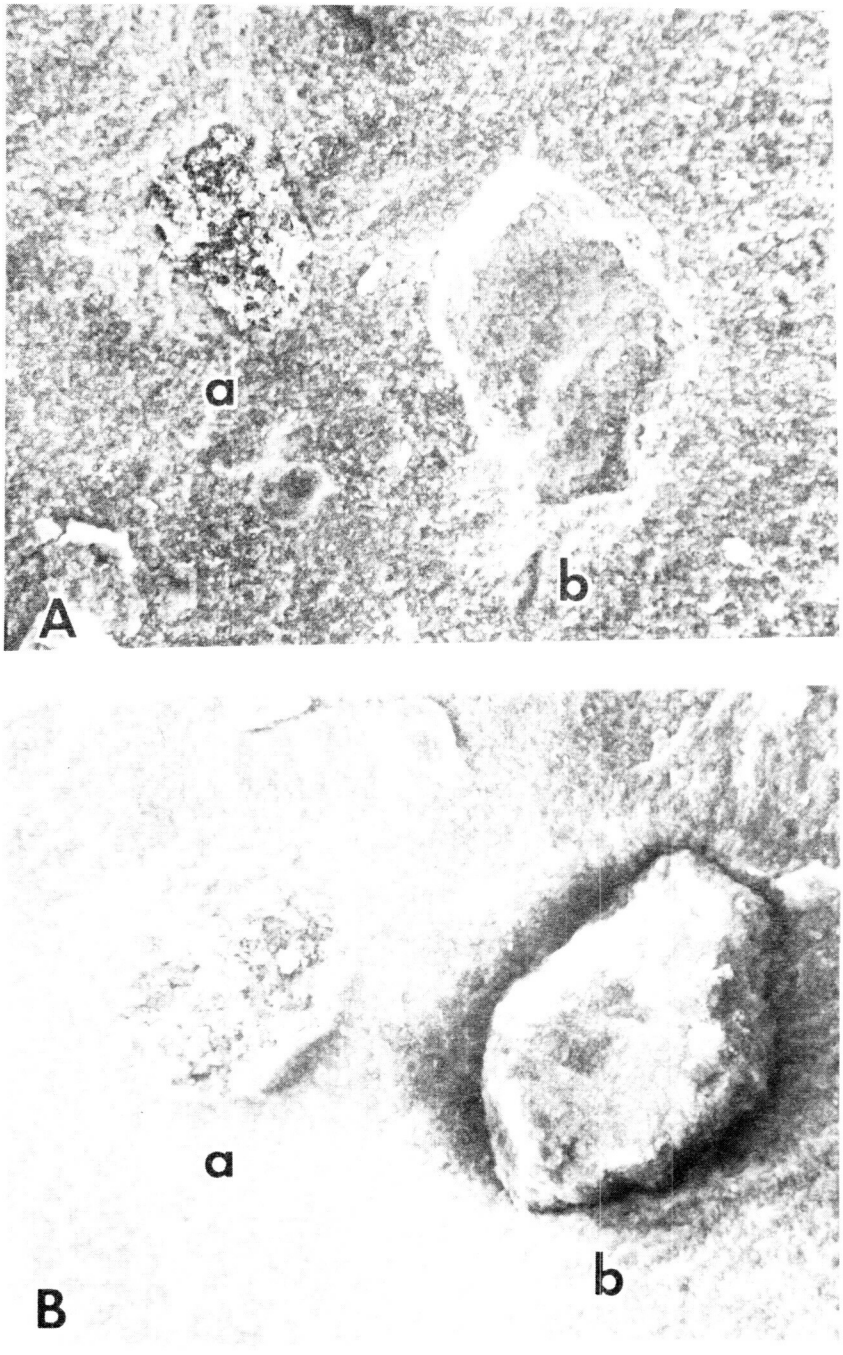

Fig. I.6.2-3

Red Spot: a; Boron, b; Si scans

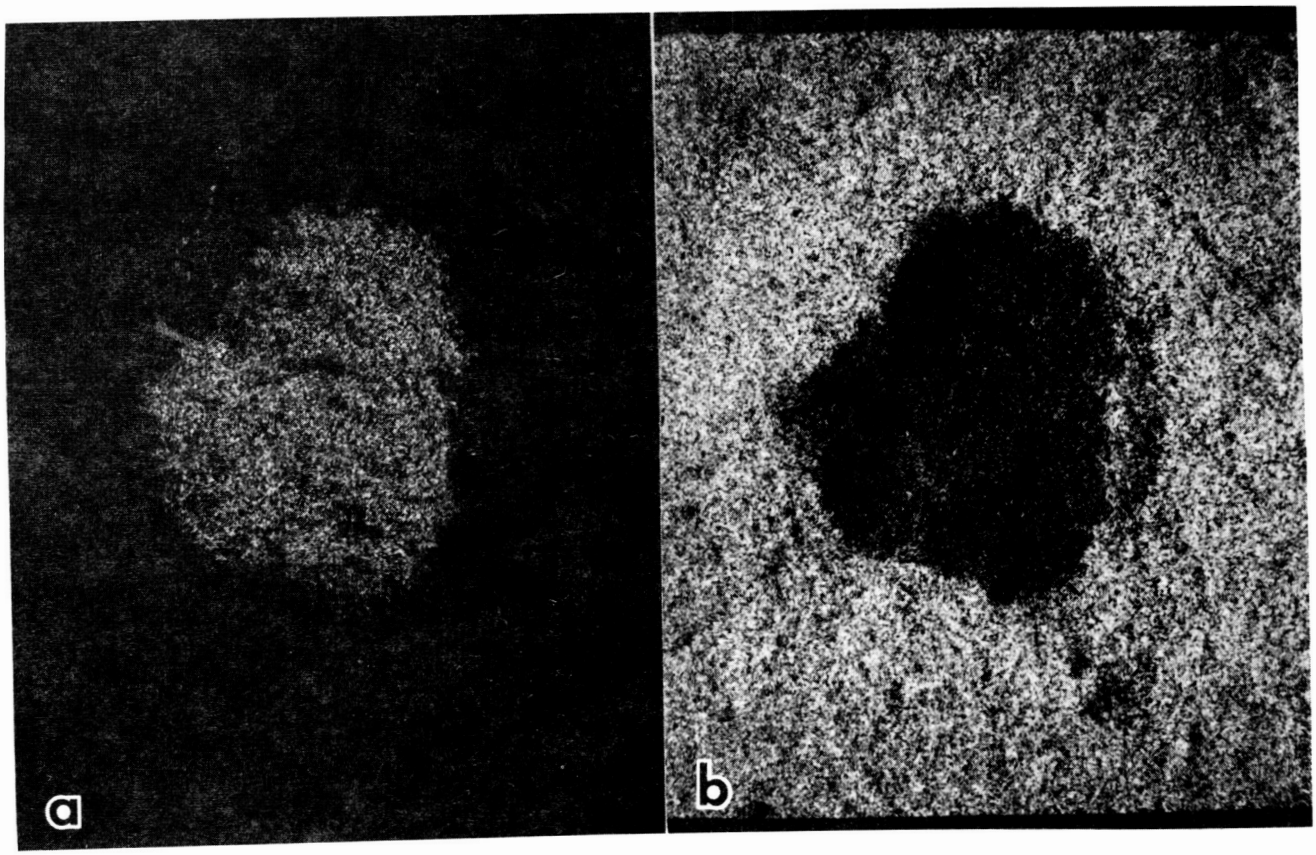

Fig. I.6.2-4

Dewaxed Body

Observations of the fracture surfaces of dewaxed test bars, Figure I.6.2-5(a), (vacuum process) show that there is a tendency for small cracks to form in certain areas and the microstructure tends to be more uniform than that observed following an argon dewaxing, Figure I.6.2-5(b). High shear mixing induced a layered or scaly appearing fracture morphology in comparison with that noted with materials produced by other mixing methods, Figure I.6.2-6. The oval-shaped defect in the figure appears to be the gray spot type of defect discussed above.

Sintered Body

Four types of defects have been identified with SEM analyses of the fracture surfaces of sintered MOR test bars prepared for the baseline characterization.

Type A: This defect has the following characteristics: i) particles of SiC powder that have sintered very little, Figure I.6.2-7; ii) the boundaries of the defect are sharply defined by the transition between sintered and unsintered zones, Figure I.6.2-8; and iii) the defect shape is nearly spherical with a diameter typically in the 25 to 50 micrometer range.

This defect is probably formed from agglomerates of SiC powder which lack the required sintering aids. The defect has little strength and is generally fractured when the sinter body is broken.

Type B: This defect is characterized by the additional sintering or grain growth which has occurred relative to that present in the SiC matrix, Figure I.6.2-9. The following characteristics are observed: i) the frequency of observation is similar to that of the gray spots noted in the green body; ii) the growth structure is continuous between defect and matrix; iii) no detectable chemical difference exists between defect and matrix; and iv) the defect shape is nearly spherical.

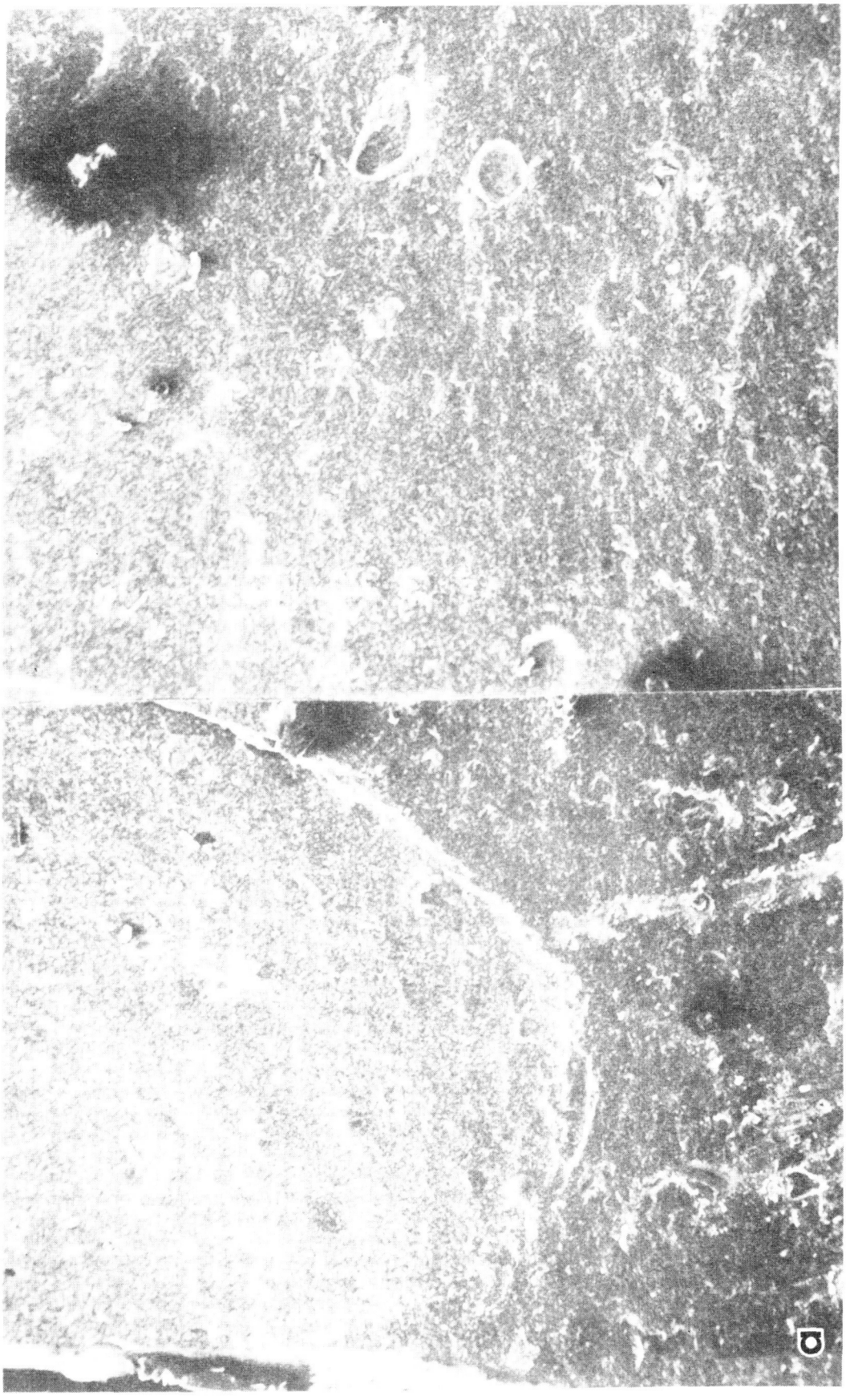

Fig. I.6.2–5a

Argon dewaxed body

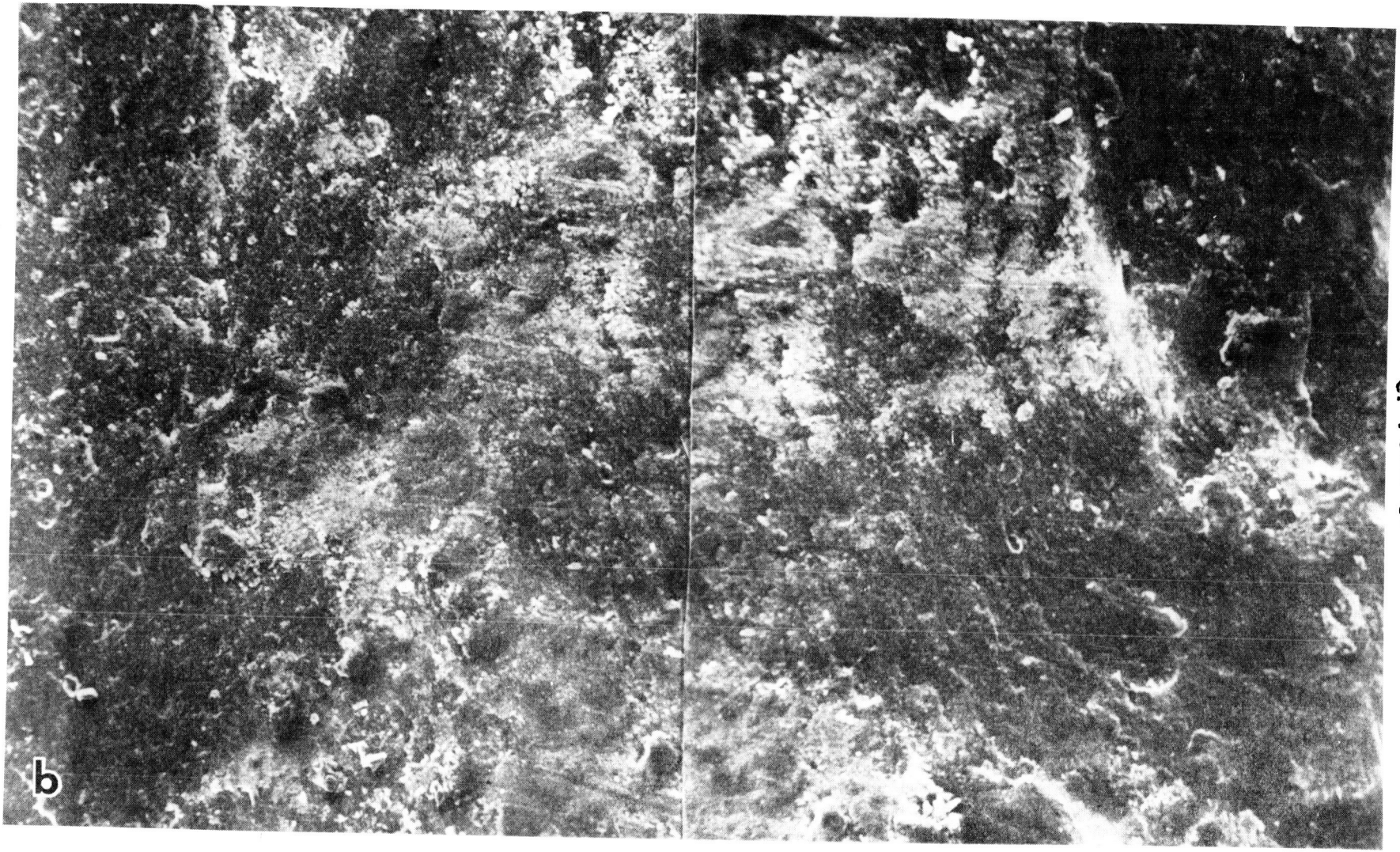

Fig. I.6.2-5b

Green, High Shear Mixing

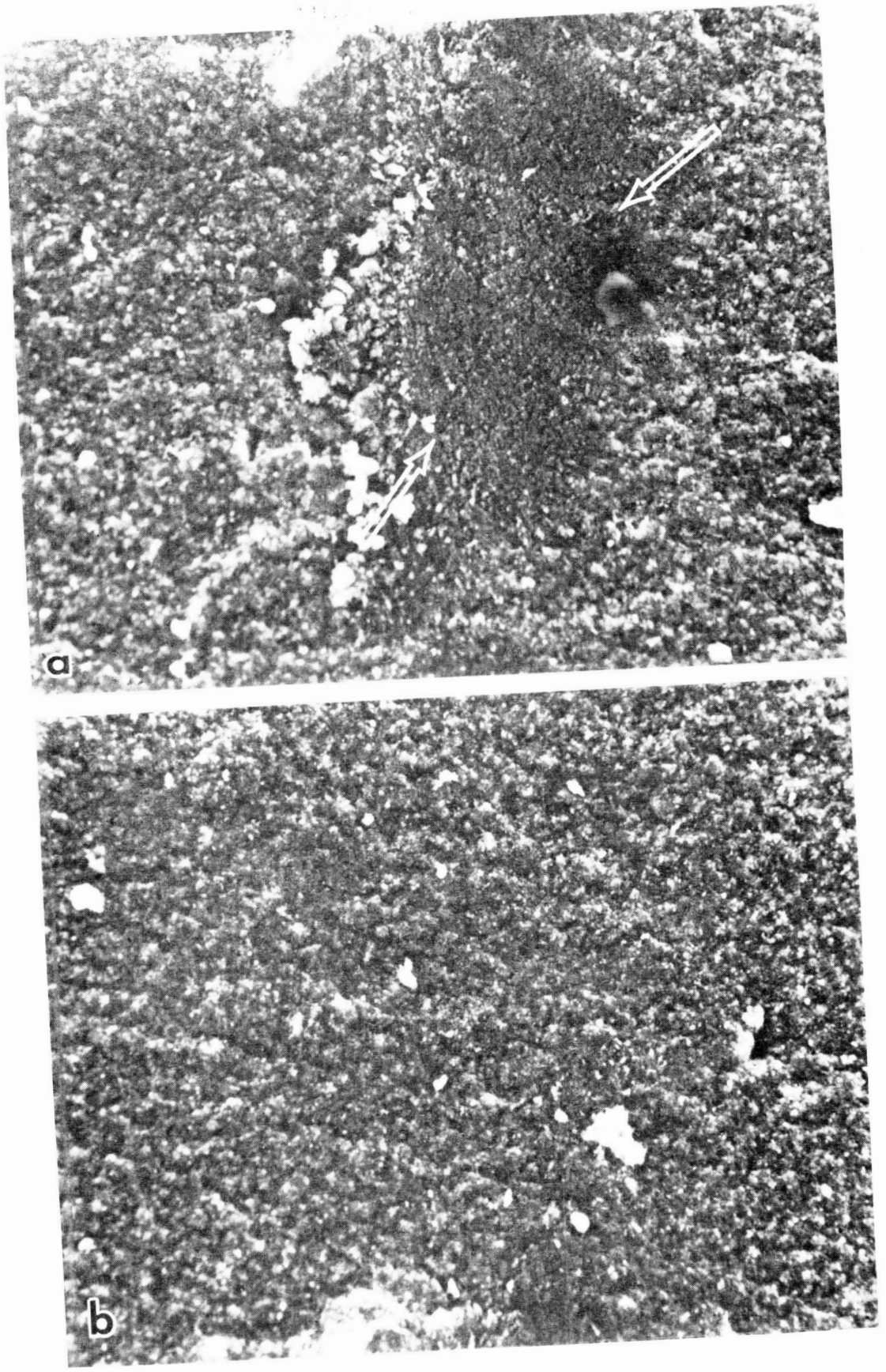

3 0 μm

Fig. I.6.2-6

Sintered, SiC agglomerate

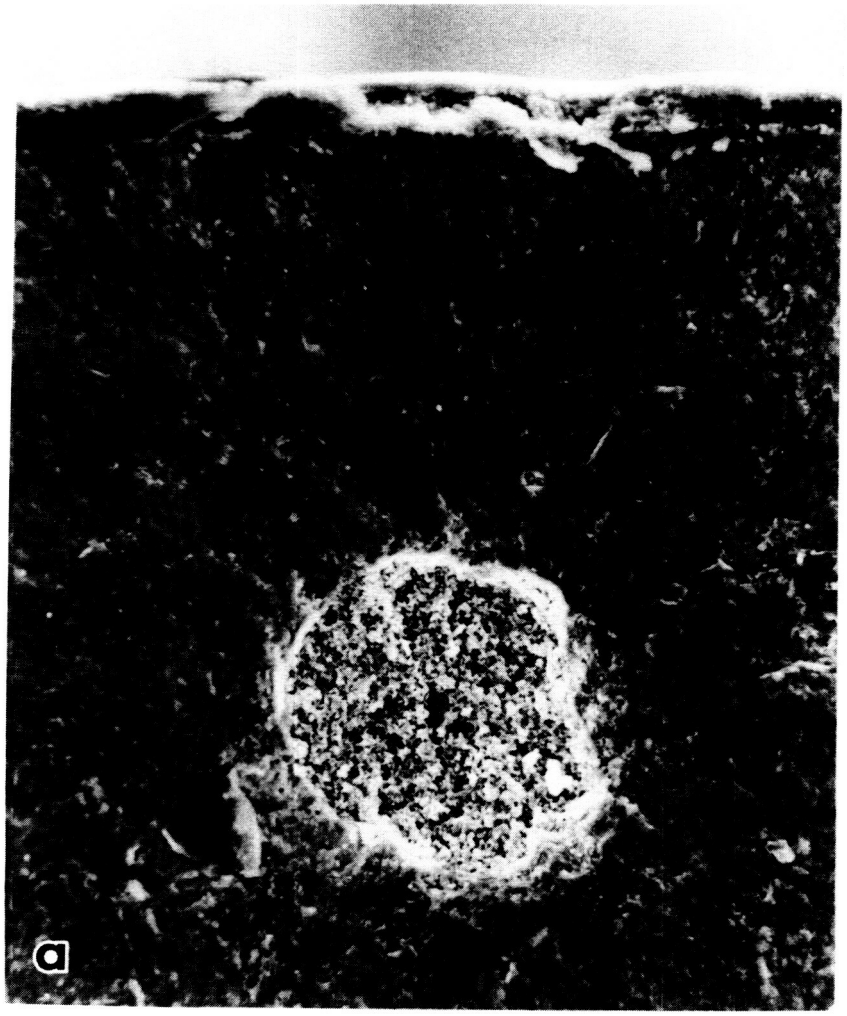

Fig. I.6.2-7

Sintered, SiC agglomerate

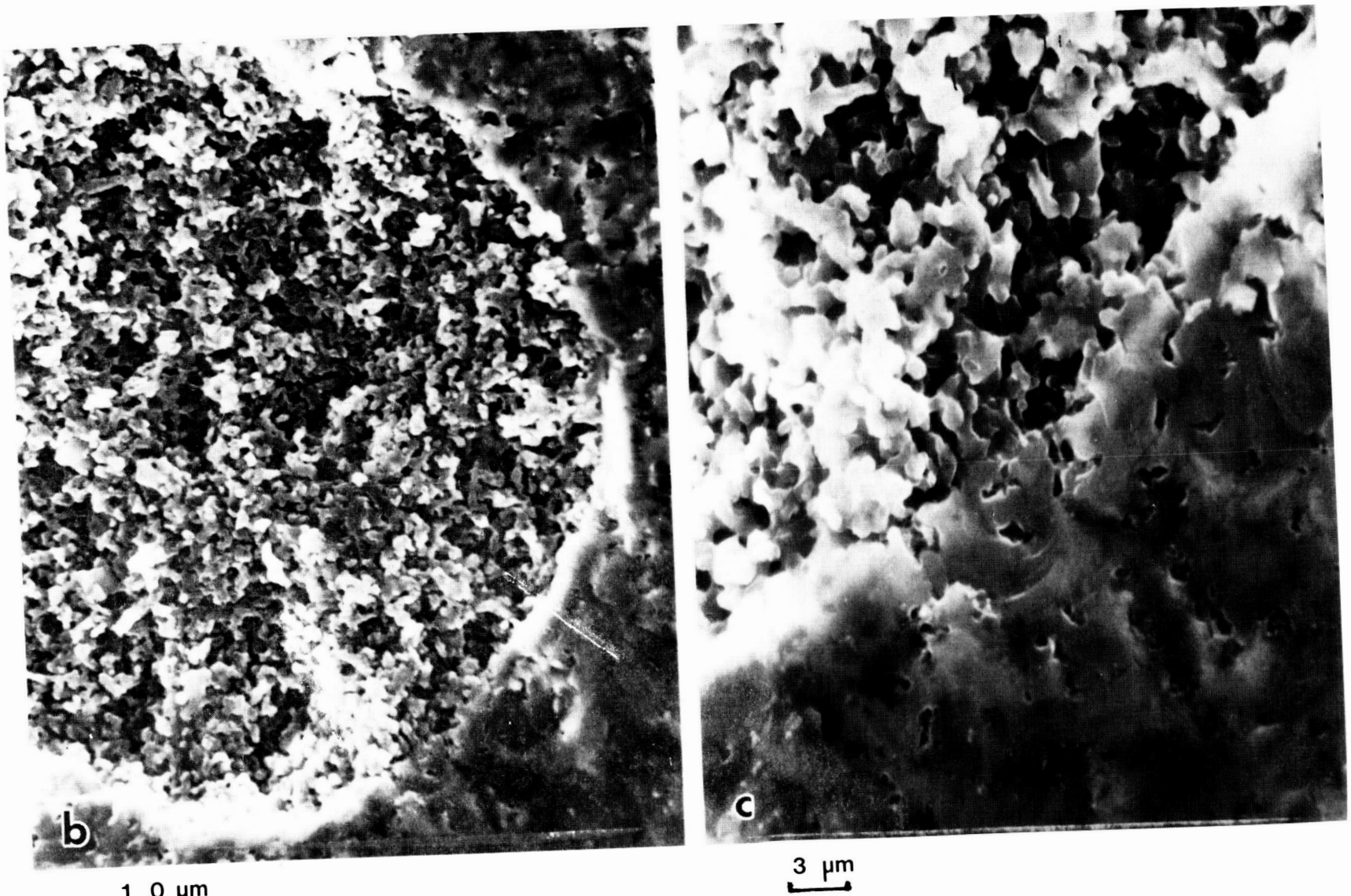

Fig. I.6.2-8

Sintered, Grey spots

Fig. I.6.2–9

This defect probably results from the sintering of the gray spot flaws noted in the green body.

. Type C: The microstructure of this type of flaw is a complex mixture of grain sizes and shapes, Figure I.6.2-10. The platelike morphology that characterizes the defect is markedly different from that of the flaw types A and B. Chemical analysis, EMPA, shows that the composition of the area is mainly boron with a low level of carbon, Figure I.6.2-11. No Si was detected.

The boron agglomerates noted in the green and dewaxed bodies are obviously the origin of this defect.

. Type D: Figure I.6.2-12 illustrates another type of defect observed in the baseline material. A relatively high concentration of Fe, as determined with EDX, is associated with the defect. The highest level of Fe was found in the surface region defining the pore. The particles within the pore, labeled A in Figure I.6.2-12(a), are relatively pure SiC.

The defect has been associated with metallic inclusions introduced into the molding mix during one of the mixing steps. It is probable that the metal inclusion melts during sintering and interacts with and penetrates into the SiC matrix leaving a pore and a surrounding region enriched in Fe.

Each of the four types of defects identified in the sintered bodies is believed capable of acting as initiation sites for failure. Since the relative ability of each type of flaw to induce fracture is expected to be determined by the size and the mechanical properties of the defect and the adjacent matrix region, it is probable that some of these flaws are more serious than others. However, the results of studies relating defect type and failure origin in the baseline materials, Section I.5, indicate that all of the defects noted are active in initiating fracture.

Sintered, Boron agglomerate

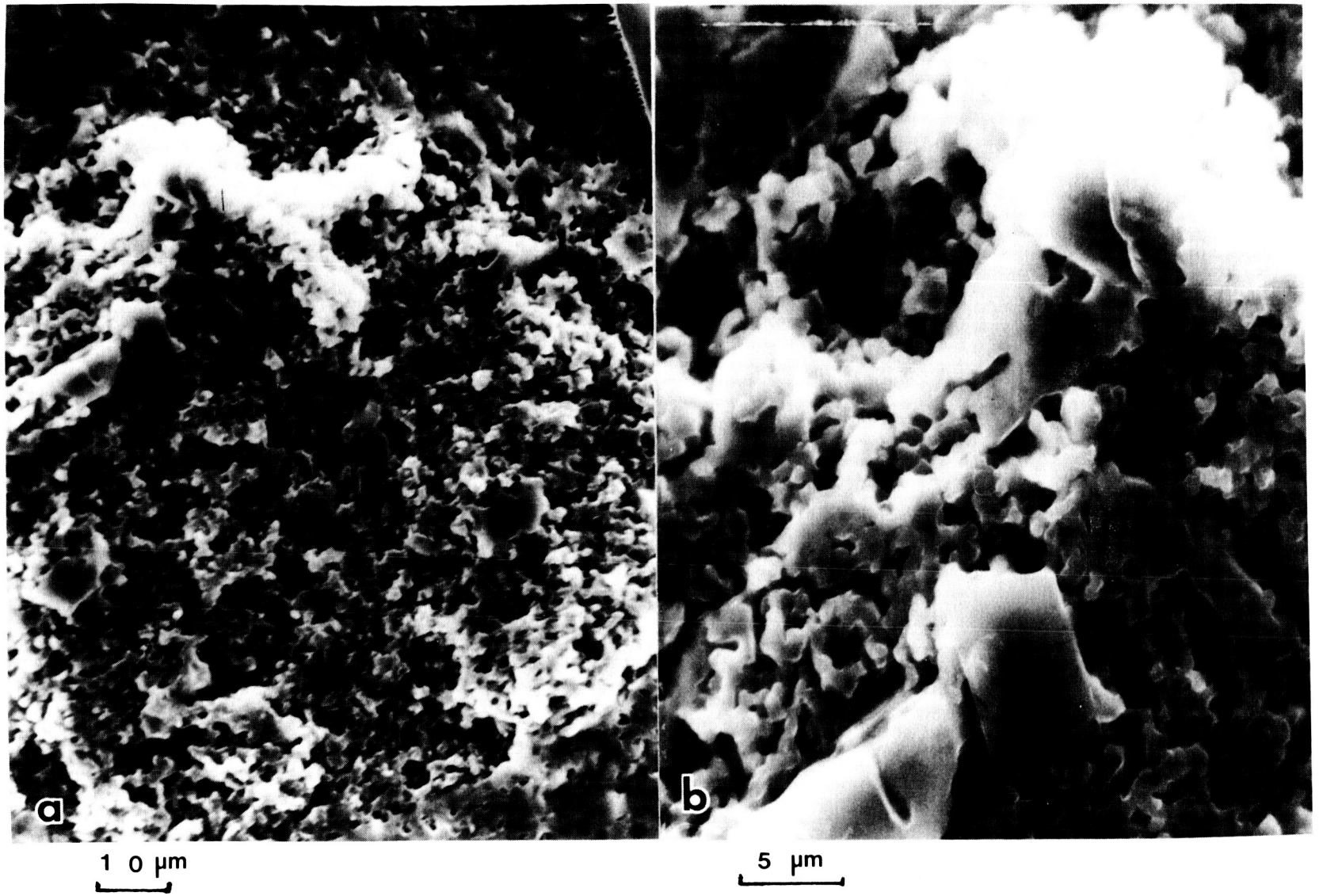

Fig. I.6.2-10

Sintered, Boron agglomerate

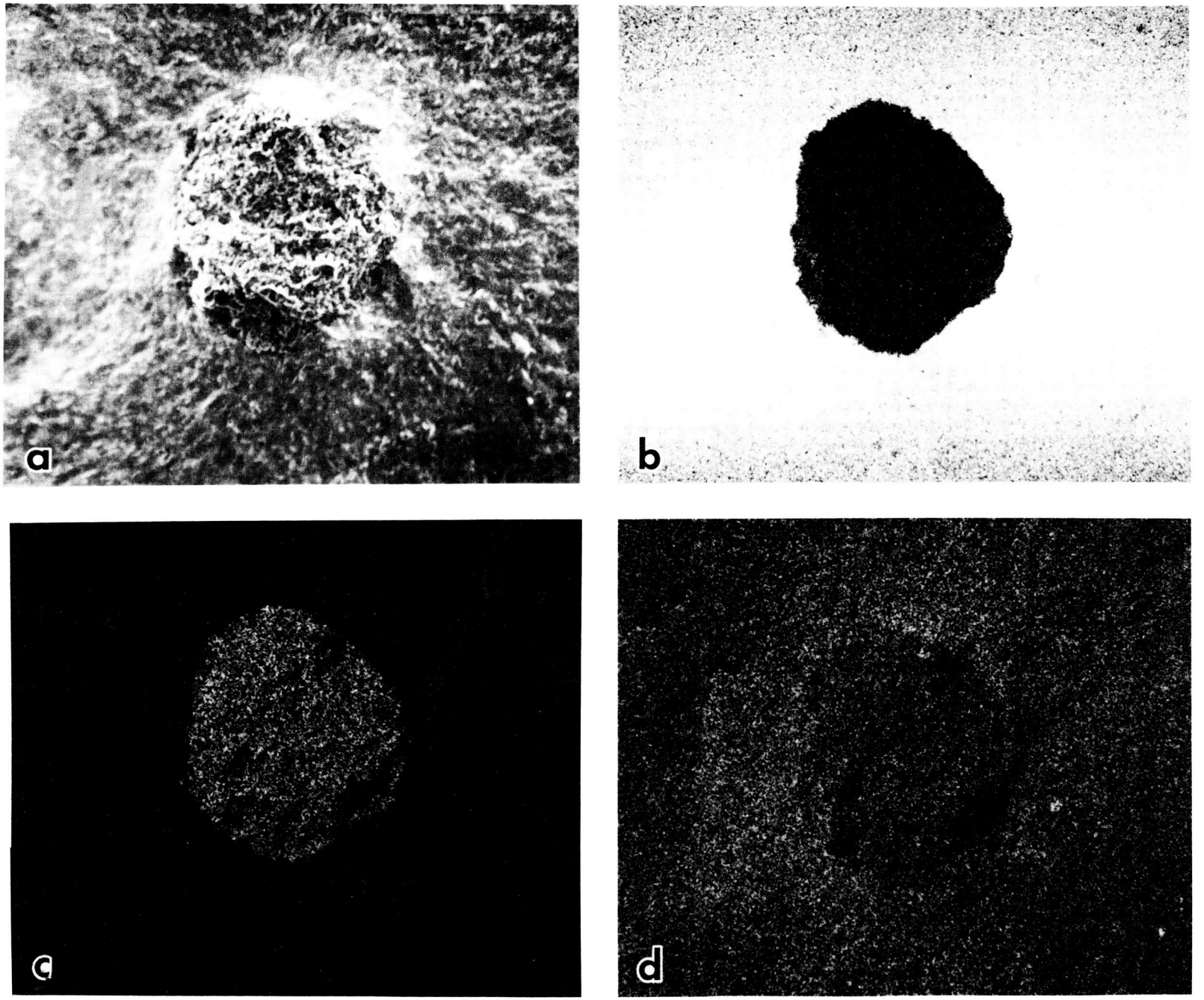

Fig. I.6.2-11

Sintered, Metallic inclusion

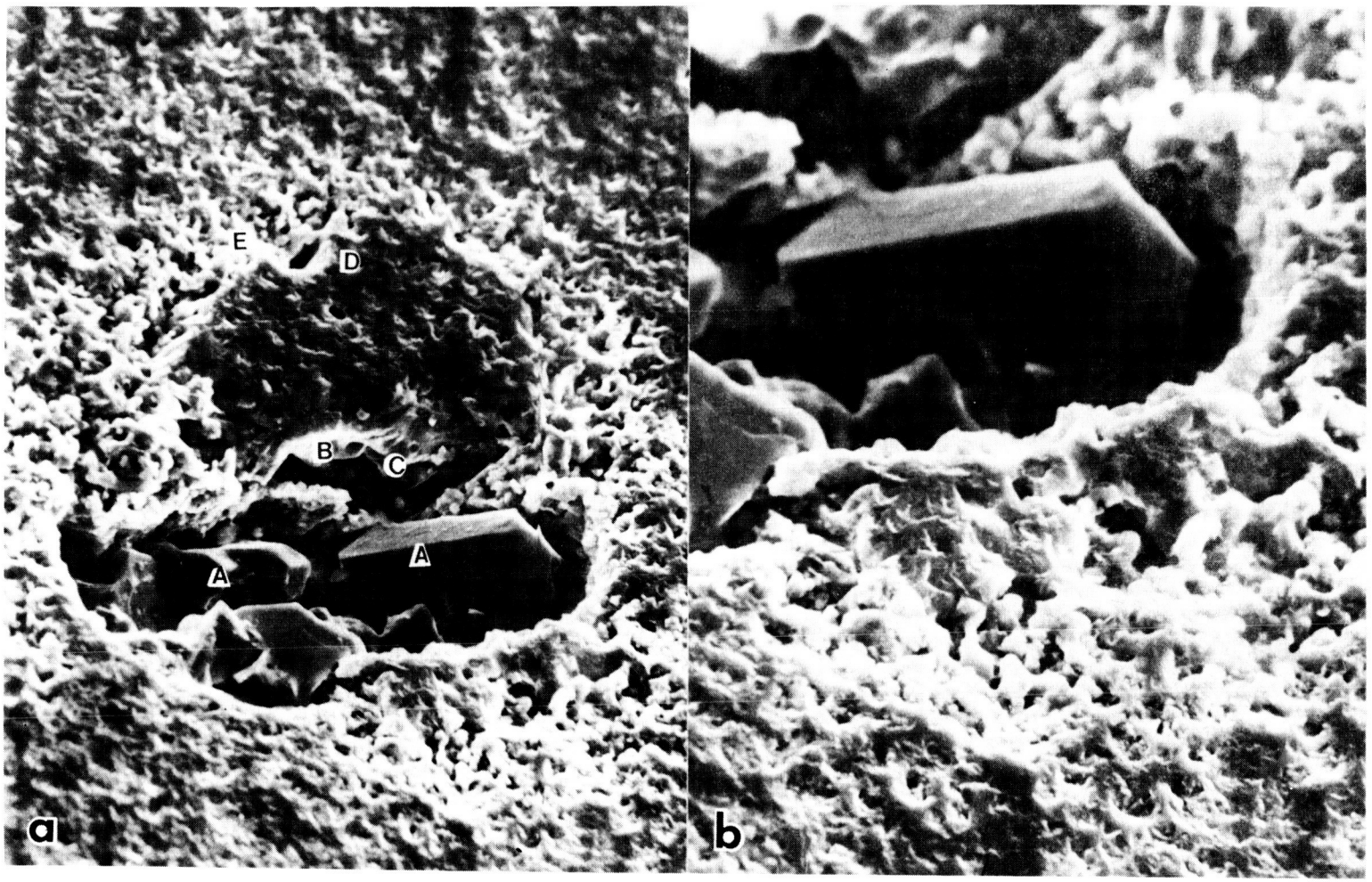

5 μm

1 0 μm

Fig. I.6.2-12

On the basis of these results and the fractographic studies described earlier, it was concluded that improvements in material preparation and batch blending procedures used in the baseline processing would be required to obtain the desired uniformity of solids and binder in the blended mix. A decision was made to evaluate fluid mixing procedures, and the results described under Task VII studies are encouraging.

Task VII - MATERIALS AND PROCESSING IMPROVEMENTS

VII.1 Objectives

This task is aimed at exploring new ideas for materials and processing improvements which are then evaluated and, if significant, fed into the Task I and Task II work plans. In this first year six studies were completed to aid in choosing the baseline process and to help plan the Task II MOR bar optimization matrices. Those studies that were planned along the lines of statistically-designed matrices are listed below:

1. Matrix 1 - Baseline Composition

2. Matrix 2 - Dewaxing Cycle

3. Matrix 3 - High-Shear Processing

4. Matrix 4 - Fluid Mixing Process

5. Matrix 5 - Argon Sintering

Matrix 1 was used in selecting the baseline composition from the best result obtained. Vacuum dewaxing and sintering processes were developed which were capable of giving acceptable densities and strengths for the baseline composition.

Matrix 2 was used to improve the dewaxing cycle. The results of this work defined the dewaxing cycle used for the baseline material.

Matrix 3 was undertaken when large and numerous agglomerates in the dry-mixed material were found to be the fracture origins in the material at low stress levels.

Matrix 4 was designed to compare the dry mixing process used for the

baseline process with a fluid mixing process designed for improved mixing homogeneity. The results demonstrated the superiority of the fluid-mixing process.

Matrix 5 was used to investigate heating rates and temperatures for sintering in an argon atmosphere and to verify that acceptable densities could be obtained by sintering in an argon atmosphere.

VII.2. Matrix 1: Baseline Composition

VII.2.1. Composition

An experiment was conducted to aid in selecting the baseline composition. Two grades of beta-SiC powder produced by Ibiden Co., Ltd (Japan) and sold under the trade name "Betarundum" were used. The two were different size fractions of the same powder: a coarser grade, Standard Fines (SF); and a finer grade, Ultra Fines (UF). Two carbon sources (lampblack and polyphenylene resin), and two levels of solids loading were investigated. A schematic of the experiment is given in Figure VII.2.1-1.

The base formulation consisted of 1 % boron and 2 % carbon equivalents as sintering aids. The mixes with carbon black (NASA 4 & 5) were dry mixed in a V blender to obtain uniformity, intermixed with the binder in a heated mixer, and molded. The mixes with the resin (NASA 7 & 8) were ball milled in toluol to obtain a more uniform distribution of the resin. The mixes were then dried, waxed and molded. In all cases, the highest loading level was initially prepared and molded. The remaining mix was then diluted to the lower solids level by a wax addition and molded.

The yield of the experiment expressed in terms of the density of the bars after sintering, is reported in Table VII.2.1-I as a percent of theoretical density. Data for three dewaxing and sintering cycles are listed. Test bars dewaxed in the conventional argon process developed for

2^3 EXPERIMENT TO

DETERMINE BASELINE COMPOSITION

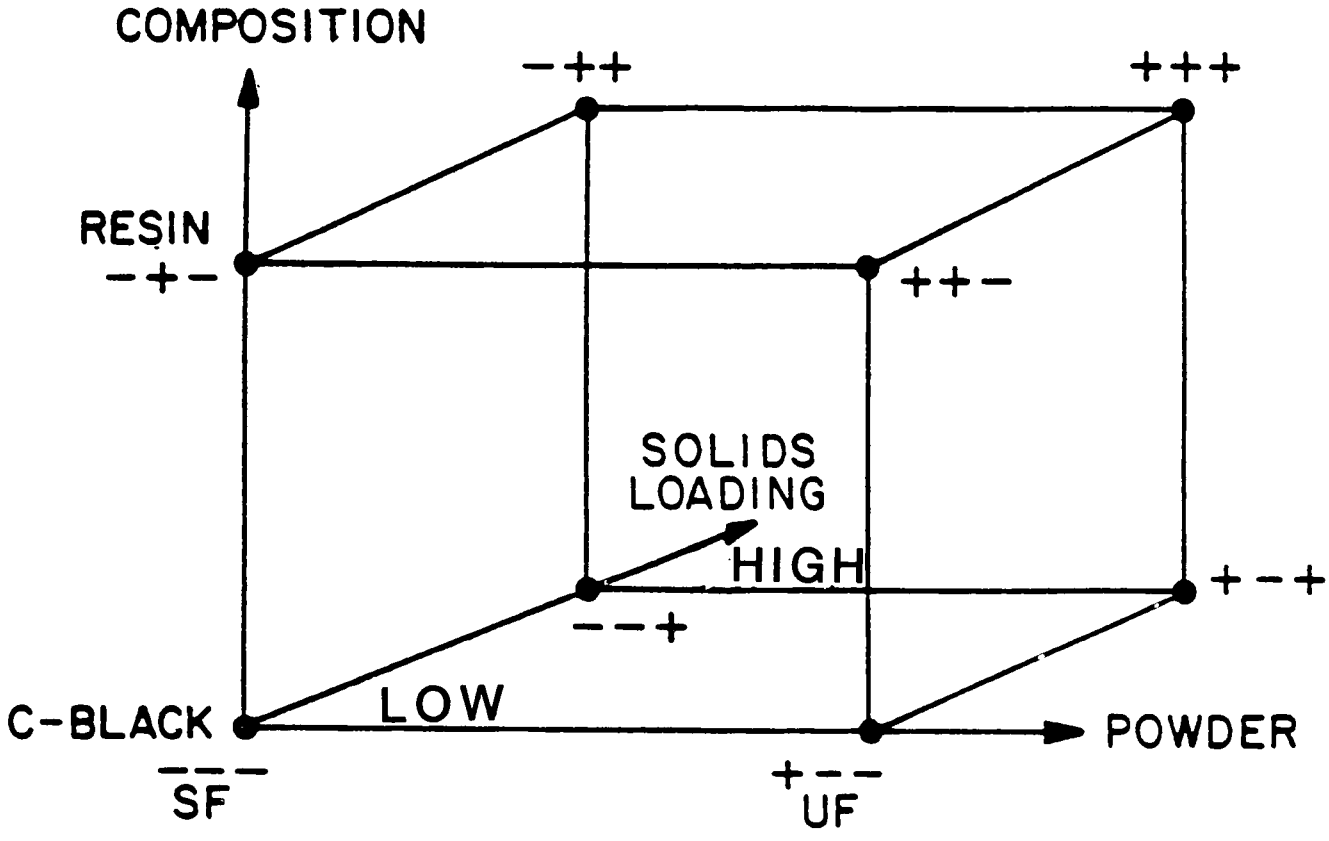

Fig. VII.2.1-1

TABLE VII.2.1-I

DEVELOPMENT OF BASELINE PROCESS

NASA No.	Loading Level	Carbon Source	SiC Source	% Theoretical Density: Conventional Ar Dewax Ar Sinter	% Theoretical Density: 2 Cycle Vac Dewax Vac Sinter	% Theoretical Density: 1 Cycle Vac Dewax Vac Sinter
4	Low	C-Black	UF	77	92	93
	High			77	92	94
5	Low	C-Black	SF	74	88	91
	High			75	89	90
7	Low	Resin	UF	70	--	--
	High			68	85	88
8	Low	Resin	SF	70	86	88
	High			70	86	88

this binder formulation exhibited very poor sintered density. Chemical analysis of these specimens, Table VII.2.1-II, revealed that the SiC was slightly oxidized during the argon dewaxing cycle with a high probability that this oxidation inhibited densification of the bars processed in the conventional manner.

TABLE VII.2.1-II. Oxygen Content: NASA 4 (61.5%) Dewaxing

	As Molded	After Dewaxing	Net Change ($\%O_2$)
Argon Dewax	1.05%	1.22%	+16.2%
Vacuum Dewax	1.05	0.97	- 8.3
		Net Inc.	24.5%

Vacuum dewaxing and sintering effectively prevented further oxidation and the improvements are shown in Table VII.2.1-II

Main effects and two-factor interactions from the three dewaxing and sintering runs are given in Table VII.2.1-III. The same trend is observed in all three of the experiments, independent of the level of final density attained. There is a strong SiC powder effect with the UF powder yielding the preferred result. As indicated in the Task I reporting, the UF particle size is finer than the SF SiC powder, and characteristically produces a denser, more finely grained structure during pressureless sintering. A strong carbon source effect is reflected in all of the data and the lampblack powder yields better results than the resin. The higher solids loading level is slightly better than the lower level. A significant SiC powder/carbon powder source interaction is noted. On the basis of these data, the composition designated as NASA 4 was selected for the baseline formulation.

TABLE VII.2.1-III

MAIN EFFECTS AND INTERACTIONS FROM 2^3 EXPERIMENT ON SINTERED DENSITY OF INJECTION MOLDED BARS

	EFFECTS ON DENSITY		
IDENTITY	CONVENTIONAL Ar DEWAX & SINTER	TWO CYCLE VAC DEWAX & SINTER	ONE CYCLE VAC DEWAX & SINTER
AVERAGE	72.7 ± 0.1	88.2	90.2
POWDER	1.2 ± 0.2	1.8	2.0
CARBON	-5.8 ± 0.2	-4.2	-3.5
POWDER-CARBON	-1.6 ± 0.2	-1.8	-1.0
SOLIDS LOADING	0.9 ± 0.2	0.8	0.5
POWDER-LOADING	-0.1 ± 0.2	0.2	1.0
CARBON-LOADING	0.2 ± 0.2	0.2	0.5
POWDER-CARBON-LOADING	0.6 ± 0.2	0.8	0

CONCLUSIONS FROM THESE DATA:

STRONG POWDER EFFECT - UF IS BETTER

VERY STRONG CARBON EFFECT - CARBON BLACK IS BETTER

SOLIDS LOADING EFFECT - HIGH IS BETTER

POWDER-CARBON INTERACTION NOTED

VII.2.2. Molding

The four material compositions described in Section VII.2.1 were initially mixed to a volume percent solids loading level qualitatively judged to be the upper limit for molding test bars. Each mixture was then diluted to provide a range of solids loading levels. The actual loading levels used to make test bars varied as a function of both carbon source (carbon black (CB) vs. polyphenylene resin) and silicon powder type (ultra fine (UF) vs. standard fine (SF)).

The specific loading levels at which bars were molded were:

Powder/Carbon Source	Volume % Solids			
(Composition Designation)	52.5	55.5	58.5	61.5
SF/CB (NASA 5)	--	X	--	X
UF/CB (NASA 4)	--	X	X	X
SF/Resin (NASA 8)	--	X	X	--
UF/Resin (NASA 7)	X	(X) (marginal)	--	--

A spiral flow test was used to quantify the moldability of various mixes. The spiral flow results obtained at 115° and 130°F die temperatures for the only loading level common to all four materials (55.5%) are presented in Table VII.2.2-I. The NASA 5 mix (standard fine/carbon black) was the optimum material for moldability with the NASA 4 mix (ultra fine/carbon black) being an acceptable alternative.

TABLE VII.2.2-I

SPIRAL FLOW DISTANCE
(Inches)

55% Volume Solids

Material Designation and Mix Composition		Spiral Flow Die Temperature	
		115°F	130°F
NASA 5	SF/C-B	5.9	(15.6)
NASA 4	UF/C-B	4.0	12.9
NASA 8	SF/Ph	2.9	13.8
NASA 7	UF/Ph	(<1.0)	8.8

(Extrapolated Estimate)

VII.3. Matrix 2: Dewaxing Cycle.

To evaluate alternate dewaxing cycles, a 2^2 configured experiment was performed in which two heating rates, 5^0 and 10^0 C per hour, and two pressure conditions, vacuum and 150 psi nitrogen, were examined. The yields of this experiment were the percent of wax removed and the sintered density. The conditions of the experiment are listed in Table VII.3-I; the negative and positive signs used in the table indicate lower and higher heating rate and pressure of each experiment.

The weight percent burnout was higher in 150 psi nitrogen than in vacuum; however, the standard deviation was also greater. The significant result observed in this experiment, shown in Table VII.3-I, is that the sintered density is the same for all four conditions. Based on equipment availability, a ramp rate of 5^0 C per hour in vacuum was chosen for the baseline dewaxing process.

VII.4. Matrix 3: High-Shear Processing.

The standard dry mixing procedures were found to be inadequate for use with the ultra-fine powders of the NASA 4 composition. Agglomerates and other inhomogeneities were not effectively reduced in the pre-molding process which delayed development of a baseline process.

A sampling procedure for characterizing the inhomogeneity size and distribution was developed and used as a control parameter for the mixing process. Sampling of both the mix during blending and observation of the fracture surfaces of the as-molded green body and dewaxed body was found to provide a quantitative measure of mix homogeneity. Fracture surfaces were examined microscopically using polarized light. The green test bars contained two types of agglomerates of approximately the same size as those found in the sintered specimens. Gray spots (believed to be wax rich nodules) were distributed throughout the test bars as quantified in Table VII.4-I. Red spots (identified as boron agglomerates) were also

TABLE VII.3-I

TASK VII MATRIX 3

NASA 4 61.5% LOADING
DEWAXING STUDY

2^2 DESIGN

VARIABLES			(-)	(+)
	(1)	HEATING RATE	5°C/hr	10°C/hr
	(2)	PRESSURE	VACUUM	150 psi N

EXPERIMENT		DEWAXED		SINTERED DENSITY	
(1)	(2)	% B/O	σ	%T.D.	σ
-	-	91.76	0.2	93.52	0.3
+	-	91.42	0.1	93.66	0.5
-	+	95.82	0.8	93.95	0.3
+	+	96.38	1.6	93.81	0.5

ALL SINTERED IN V-23 - 5 M.O.R. BARS EACH
NO SIGNIFICANT DIFFERENCE IN GROUPS OF SINTERED BARS

Table VII.4-1

NODULAR AGGLOMERATES IN MIXED MATERIAL PREPARED FOR MOLDING

MATERIAL/MIXING TECHNIQUE	GRAY SPOTS LARGEST (μm)	GRAY SPOTS TYPICAL (μm)	GRAY SPOTS FREQUENCY (#/mm^2)	BORON AGGLOMERATES OBSERVED SIZE (μm)	BORON AGGLOMERATES OBSERVED FREQUENCY (#/mm^2)
NASA 4B (55.5) REFERENCE	62-120	25-80	47		
1000 gm BATCH NASA 4G (55.5) HOT ROLL MIX	50-75	25-50	23	12-87	0.34
500 gm BATCH NASA 4G (55.5) HOT ROLL MIX	50-75	25-35	14	12-87	0.16
NASA 4G (55.5) BASE LINE HI SHEAR MIX	50-100	25-75	12	12-87	0.14
NASA 4G (55.5) SURFACTANT HI SHEAR MIX	50-75	25-35	23	12-62	0.29

observed, but with much lower frequency; a ratio of approximately 1:100. These agglomerates are discussed in detail in Section I.6.2.

Experiments were conducted to determine the effects of alternate mixing techniques on the size and frequency of the agglomerates. The standard mixing process incorporated a double-bladed planetary mixer[4]. Two additional high shear mixing techniques were evaluated as supplemental procedures: hot roll[5] extrusion and Haake mixing[6]. Test results, reported in Table VII.4-I, showed that both procedures significantly improved the homogeneity of the material. Although hot roll mixing appeared to yield the preferred result, it had two distinct disadvantages. First, only very small amounts of material (~ 40 g) could be processed at one time. Secondly, the results were very sensitive to operator technique, requiring constant attention and interaction.

Other procedures were evaluated as a means of reducing the agglomerate size and frequency of occurrence. Dry powder screening and treating the powders with a surfactant prior to the blending step were tried but proved to be ineffective, Table VII.4-I. The Haake high shear process provided the most effective means for improving homogeneity and was selected for processing the baseline material.

VII.5 Matrix 4 - Fluid Mixing

It is well recognized in the field of ceramics that fluid processing will result in better mixing than dry processing techniques. Consequently a research effort was initiated to study the feasibility of using fluid processing to prepare injection molding batches. It was thought that this processing innovation would reduce the agglomerate size and result in improvements in the silicon carbide strength.

---

[4]Ross Mixer: Charles Ross and Son, Hauppauge, N.Y.

[5]Hot Roll Mill: Farrel Co., Ansonia, Conn.

[6]Haake Mixer: Haake Inc., Saddle Brook, N.J.

The fluid mixing process consists of:

- Dissolving the injection molding binders in a solvent (toluol)
- Mixing the solid ingredients (silicon carbide plus sintering aids) in toluol
- Combining the two mixtures
- Removing the toluol by evaporation and drying

The ingredients were batched such that the dried mixture contained the correct amount of solids and injection molding binders. It was intended that the dried batch would act as a "feed stock" to the injection molding machine where it would be melted and injection molded. A small amount of binder was added prior to molding (referred to as "waxing") when improved moldability was desired.

Figure VII.5-1 illustrates how the fluid mixing process is incorporated into the entire processing sequence.

The fluid mixing process, described above, was used to make two batches of material; 4E and 12A. The results of the initial fluid processing experiments are presented in Table VII.5-I in terms of agglomerate size after drying, waxing and molding. The sintered strengths are also presented.

Table VII.5-I. Maximum Agglomerate Size
(micrometers)

Batch No.	Drying	Waxing	Molding	Strength (MPa)
4E	ND	38	38	388 (56.3 Ksi)
12A	ND	37	38	Processing not Complete

ND = Not Detected

INJECTION MOLDED SiC PROCESS FLOW SHEET
INCORPORATING THE FLUID MIXING PROCESS

POWDER PREPARATION

FLUID BLEND SINTERING ADDITIVES
WITH SiC

FLUID BLEND SOLIDS WITH INJECTION MOLDING BINDERS
(BINDERS DISSOLVED IN FLUID)

REMOVE FLUID BY DRYING

INJECTION MOLD

BINDER REMOVAL

SINTER

MACHINE

STRENGTH EVALUATION

Fig. VII. 5-1

The data indicate that the agglomerate size is significantly reduced with the fluid mixing procedure and that the strengths are significantly higher.

The data generated thus far indicate a significant reduction in the agglomerate size. The available data from the fluid mixing process are plotted in Figure VII.5-2 for agglomerate size and Figure VII.5-3 for strength. Insufficient data have been generated to define the process capability with respect to agglomerate size, however, the reduction in the agglomerate size of the fluid mixing process was found to be statistically significant.

Critical analysis of the actual fluid mixing process revealed many opportunities for process improvements which will be carried out in future Task VII experiments. However, it has been decided that the fluid mixing process will be applied in Task II.

VII.6. Matrix 5 - Argon Sintering

The baseline sintering process was carried out in vacuum at 2100°C for 10 minutes. The sintered densities achieved were in the range of 93-94 % of theoretical. A low density case was observed around each sample, indicating that some SiC dissociation was occurring. Consequently, several experiments were performed to develop conditions for successful sintering using an argon atmosphere. This has been shown in prior research at Ford to result in high densities without evidence of dissociation.

An experiment (2^2) was designed to evaluate the effect of sintering temperature and the rate of temperature increase on the sintered density

Maximum Agglomerate Size, Samples Processed by Three Mixing Methods

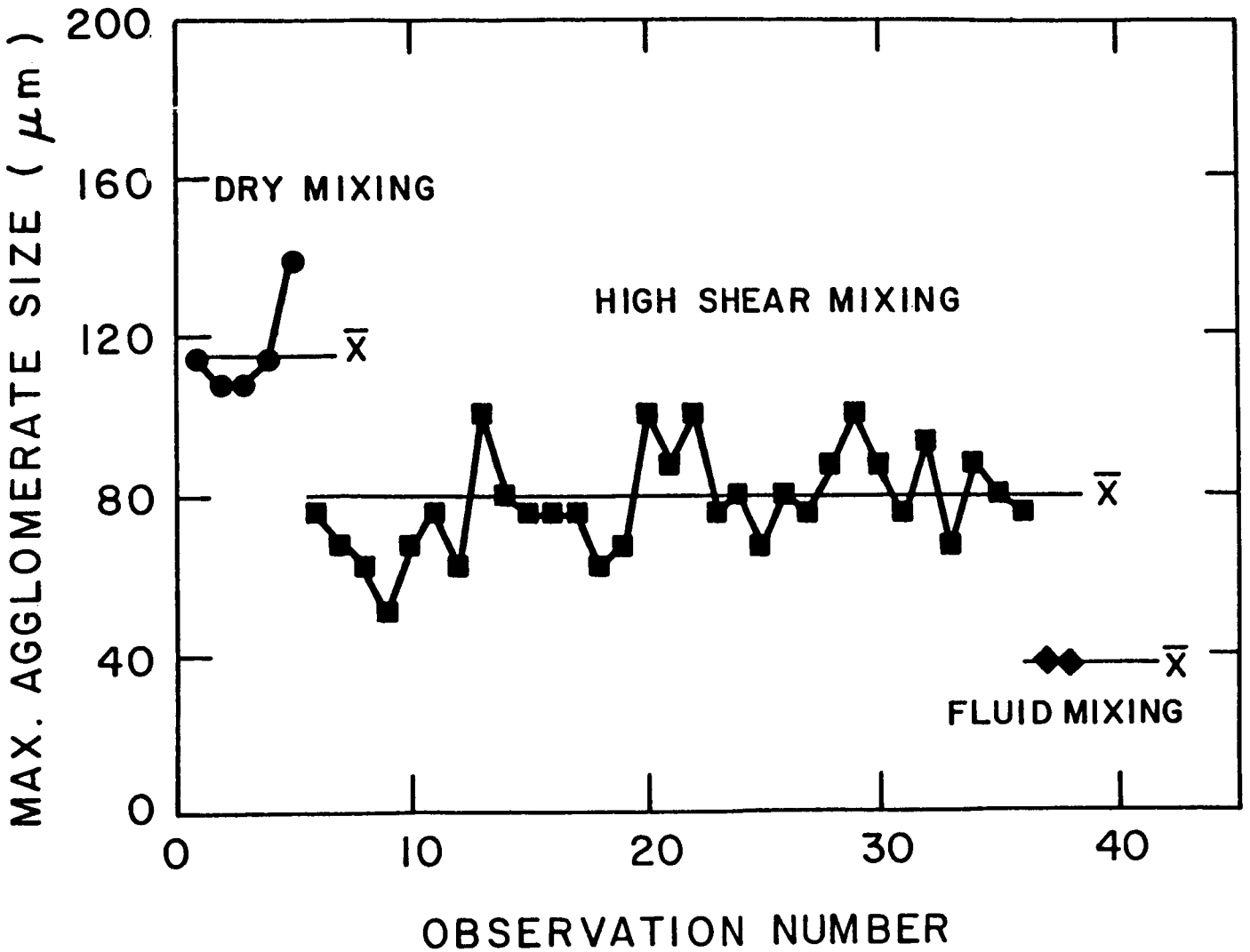

Fig. VII 5-2

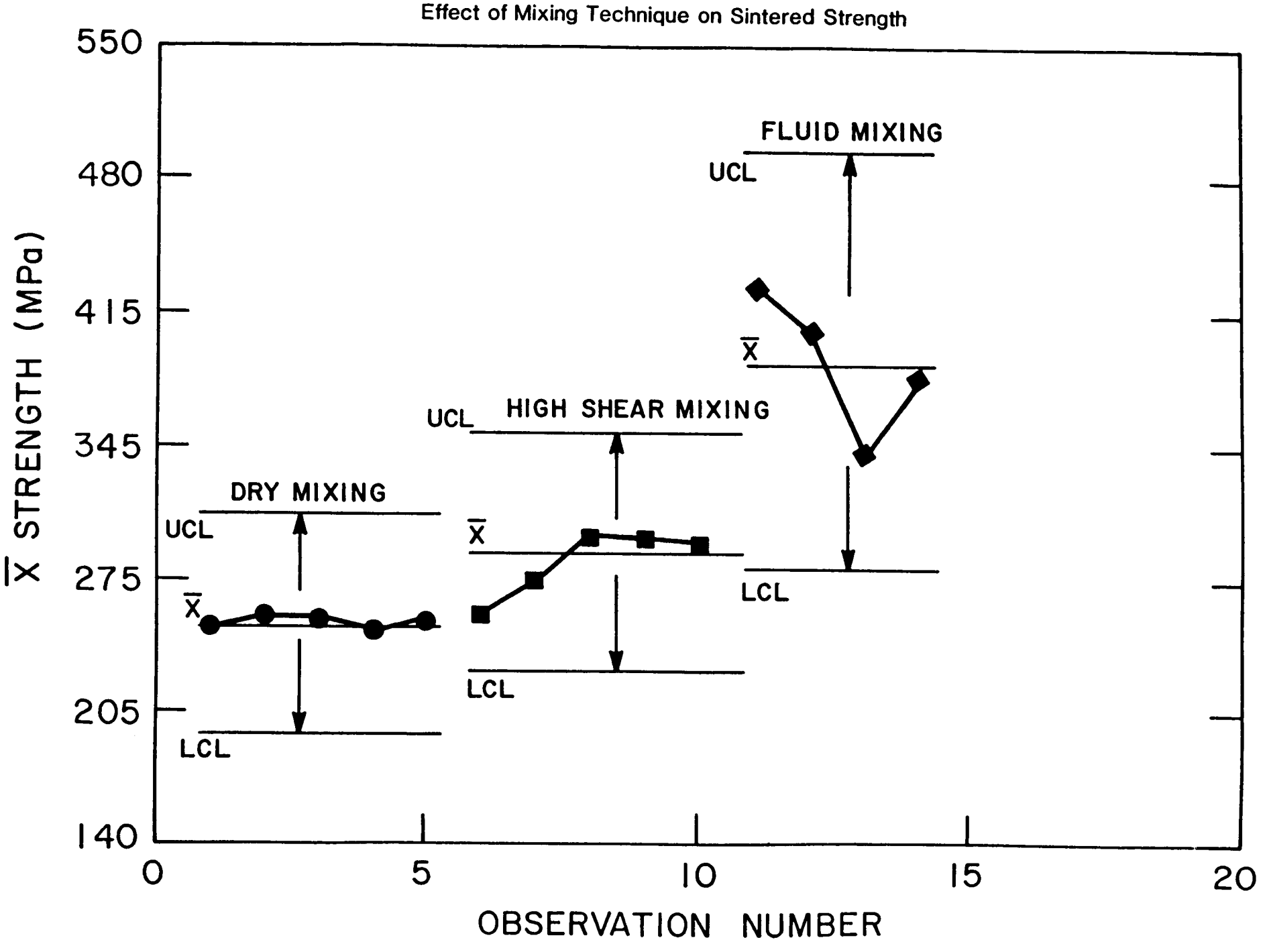
Effect of Mixing Technique on Sintered Strength
550
480
415
345
275
205
140
$\bar{X}$ STRENGTH (MPa)
0
5
10
15
20
OBSERVATION NUMBER
FLUID MIXING
UCL
$\bar{X}$
LCL
HIGH SHEAR MIXING
UCL
$\bar{X}$
LCL
DRY MIXING
UCL
$\bar{X}$
LCL

Fig. VII 5-3

of the NASA 4 material. The sintering time was constant at 10 minutes. An argon atmosphere was used.

The results are presented graphically in Figure VII.6-1, with the arrow indicating the line of steepest assent. A statistical analysis indicates that only the main effects (temperature and rate) are statistically significant at the 0.001 level. The interaction between the two variables is not found to be significant.

The data are expressed mathematically in equation 1

$$\text{Density} = 92.42 + 1.67(T) - 0.97(R) \qquad (1)$$

where T is a unit of temperature (equal to 25°C) and measured above 2000°C and R is a unit of rate equal to 2.5°C/min. Evaluation of this equation indicates that an as-sintered density of > 99% could be achieved if the temperature were increased to 2200°C and the rate decreased to 2.5°C/min. However, experience indicates that grain growth is a concern under these conditions.

Further Task VII experiments are planned to optimize the argon sintering conditions for the injection molded SiC system.

VII.7. Fractographic Analysis of Baseline Trial

This study was undertaken prior to running the baseline in order to determine the failure origins in the 4G materials prepared with high-shear processing. Machined test specimens of 4G composition (prepared with baseline process) were examined by x-ray analysis to determine the location of resolvable defects. The limit of resolution for metallic inclusions and voids is 150 and 250 micrometers, respectively. X-ray maps were made of both the 0.98 cm width and 0.49 cm thickness so that the position of the flaws accurately determined. Metallic inclusions appeared

Graphical Results of Matrix 7
Showing the Sintered Densities
for Each Experimental Condition.
The arrow is the line of steepest assent.

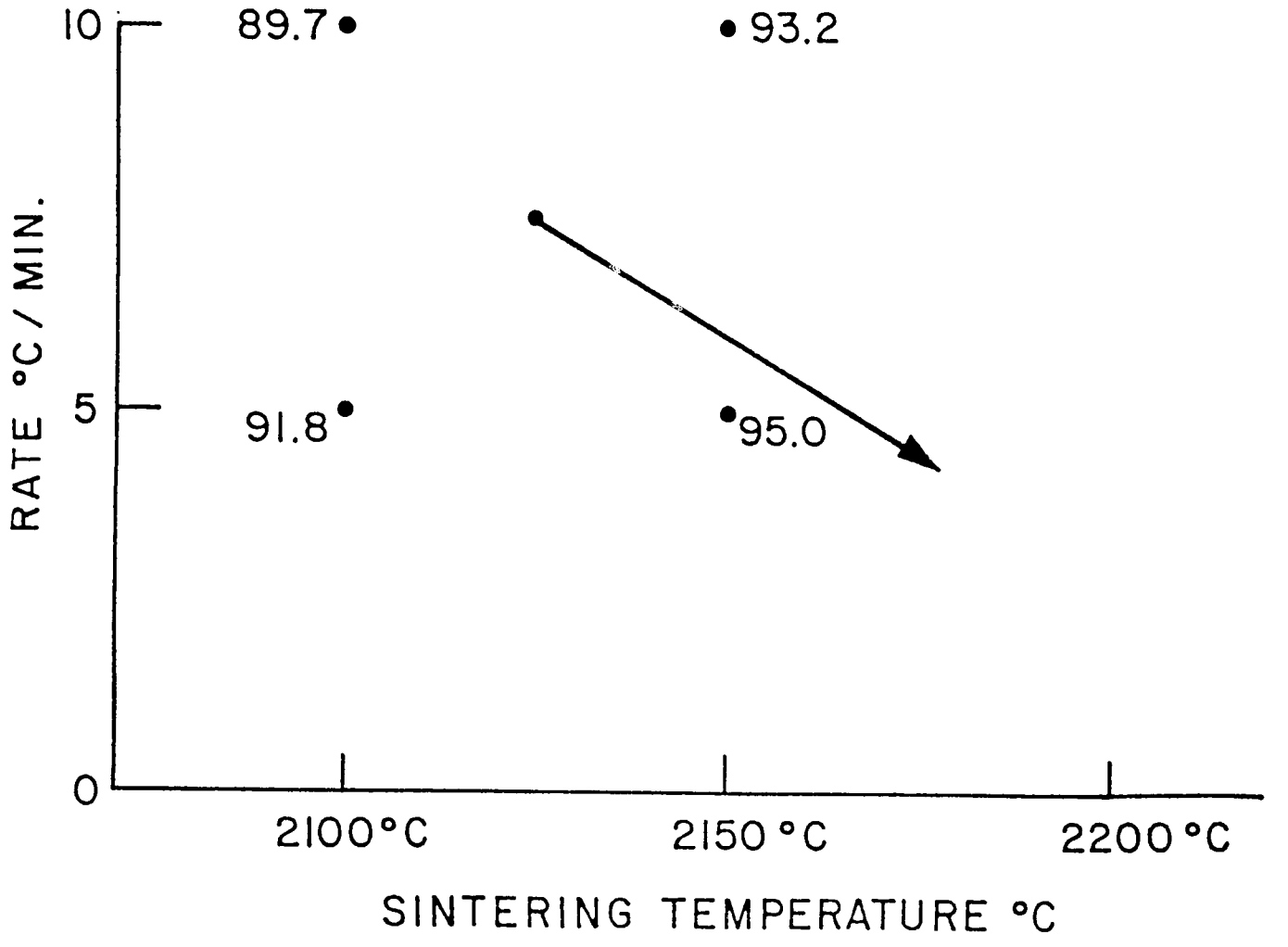

Fig. VII.6-1

as distinctly white areas. Pores were less sharply defined and appeared as slightly darker areas. A preliminary study was made to correlate x-ray detectable defects and the physical properties and fractography of bars from sintering run V-24. MOR bars were classified into four subgroups according to the location and size of the defects and then broken.

The average strengths were as follows:

Type of Flaw	Avg. (MPa)	n
X-ray clean (XC)	255	5
Small defects (S)	292	5
Large defects, near surface, compression side (LS)	275	5
Large defects, near center line (LC)	283	5
TOTAL	276	20

As indicated in the results, there is little correlation between the location of the x-ray resolvable defect and the average strength of the test bars for each grouping.

Examination of the fracture surfaces after testing, Table VII.7-I, showed that the majority of the failure origins were due to flaws whose size was below that resolvable by x-ray analysis. Figure VII.7-1 shows optical micrographs under polarized light (A & B) and an SEM micrograph (C) of a failure origin identified as a metallic inclusion. The defect is shown at higher magnification in Figure VII.7-2, and the details indicate the inclusion has melted and diffusion of the metallic elements into the SiC structure has taken place during sintering. Figure VII.7-3 illustrates a typical porous area which acted as a failure origin.

TABLE VII.7-I

FAST FRACTURE FLEXURAL STRENGTH DATA FOR SINTERED SiC

NASA 4G (V-24 Sintering)

Flaw Type	Fracture Strth. (MPA)	Fracture Strength (Ksi)	Fracture Origin
LS	304	44.03	Sub-surface circular porosity, 2-pc. failure
LS	249	36.14	Same
LS	263	38.19	Same
LS	245	35.51	Surface failure, two-piece
LS	314	45.48	Surface failure, three-piece
LC	238	34.49	Sub-surface circular porosity, two-piece
LC	374	39.68	Surface-associated circular porosity, 2-pc.
LC	317	46.04	Sub-surface porosity, three-piece
LC	386	41.53	Sub-surface circular porosity, two-piece
LC	302	43.75	Sub-surface porosity near corner, three piece
XC	222	32.23	Surface porosity and inclusion, two-piece
XC	230	33.31	Sub-surface circular pore, two-piece
XC	307	44.52	Surface porosity, two-piece
XC	242	35.08	Sub-surface porosity, two-piece
XC	251	36.44	Surface porosity, two-piece
S	300	43.46	Sub-surface, non-circular porosity, two-piece
S	266	38.55	Sub-surface, circular pore, two-piece
S	314	45.55	Sub-surface, circular pore, three-piece
S	270	39.21	Sub-surface porosity, two-piece
S	308	44.64	Surface associated failure

FRACTURE SURFACE
METALLIC INCLUSION

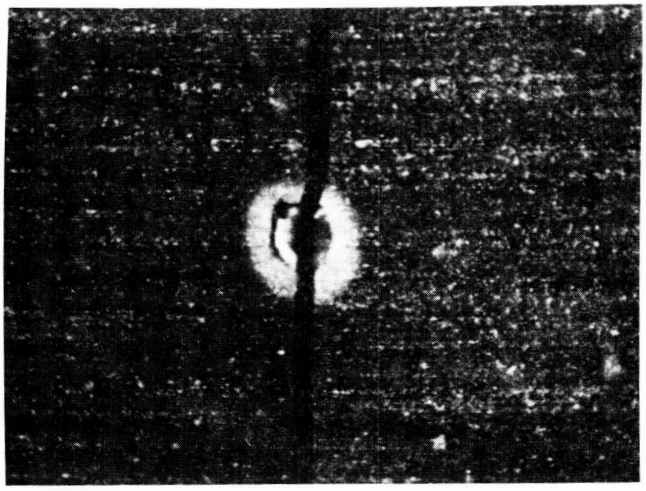

POLARIZED LIGHT

75X

TENSILE SURFACE

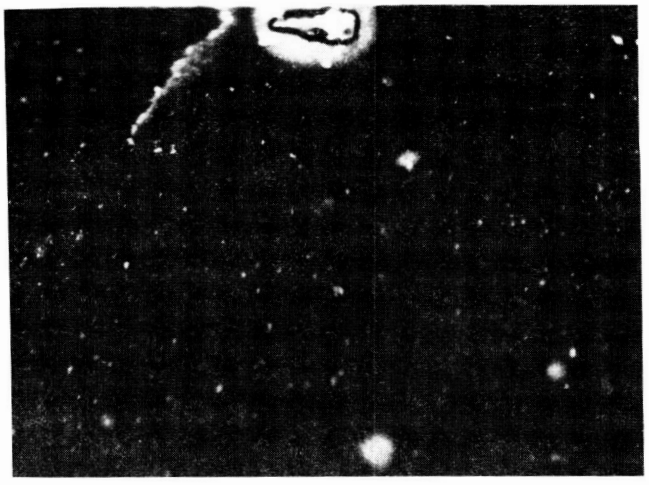

POLARIZED LIGHT

75X

FRACTURE SURFACE

S.E.M.

50X

FRACTURE SURFACE

Fig. VII.7-1

SEM Micrographs of Fracture Surface Showing Iron-Rich Flaw Origin

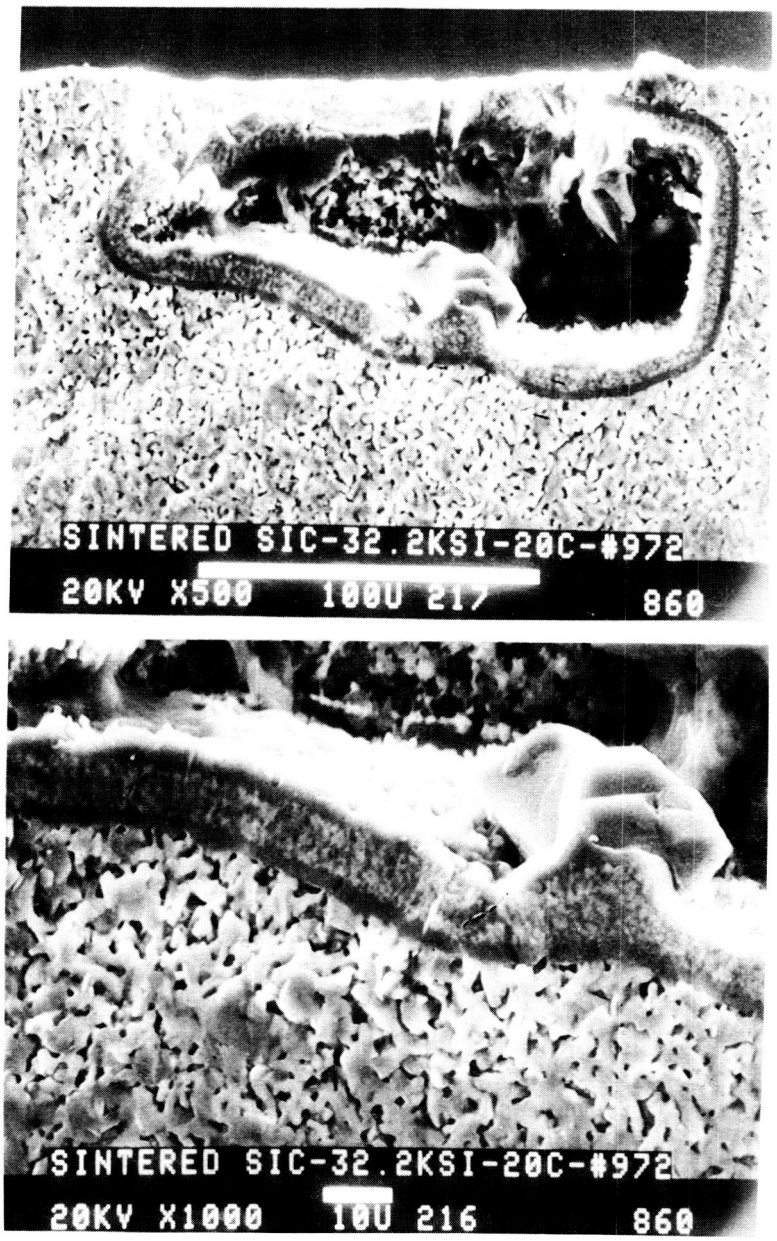

Fig. VII.7-2

Micrographs of Typical Porous Inclusions

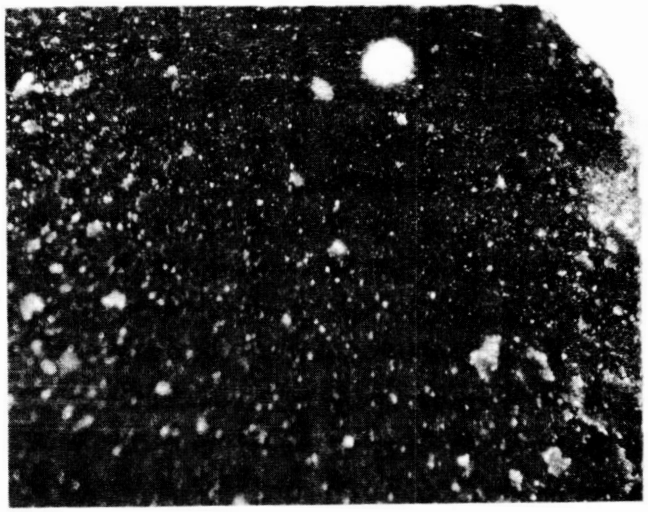

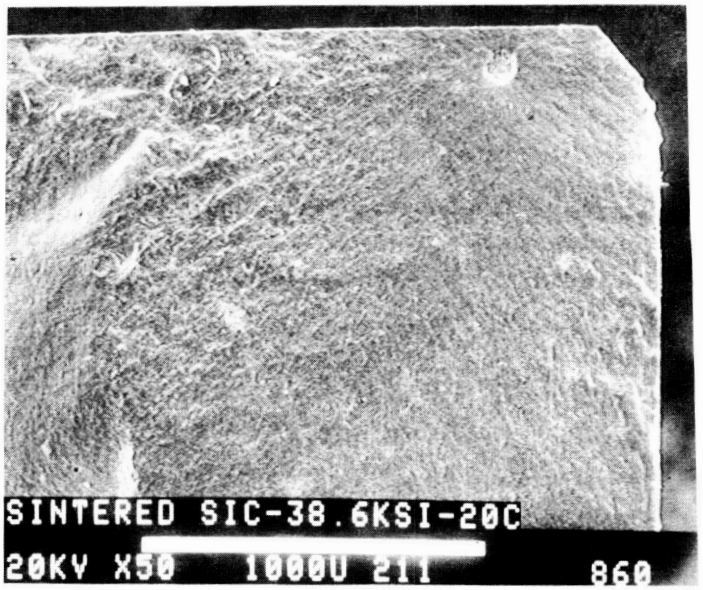

Fig. VII.7-3

FUTURE PLANS

Task II: Improve SiC Properties

II.1. General Considerations

The strength of any ceramic can generally be expressed by the Griffith equation

$$\text{strength} \sim K_I E / c^{1/2}$$

where K_I is the fracture toughness, E is the elastic modulus and c is the flaw size. K_I and E are generally thought to be controlled by the sintering process while c is generally a function of the fabrication process. The first year of the program has concentrated on improvements in silicon carbide properties by improving the fabrication processing steps, i.e. reducing the flaw size of the material.

Research in the program's first year has identified the critical, strength controlling defect as "agglomerates" which occur in the injection molded body. (The term "agglomerates" is meant to be synonymous with nodules, gray spots or unwetted agglomerates.) Close examination of the process revealed that the agglomerates originated in the "mixing" process. Research into the mixing process revealed that the agglomerate size could be reduced with corresponding improvements in the final strength, Figure II.1-1. Regression analysis of these data resulted in the following empirical relation between the strength of injection molded silicon carbide and flaw size, c, in micrometers

$$\text{strength} = 10 + 280\ c^{-1/2}$$

in the flaw size range of 40 - 120 micrometers. Projections using this model indicate that strengths of 66 Ksi (455 MPa) could be expected if the agglomerate size were reduced below the limit of detection (25 micrometers).

Mean Strength of 1.M. SiC as Function of Agglomerate Flaw Size

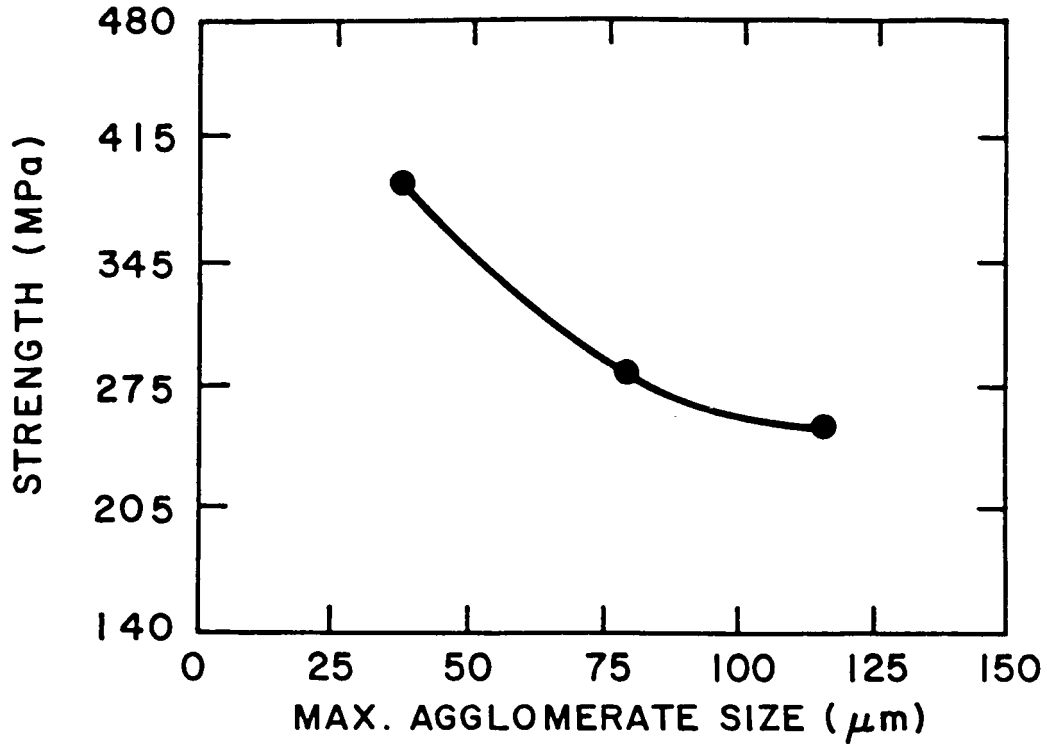

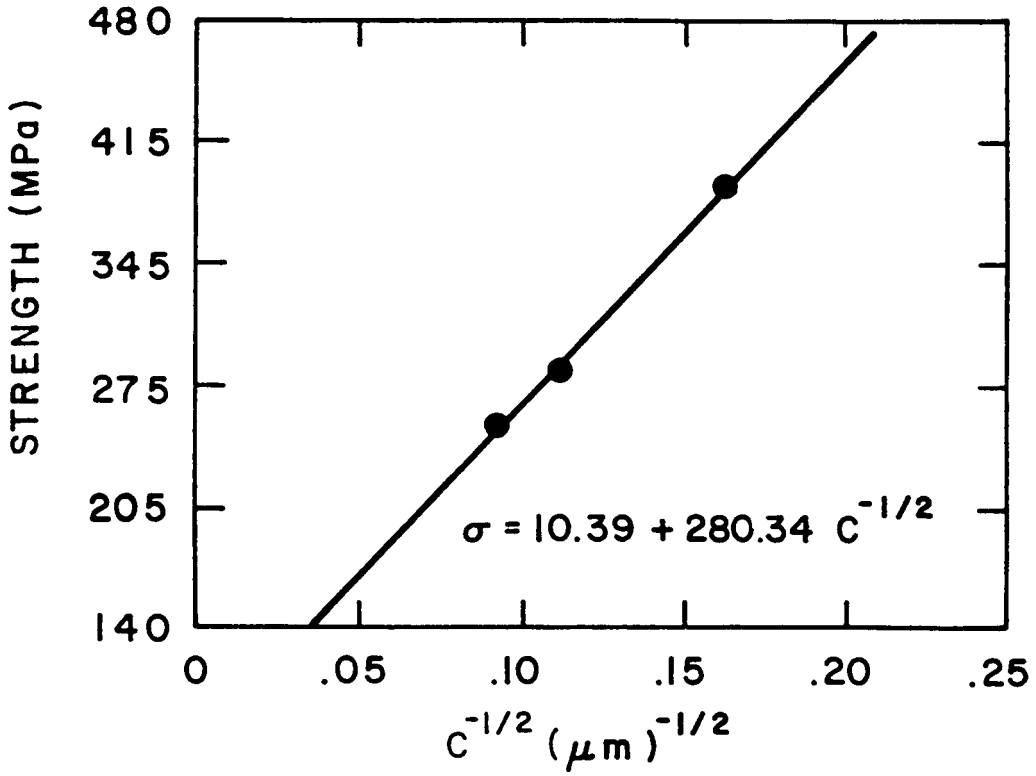

Fig. II.1-1

C-7

Likewise further strength improvements would be expected if the sintered density could be improved from the 93-94 % level to >99 %. Increases in sintered density result in an increase in E. The sintering experiments performed during the program's first year suggest that these improvements are possible.

Finally, the fracture toughness of the SiC could be expected to be improved through microstructural optimization. A fiber strenthening approach is an alternative approach for increasing toughness.

Considering the many opportunities for improvements which have evolved during the program's first year, Ford and NASA have agreed that the best-effort goals of the program be revised upwards as follows:

Room Temp. Strength: 550 MPa (80 Ksi)
Weibull Modulus: 16

It is expected that these objectives will be accomplished through the Task II and Task VII experiments described below.

II.2. Task II. MOR Bar Matrix Study

Task II will consist of two iterations of designed experiments to define the main effects and first order interactions of variables deemed important to the process. The first iteration will concentrate on minimizing the critical flaw size and improving the sintered density of the injection molded SiC. The second iteration will concentrate on optimizing the sintering behavior to achieve a 99 % dense article having a homogeneous microstructure and an improved fracture toughness.

Based on the experience gained during the first year of the program, five key variables were identified for the first iteration of Task II. Specifically, a 2^{5-1} experimental design will be used in studying the parameters. The variables, outlined in Table II.2-I include:

TABLE II.2-I

Proposed Task II Experimental Designs

Matrix II.1

Purpose: Improve the Strength by reducing the agglomerate size and increasing the sintered density

Responses: Sintered density and Sintered strength

Design: 2^{5-1} - Main effects and 2-factor interactions

Variables:

1) Fluid Mix Procedure (A vs B)
2) Solids Loading (55 % vs 60 %)
3) Binder Removal Procedure (Vacuum vs Argon)
4) Sintering Time (30 min vs 60 min)
5) Sintering Temperature (2125 °C vs 2175 °C)

Matrix II.2

Purpose: Improve the strength by increasing the sintered density and increasing the fracture toughness

Responses: Sintered density, fracture toughness, sintered strength

Design: 2^{5-1} - Main effects and 2-factor interactions

Variables: To be determined from on-going Task VII experiments

1) Two variations of the fluid mixing process

2) Two solids loading levels (55 and 60 %)

3) Two binder removal procedures using vacuum and argon atmospheres

4) Two sintering times (30 min and 60 minutes)

5) Two sintering temperatures (2125 and 2175°C)

The study of variable 1 is designed to minimize the flaw size of the material, specifically the agglomerates. The study of variables 2 to 5 is designed to improve densification. In the study of variable 2, the effect of green density will be investigated; the effect of contamination during binder removal will be evaluated through variable 3; and the study variables 4 and 5 will provide the basis for optimizing the sintering conditions.

II.3. TASK VII Studies

Task VII work will continue to supply support information which will input into the other tasks. Work in the next year will investigate the fluid mixing process, the source of sintering additives, the binder removal process and the sintering process.

The timing chart for the remainder of the Phase I of the program is shown in Figure II.3-1.

PROGRAM TIMING CHART
PHASE I

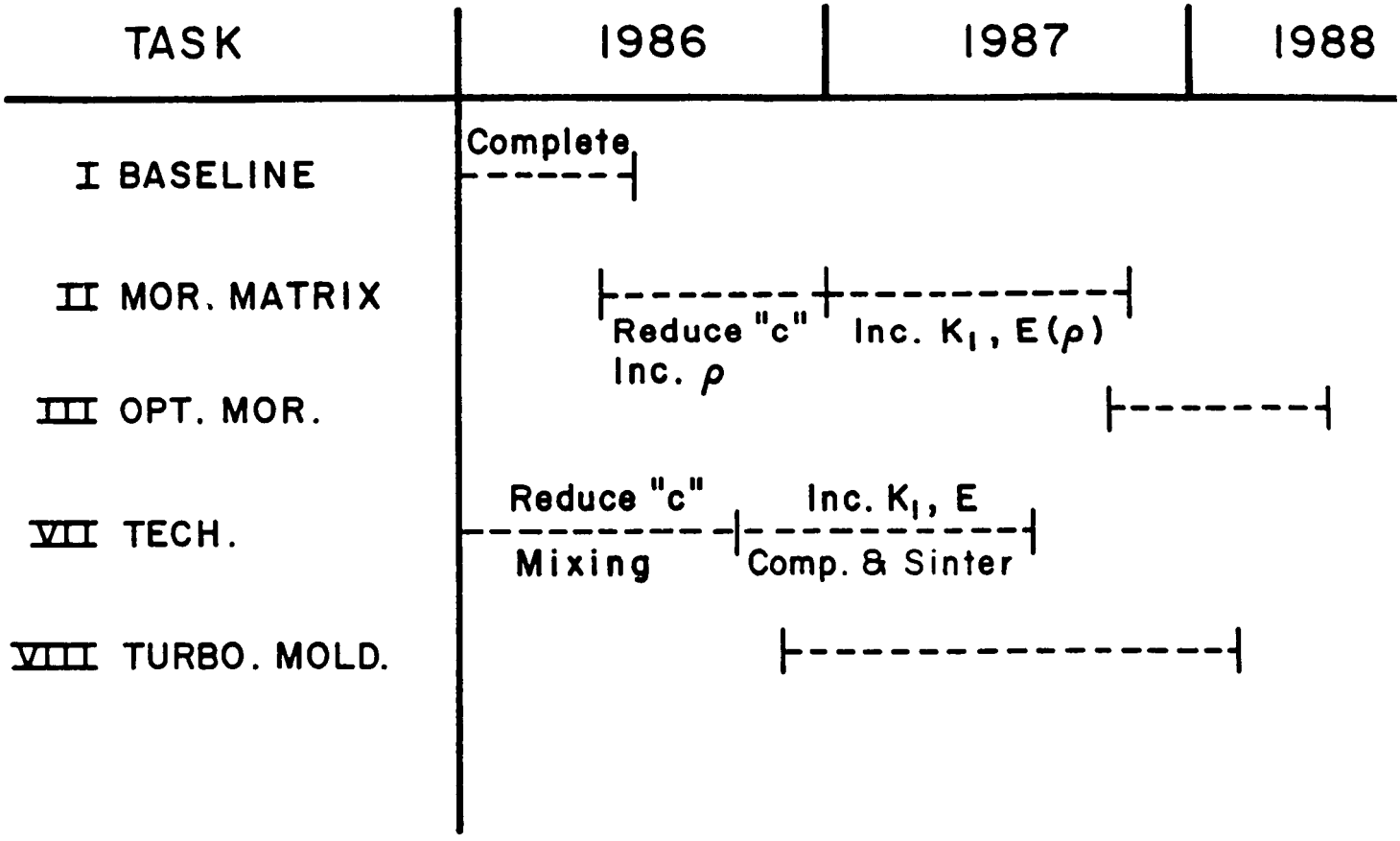

Fig. II.3-1

1. Report No.	2. Government Accession No.	3. Recipient's Catalog No.
NASA CR-179477		

4. Title and Subtitle	5. Report Date
Improved Silicon Carbide for Advanced Heat Engines	September 1986
	6. Performing Organization Code

7. Author(s)	8. Performing Organization Report No.
T.J. Whalen and W.L. Winterbottom	None
	10. Work Unit No. 533-05-01

9. Performing Organization Name and Address	11. Contract or Grant No.
Ford Motor Company Scientific Laboratory Dearborn, Michigan	NAS3-24384
	13. Type of Report and Period Covered: Contractor Report Annual

12. Sponsoring Agency Name and Address	14. Sponsoring Agency Code
National Aeronautics and Space Administration Lewis Research Center Cleveland, Ohio 44135	

15. Supplementary Notes

Project Manager, Nancy J. Shaw, Materials Division, NASA Lewis Research Center.

16. Abstract

This report describes work performed in the first year of the program conducted for NASA to develop silicon carbide materials of high strength and to form components of complex shape and high reliability. The approach has been to adapt a beta-SiC powder and binder system to the injection molding process and to develop procedures and process parameters capable of providing a sintered silicon carbide material with improved properties. The initial effort has been to characterize the baseline precursor materials (beta silicon carbide powder and boron and carbon sintering aids), develop mixing and injection molding procedures for fabricating test bars, and characterize the properties of the sintered materials. Parallel studies of various mixing, dewaxing, and sintering procedures have been carried out in order to distinguish process routes for improving material properties. A total of 276 MOR bars of the baseline material have been molded, and 122 bars have been fully processed to a sinter density of approximately 95 percent. The material has a mean MOR room temperature strength of 43.3 ksi (299 MPa), a Weibull characteristic strength of 45.8 ksi (315 MPa) and a Weibull modulus of 8.0. Mean values of the MOR strengths at 1000 °C, 1200 °C and 1400 °C are 41.4 ksi, 43.2 ksi, and 47.2 ksi, respectively. Strength controlling flaws in this material were found to consist of regions of high porosity and were attributed to agglomerates originating in the initial mixing procedures. The mean stress rupture life at 1400 °C of five samples tested at 172 MPa (25 ksi) stress was 62 hours and at 207 MPa (30 ksi) stress was 14 hours. New fluid mixing techniques have been developed which significantly reduce flaw size and improve the strength of the material. Initial MOR tests indicate the strength of the fluid-mixed material exceeds the baseline property by more than 33 percent. Future plans for the development of the fluid-mixing process to reduce flaw size and increase density and the optimization of sinter-body microstructure to increase toughness of the silicon carbide materials have been approved.

17. Key Words (Suggested by Author(s))	18. Distribution Statement
Silicon carbide Injection molding	[redacted]

19. Security Classif. (of this report)	20. Security Classif. (of this page)	21. No. of pages	22. Price*
Unclassified	Unclassified	102	A06

[redacted]